12-1985

Modeling Soil Erosion with Emphasis on Steep Slopes and the Rilling Process

Digital Object Identifier: https://doi.org/10.13023/kwrri.rr.162

Michael C. Hirschi
University of Illinois at Urbana-Champaign

Billy J. Barfield
University of Kentucky

Ian D. Moore
CSIRO, Australia

Research Report No. 162

MODELING SOIL EROSION WITH EMPHASIS ON STEEP SLOPES AND THE RILLING PROCESS

by

Michael C. Hirschi
Assistant Professor
Department of Agricultural Engineering
University of Illinois - UC
Urbana, Illinois
(Former Research Specialist, University of Kentucky)

Billy J. Barfield
Professor
Principal Investigator
Department of Agricultural Engineering
University of Kentucky
Lexington, Kentucky

and

Ian D. Moore
Senior Research Scientist
Co-Principal Investigator
CSIRO, Division of Land and Water Resources
Canberra, Australia
(Former Assistant Professor, University of Kentucky)

Project Number: B-072-KY (Post-completion Report)
Agreement Number: 14-34-0001-0224 (FY 1980)
Period of Project: October 1979 - September 1983

Water Resources Research Institute
University of Kentucky
Lexington, Kentucky

The work upon which this report is based was supported in part by funds provided by the United States Department of the Interior, Washington, D. C., as authorized by the Water Research and Development Act of 1978, Public Law 95-467.

December 1985

DISCLAIMER

The contents of this report do not necessarily reflect the views and policies of the United States Department of the Interior, Washington, D. C., nor does the mention of trade names or commercial products constitute their endorsement or recommendation for use by the United States government.

ABSTRACT

A soil erosion model, known as KYERMO, was developed for use in soil erosion research. The model was written in Microsoft FORTRAN, which is a subset of the ANSI FORTRAN 77 standard, allowing the model to be run on an IBM-PC as well as a mainframe computer. The model structure consisted of many interrelated subroutines which facilitated model development, testing, and future expansion.

A sensitivity analysis of the detachment component was performed, examining the number of rills, the number of space and time steps, and the detachment parameters. This analysis indicated that the model performed as expected for the detachment limiting case.

Field plots for the collection of justification data were designed and constructed on steep slopes (28 and 30.5 percent). Their surfaces were shaped to provide controlled rill patterns. Rainfall was applied through use of an irrigation nozzle rainfall simulator.

The field simulations included initial full plot (22.1 m) runs on unrilled surfaces with two and six rill watersheds, full plot runs on established surfaces, and half plot runs on established surfaces. Eight field simulations were conducted. Measured or sampled quantities included runoff rate, delivered sediment concentration, delivered sediment size distribution, rainfall intensity, soil moisture content, plot surface shape, and rill cross-sections.

Each of the field erosion events was simulated using KYERMO.

Hydrologic parameters were fitted to provide the proper runoff characteristics to allow justification of the erosion component of the model. The detachment parameters were initially set using parameters and relationships from the literature. Prediction was comparable to that reported by other researchers. The detachment parameters were then fitted individually to gain insights about their effects. The resultant values were then considered in light of plot characteristics. These analyses indicated that a more complete knowledge of the rill bed particle size distribution could be used to increase accuracy and that soil structure changes due to tillage should be considered. The detachment rate was found to be the limiting factor rather than the sediment transport rate.

DESCRIPTORS: Erosion, Sediment Erosion, Erosion Rates, Slope Stability, Model Studies, Slopes, Slope Degradation, Rill Erosion, Rain, Rills

IDENTIFIERS: Long Steep Slopes, Rilling Process, Modeling Erosion.

FOREWORD

This report expands upon the literature review and model development provided by Hirschi, Barfield, and Moore (1983). Model enhancements and corrections subsequent to that report were made prior to the analyses presented in this volume. Additionally, the work reported in this volume was presented as a portion of a dissertation presented to the University of Kentucky graduate school by the senior author as partial fulfillment of the requirements for the degree of Doctor of Philosophy. Material from that dissertation was used extensively in the preparation of this report.

ACKNOWLEDGEMENTS

The authors wish to acknowledge the support and cooperation of Kentucky Utilities Company in providing the field research site and personnel to assist in the site construction. We specifically wish to thank Bob Bowling and his fine crew at the Tyrone Power Plant for their assistance in constructing the erosion plots and for operating the pumps to supply water to our site. We also wish to acknowledge Lloyd Dunn and Jim Wilson for their help with the instrumentation and data collection for this study. Only through their assistance could this study have been completed.

TABLE OF CONTENTS

LIST OF FIGURES

LIST OF TABLES

CHAPTER 1 INTRODUCTION

Soil erosion is not a new problem. It is a complex process with numerous hydrologic interrelationships. Only in the past century has prediction and control been pursued in earnest. Only partial success in prediction has been obtained. Techniques have been developed to predict long-term erosion well enough for use in planning, but detailed research efforts into specific subprocesses that govern erosion are still necessary.

The erosion process becomes an even greater problem when soil is exposed for long periods of time and when steep slopes are encountered. Both situations occur during surface mining. The problem of soil erosion during surface mining has been recognized for a long time, but very little erosion data for steep slopes has been collected. Shallow-slope models have been utilized in the absence of steep-slope models, with varying success. A new model, applicable to steep slopes, is needed to obtain accurate estimates of erosion on steep slopes.

The study described in this report dealt with the development and justification of a soil erosion model that can be used to predict erosion on steep slopes. The rilling process was deemed as one of the most important elements of soil erosion, especially on steep slopes. For this reason, rill erosion mechanics were emphasized in the model development and the experimental portions of the study.

It is anticipated that this effort will ultimately lead to simplified models for use in the mining industry. The model is not

limited to surface mining, but should be equally useful for research use for agricultural soils and situations. It is hoped that further development will continue with this model so that it can be used for future research and development aimed at reducing the alarming rate at which our agricultural soils are being lost, to help the mining industry minimize soil loss from their operations and to put surface mined areas back into useful production after the minerals have been removed. The model was written in Microsoft FORTRAN to be run on an IBM PC microcomputer. Microsoft FORTRAN is a subset of the ANSI FORTRAN 77 standard. Therefore, the model can be run on other computers also. It was written as interconnected subroutines so that new relationships can be added as they become available.

CHAPTER 2 MODEL DEVELOPMENT

The Kentucky Erosion Model (KYERMO) was developed as a research tool to isolate the important aspects of the rainfall/runoff/erosion process. The development goals were to:

1) Develop an overall framework for the erosion process to facilitate further research,

2) Predict overall sediment yield and average rill cross-sections under controlled surface shape conditions on a steep slope as a first step to modeling the erosion process on a random surface, and

3) Model the rilling process due to its importance and a lack of knowledge about its prediction.

The model consisted of a main program and 37 subroutines and functions. It was written in Microsoft FORTRAN. The Microsoft FORTRAN is compatible with FORTRAN 77, so the program can be run on other computers with few modifications. Most of the simulations for the work that follows were run on an IBM 3081 mainframe.

In the following section, a description is given of the computer model structure and the methodology for defining rill drainage patterns. This section is followed by descriptions of the algorithms for computing runoff, erosion, and sediment transport. The reader who is interested only in the computational algorithms may wish to skip to that section.

MAIN PROGRAM AND SUPPORT PROGRAMS

The framework for the model is in the MAIN program of KYERMO. Support programs labeled as INITIA, PRINTO, RAINFA, MOVE, PRINT1, PRINT2, PRINT3, PRINT4, PRINTR, JCTN, and CRASH provide initialization, bookkeeping, and output capabilities. The support programs are called from MAIN (except for PRINTR and JCTN, which are called from INITIA). Each will be discussed in subsequent paragraphs. A full listing was presented by Hirschi (1985).

The MAIN program's structure is represented by the flowchart in Figure 2.1. The generation and routing calls are to sub-main programs rather than to the actual subroutines to facilitate changes in program structure as the program is improved through experience and further research.

The INITIA subroutine is the parameter input and initialization routine for KYERMO. It reads parameter values from disk files and sets up the variables for use by the rest of the model. INITIA also accesses the subroutine PRINTO which prints all the input parameters if desired. A list of all inputs is given in Table 2.1.

The JCTN subroutine is called from INITIA to set the rill flow junction parameters, RJCTN, for each rill watershed on each slope increment. The RJCTN parameter for each rill watershed on a slope increment is calculated for each rill watershed on the increment immediately upslope. RJCTN represents the fraction of flow and sediment travelling from the upslope rill watershed to the rill watershed under consideration. The subscripts of RJCTN are then (J, M,

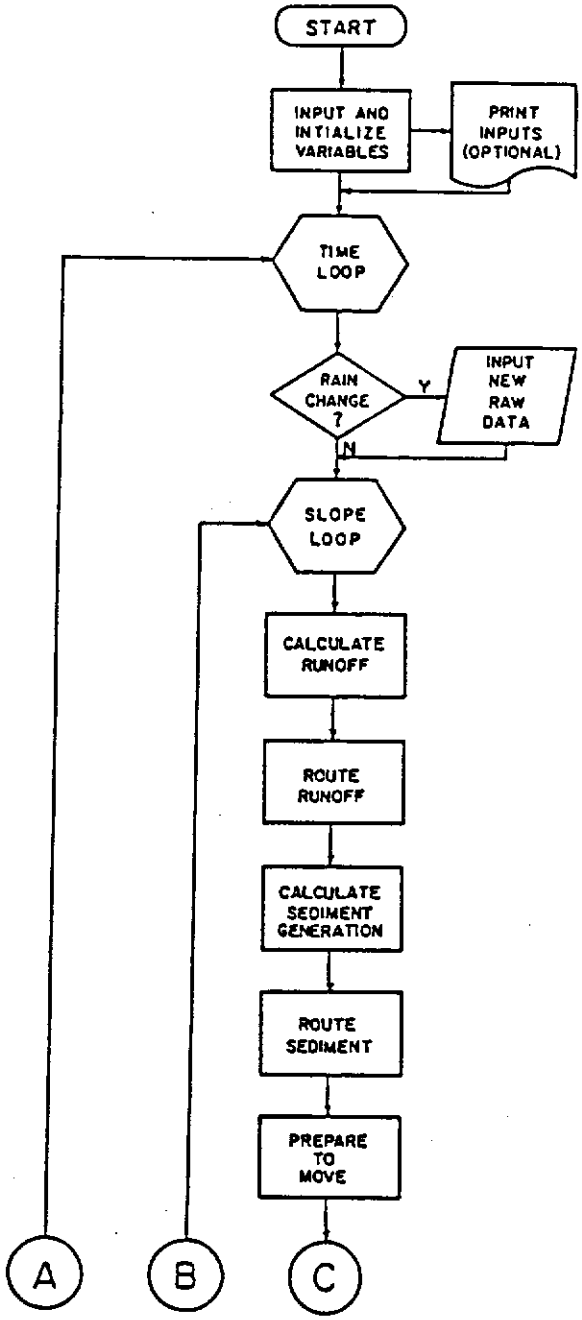

Figure 2.1 MAIN Program Flowchart (continued on next page)

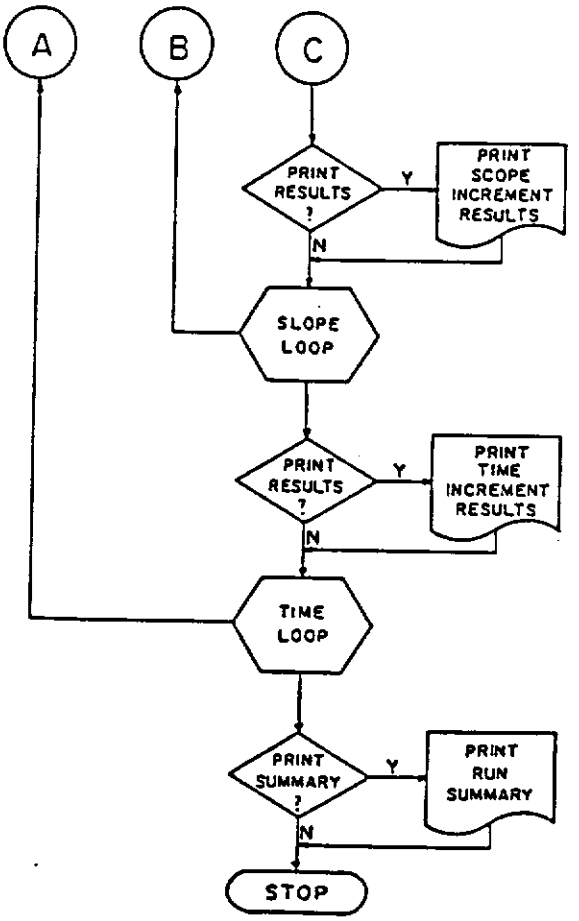

Figure 2.1, continued MAIN Program Flowchart

Table 2.1 INITIA Inputs

Variable Name	Dimension	Variable Description (Units)
HPL	1	Horizontal Plot Length (m)
PW	1	Plot Width (m)
NJ	1	Number of Plot Incrmeents (-)
NR(J)	10	Number of Rills in Each Increment (-)
NSEG(J,M)	10,10	Number of Initial Sediments in Each Rill (-)
NSS(J,M,MJ)	10,10	Number of Sub-Segments for Each Segment (-)
SO(J)	10	Plot Increment Slope (m/m)
HLINC(J)	10	Horizontal Plot Increment Length (m)
TS	1	Simulation Time (min)
DTM	1	Time Step (min)
ITRS	1	Time of Initial Rain Start (min)
TCELS	1	Ambient Temperature (^{o}C)
KS(L)	2	Lab Saturated Hydraulic Condition (cm/hr)
SMC(L)	2	Lab Saturated Moisture Content (cc/cc)
B(L)	2	Log-Log Slope or Moisture Rel. Curve (-)
XI(L)	2	Log-Log Intercept of Moisture Rel. Curve (cmH_2O)
DMM(I)	10	Sediment Type Diameter (mm)
SS(I)	10	Seidment-Type Specific Gravity (-)
FDMM(I)	10	Maxtrix Fraction of Sediment Type (-)
FDMMRD(I)	10	Rain Detached Fraction of Sediment Type (-)
DS(L)	2	Final Degree of Saturation (-)
MC(L)	2	Initial Moisture Content (cc/cc)
PCL(L)	2	Percent Clay (%)
EF	1	Infiltration Rate Criterion (cm/hr)
EV	1	Infitlration Volume Criterion (cm)
LI(J)	10	Upper Layer Thickness (cm)
N(J,M)	10,10	Rill Manning 'n'(-)
NS(J,M)	10,10	Sheet Manning 'n' (-)
RWSW(J,M)	10,10	Rill Watershed Width (-)
ISSD	1	Sheet Trans Eq Choice (-) (0 = Yalin, 1 = Yang)
IRSD	1	Rill Trans Eq Choice (-) (0 = Yalin, 1 = Yang)
RR(J)	10	Plot Increment Random Roughness (cm)
CC	1	Bubenzer-Jones Coefficient (g/min)
E1	1	Bubenzer-Jones Intensity Exponent (-)
E2	1	Bubenzer-Jones Energy Exponent (-)
E3	1	Bubenzer-Jones Percent Clay Exponent (-)
E4	1	Quansah Percent Slope Exponent (-)

Table 2.1 INITIA Inputs (Continued)

Variable Name	Dimension	Variable Description (Units)
PSM	1	Maximum Potential Soil Splash (-)
PS3	1	Potential Soil Splash at 3 Drop Diameters (-)
ARDET(L)	2	Foster Detach Ed Coefficient (g/min)
BRDET(L)	2	Foster Detach Ed Exponent (-)
PO0	1	Print Option (-)
PO1	1	Print Option 1 (-)
PO2	1	Print Option 2 (-)
PO3	1	Print Option 3 (-)
PO4	1	Print Option 4 (-)
PI1	1	Print Option 1 Frequency (Increments)
PI2	1	Print Option 2 Frequency (min)
PI4	1	Print Option 4 Frequency (Increments)
RX(J,M,MJ)	10,10,80	Initial Rill Cross-Section (x Value) (cm)
RY(J,M,MJ)	10,10,80	Initial Rill Cross-Section (y value) (cm)
ICSH	1	Critical Tractive Force Option (-)
CSH	1	Matrix Material Critical Tractive Force (N/m^2)
FCFS	10	Fraction of Surface Covered by Potential Surface Storage (-)
SSS	10,10	Average Rill Watershed Sideslope (cm/cm)

MP) where J represents the slope increment, M represents the rill watershed under consideration on J, and MP represents the rill watershed on the previous (upslope) increment, J-1, delivering water and sediment to M. This concept is shown in Figure 2.2 and Table 2.2. The upper slope increment has no flow from upslope, so all of its RJCTN values are zero. Rill watersheds are delineated on the second slope increment, each getting a flow fraction from upslope proportional to their width relative to the width(s) of the upslope watersheds, as shown in Figure 2.2 and Table 2.2. Two of those rill watersheds contribute to one of the watersheds on the lower increment, giving two values of RJCTN equal to 1 for the second rill watershed on the lower increment. The RJCTN values are then used to transfer the water flow and sediment delivery between slope increment during the simulation.

The RAINFA subroutine is a second input subroutine. It reads rainfall intensity, drop size distribution, and energy data as the program runs. It is accessed at times that are specified during each read operation. Future modifications could be made to the model to have options for 1) natural rainfall energy and drop-size distribution for the given intensity, 2) Kentucky Rainfall Simulator (Moore, Hirschi, and Barfield, 1983) energy and drop-size distribution, 3) Rainulator (Meyer and McCune, 1958) energy and drop-size distribution, or 4) the option to specify all rainfall characteristics. At the present time the only option is 4). A list of the inputs is given in Table 2.3.

The MOVE subroutine is utilized before each space or time increment to reset those variables that are to be utilized again. It also

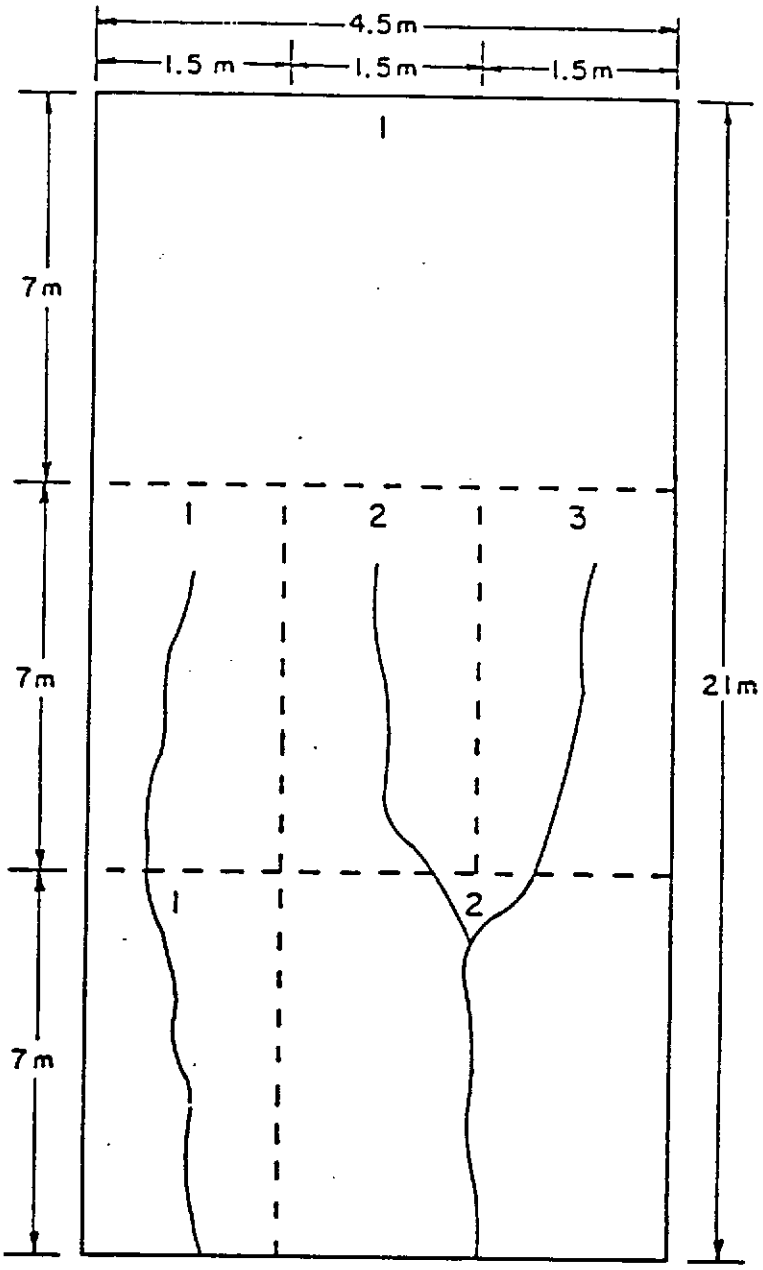

Figure 2.2 Example Plot Configuration for RJCTN Calculation

Table 2.2 RJCTN Values for Configuration of Figure 3.2

	1			2			3		
Slope	Upslope Rill			Upslope Rill			Upslope Rill		
Increment	1	2	3	1	2	3	1	2	3
1	0	0	0	0	0	0	0	0	0
2	0.333	-	-	-	0.333	-	-	-	0.333
3	1.000	0	0	0	1.000	1.000	-	-	-

Table 2.3 RAINFA Inputs

Variable Name	Dimension	Variable Description (Units)
RAIN	1	Rainfall rate (cm/hr)
EKRAIN	1	Rainfall kinetic energy (joules/cc)
TR	1	Rainfall duration (min)
TRS	1	Next rainfall start time (min)
FRDMM	28	Fraction of rainfall volume in each drop size class (-)
EKK	28	Kinetic energy of each drop size class (joules/cc)

calculates statistics for the PRINT2 and PRINT3 subroutines. It also sends hydrologic and sediment data to disk files for further analysis at a later time.

The CRASH subroutine is provided to print currently available values of the normally output variables in the event of certain errors. The CRASH subroutine can be called from RLCSSH or DEPDIS in the event of nodal point problems or the prediction of negative or infinite depths in the flow depth computation routine, from SLUFF in the event of nodel point problems, and from PRINT4 if the number of nodal points exceeds the set dimension. The subroutine simply prints an error message and then calls each print routine before terminating the run.

The output subroutines (PRINT1, PRINT2, PRINT3, and PRINT4) print the statistics and run information for KYERMO. All have on/off options specified in INITIA. The PRINT1 routine outputs after specified slope increments. The PRINT2 routine outputs after specified time increments. The PRINT3 routine outputs after the run is completed. The PRINT4 subroutine prints the rill watershed soil surface coordinates. The x-value is the distance of the point from the left edge of the rill watershed (looking uphill). The y-value is the soil surface height of the point above a datum defined by the initial surface coordinates. All of the output subroutines have print options set by inputs to INITIA to provide output only when desired. The output parameters are given for all print routines in Tables 2.4a, b, c, and d respectively.

The framework formed by the MAIN program and its support routines is then filled in with the following four components:

Table 2.4a PRINT1 Output Variables

Variable	Variable Description (Units)
J	Current Slope Increment (-)
I	Current Time (min)
HDDSL	Horizontal Distance Downslope (m)
F(J)	Infiltration Rate (cm/hr)
V(J)	Infiltrated Volume (cm)
QO	Interflow Out of Increment (cm/hr)
QI	Intreflow into Increment (cm/hr)
RO(J)	Runoff Rate (cm/hr)
SSTO(J,2)	Surface Storage Filled (cm)
RC	Rate Continuity (%)
M	Rill Watershed under Consideration (-)
QSHEET(J,M)	Sheet Flow Rate (cc/sec)
QRILL(J,M)	Rill Flow Rate (cc/sec)
I	Sediment Particle Type under consideration (-)
RDET(I,J)	Raindrop Detachment Rate (g/min)
DM(I,M)	Rill Flow Matrix Detachment Rate (g/min)
DD(I,M)	Rill Flow Deposited Detachment Rate (g/min)
SMASS(M)	Sloughed Soil Mass (g)
SST(I,M)	Sheet Flow Transport Rate (g/min)
RT(I,M)	Rill Flow Transport Rate (g/min)
DEP(I,J,M)	Deposition Rate (g/min)
QSRILL(I,J,M)	Sediment Delivery Downslope (g/min)

Table 2.4b PRINT2 Output Variables

Variable	Variable Description (Units)
T	Current Time (min)
RORTOT	Total Runoff Rate (l/min)
SEDRTO	Total Sediment Delivery Rate (kg/min)
TSPWFR	Total Sediment Plus Water Flow Rate (l/min)
QRILL (NJ,M)	Rill Flow Rate (cc/sec)
QSRILL (I,NJ,M)	Sediment Delivery Rate (kg/min)
ROTL	Cumulative Runoff (l)
ROTCM	Cumulative Runoff (cm)
SDKG	Cumulative Sediment Delivery (kg)
SDMTHA	Cumulative Sediment Delivery (MT/ha)
SDTAC	Cumulative Sediment Delivery (T/ac)
WSDL	Cumulative Water and Sediment Delivery (l)
NSDKG	Cumulative Water and Sediment Delivery (kg)
RTOT	Cumulative Rainfall (cm)
RTOTL	Cumulative Rainfall (l)
VC	Volume Continuity (%)
VC1	Delivery/Storage Volume Continuity (%)
NUM(I)	Sorted Sediment Type (-)
PFW(I)	Percent Finer by Weight (%)

Table 2.4c PRINT3 Output Variables

Variable	Variable Description (Units)
RTOT	Total Rainfall (cm)
RTOTL	Total Rainfall (l)
ROTL	Total Runoff (l)
ROTCM	Total Runoff (cm)
CN	Equivalent Curve Number (-)
SDKG	Sediment Delivery (kg)
SDMTHA	Sediment Delivery (MT/ha)
SDTAC	Sediment Delivery (T/ac)

Table 2.4d PRINT4 Output Variables

Variable	Variable Description (Units)
RX(J,M,MJ)	X-Coordinate of Rill Cross Section Nodal Point (cm)
RY(J,M,MJ)	Y-Coordinate of Rill Cross Section Nodal Point (cm)

1) Runoff generation component,

2) Runoff routing component,

3) Sediment generation component, and

4) Sediment routing component.

Each of these components will be discussed in subsequent sections.

RUNOFF GENERATION COMPONENT

The runoff generation component consists of its sub-main program, RUNGEN, and four subroutines: SURSTO, INFILT, INTERF, and RUNOFF. The INTERF subroutine is a dummy subroutine at the present time. It is planned to include an interflow component at some future time. Accordingly, no discussion of INTERF is necessary. The other three subroutines calculate surface storage, infiltration rate, infiltrated volume, and runoff rate.

The subroutine SURSTO utilizes the plot slope and an index of surface roughness termed "random roughness" (Allmaras et al., 1966) to estimate total available surface storage using curves developed by Linden (1979), as presented in Figure 2.3. The representation of these curves for use in KYERMO was developed by fitting a four-point Lagrangian function through the inflection points on Linden's curves. Linden found that no appreciable storage existed on slopes above 20% (in the range of random roughness examined), so 20% is used as an upper limit. The equations are shown in Figure 2.4.

The data of Moore (1979) was used to develop an equation to

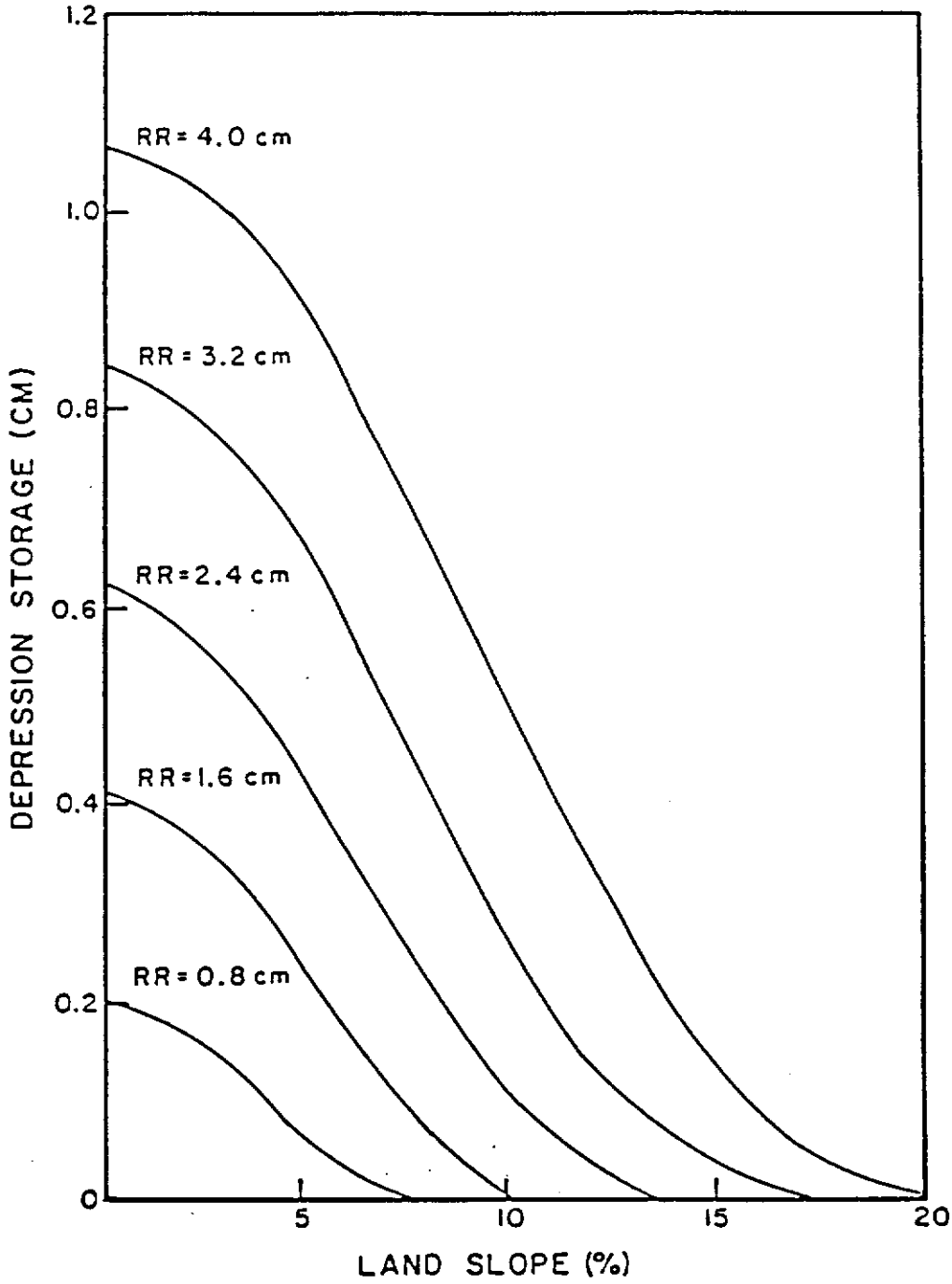

Figure 2.3 Upper Limit of Depressional Storage Versus Land Slope and Surface Roughness (after Linden, 1979)

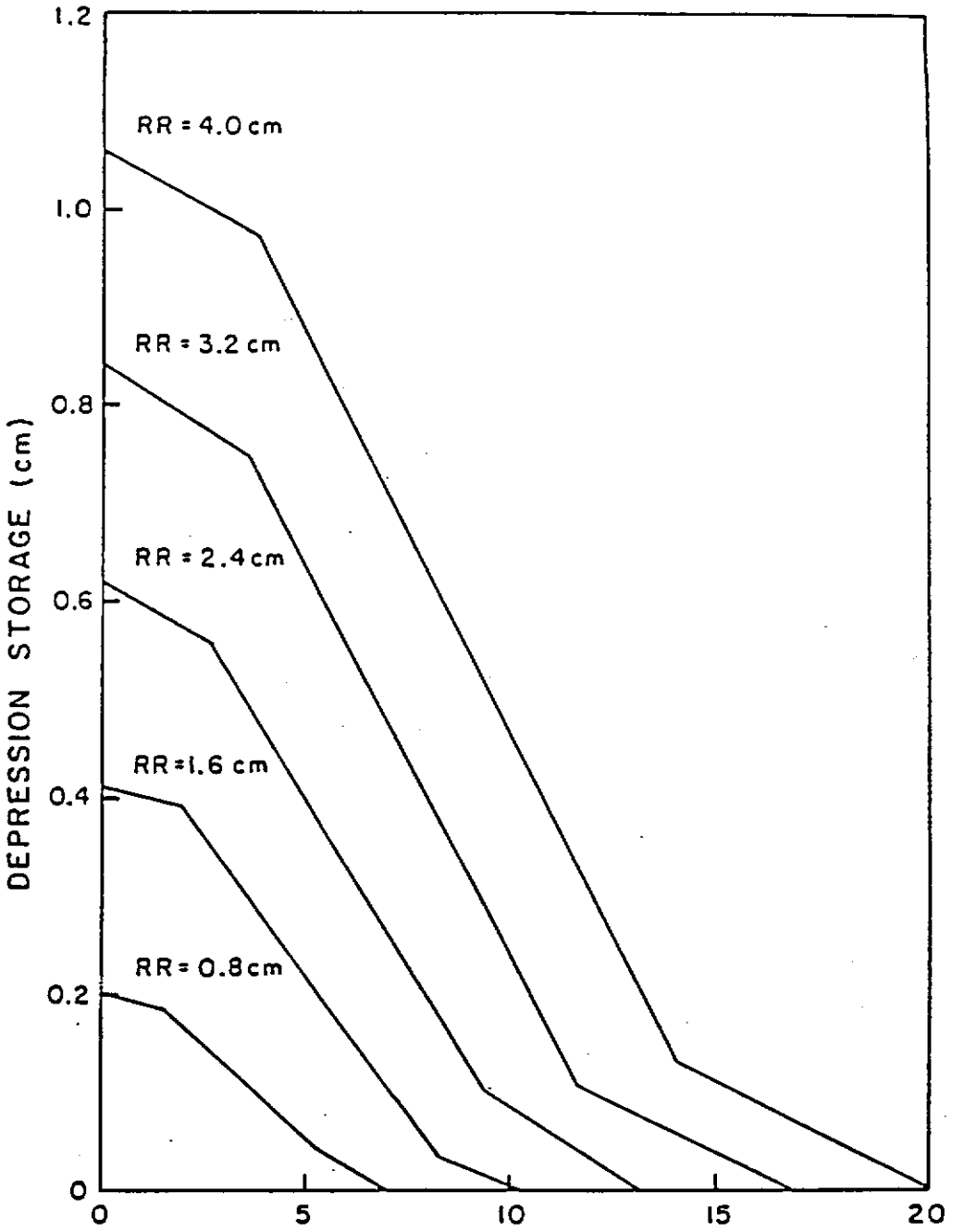

Figure 2.4 Lagrangian Representation of Linden (1979) Surface Storage Function

predict the change in random roughness due to rainfall inpact. The equation is:

$$\frac{RR}{RR_0} = 0.9644e^{-1.989KE} \qquad (2.1)$$

where RR is random roughness, RR_0 is initial random roughness, and KE is the cumulative applied kinetic energy (joules/cm^2). Although this is the "best fit" equation for Moore's data, a more correct relationship would have a coefficient of one, taking the form of:

$$RR = RR_0e^{-k(KE)} \qquad (2.2)$$

where k would be approximately equal to two. Equation 2.1 is used in KYERMO, because it represents the only available relationship for rainfall degradation of random roughness. Moore's data and Equation 2.1 are shown in Figure 2.5.

The subroutine INFILT is the most involved subroutine in the runoff generation component. It is based upon the Moore (1981a) and Moore and Eigel (1981) extension of the Green-Ampt-Mein-Larson (GAML) model which was developed by Mein and Larson (1971) as an extension of the Green and Ampt (1911) equation. A modification of the Moore (1981a) work for use in this model is the use of the "field saturation" concept as outlined by Hirschi, Larson and Slack (1980) and Hirschi (1980).

The GAML infiltration rate equation is,

$$f = K(1 + \frac{IMD(S_{av})}{F}) \qquad (2.3)$$

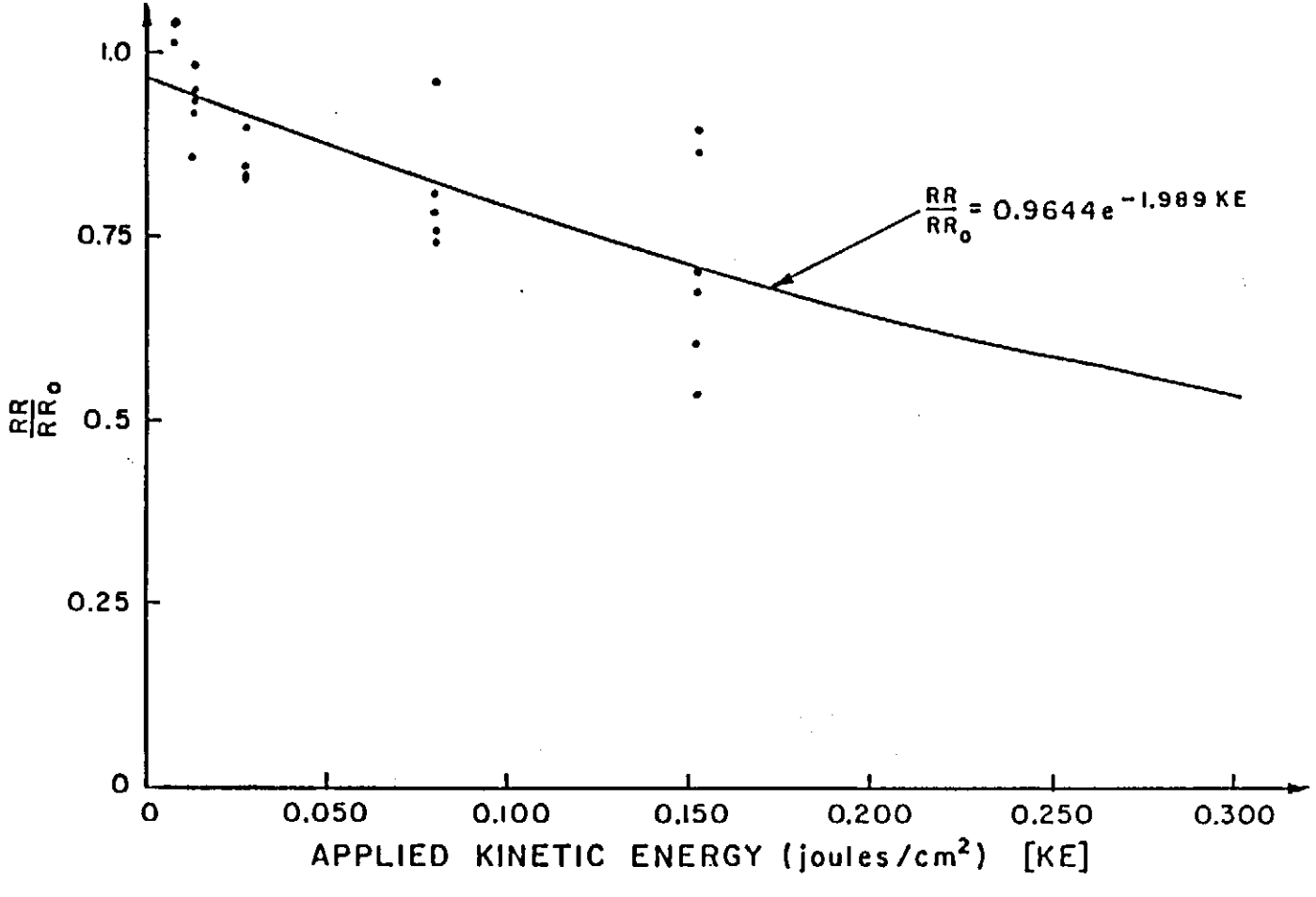

Figure 2.5 Random Roughness Degradation Function (data from Moore, 1979)

At all times, if the rainfall rate is less than the infiltration rate, the value of f is limited to the rainfall rate.

Moore and Eigel (1981) modified the GAML model to account for a two-layered system. Since the two layer system is appropriate for the plots to be studied, the final rate equation of Moore and Eigel was used in KYERMO. Moore and Eigel's equation was modified by making "field saturation" substitutions, resulting in,

$$f = K_{fs1}\left(1 + \frac{S_{av1}\ IMD_1}{F}\right) \qquad \text{for } L<L_1$$

$$f = K_{fs2}\frac{(H + F - F_1)}{(E + F - F_1)} \qquad \text{for } L>L_1 \tag{2.4}$$

where K_{fs1} and K_{fs2} are "field saturation" conductivities for layers 1 and 2, respectively, F and f are as previously defined, L is the depth to the wetted front, L_1 is the depth of the upper layer (the lower layer is assumed infinite), F_1 is the infiltrated volume stored in the upper layer, S_{av1} and IMD_1 are the average suction across the wetted front and the initial moisture deficit, respectively, for the upper layer, and H and E are as follows:

$$H = IMD_2\ (L_1 + S_{av2})$$

$$E = L_1\ IMD_2\ K_{fs2}/K_{fs1} \tag{2.5}$$

where S_{av1} and IMD_1 are the average suction across the wetted front

and the initial moisture deficit, respectively, for the lower layer.

The final equations are solved at each time interval by iteration until the values of f and F change by less than small, user-selected amounts. A small amount of numerical instability was found at the interface between the two layers, but this is remedied by recalculating the values using the upper layer equation if the rate immediately after crossing the interface is larger than the previous value. An example output is shown in Figure 2.6. Development details were presented by Hirschi (1985).

In the RUNOFF subroutine, an exponential relationship proposed by Tholin and Keifer (1960) is utilized,

$$RO = (R-f)(1-e^{-(P-F)/SS}) \qquad (2.6)$$

where RO is the runoff rate, f and F are as defined before, R is the rainfall rate, P is the accumulated rainfall volume and SS is the total available surface storage. If there is no surface storage (i.e. SS=0), RO is assumed equal to (R-f). Equation 2.6 allows runoff to occur while the surface storage is only partially filled. It is assumed that rainfall excess that does not become runoff goes into surface storage.

The runoff function described by equation 2.6 gives the correct trend, but does not converge to runoff equalling rainfall minus infiltration when the potential surface storage is filled, but will only do so as (P-F) gets very large. A correction term was added that is equal to one when the surface storage is zero, and is equal to zero when the surface storage is equal to the potential storage. The final

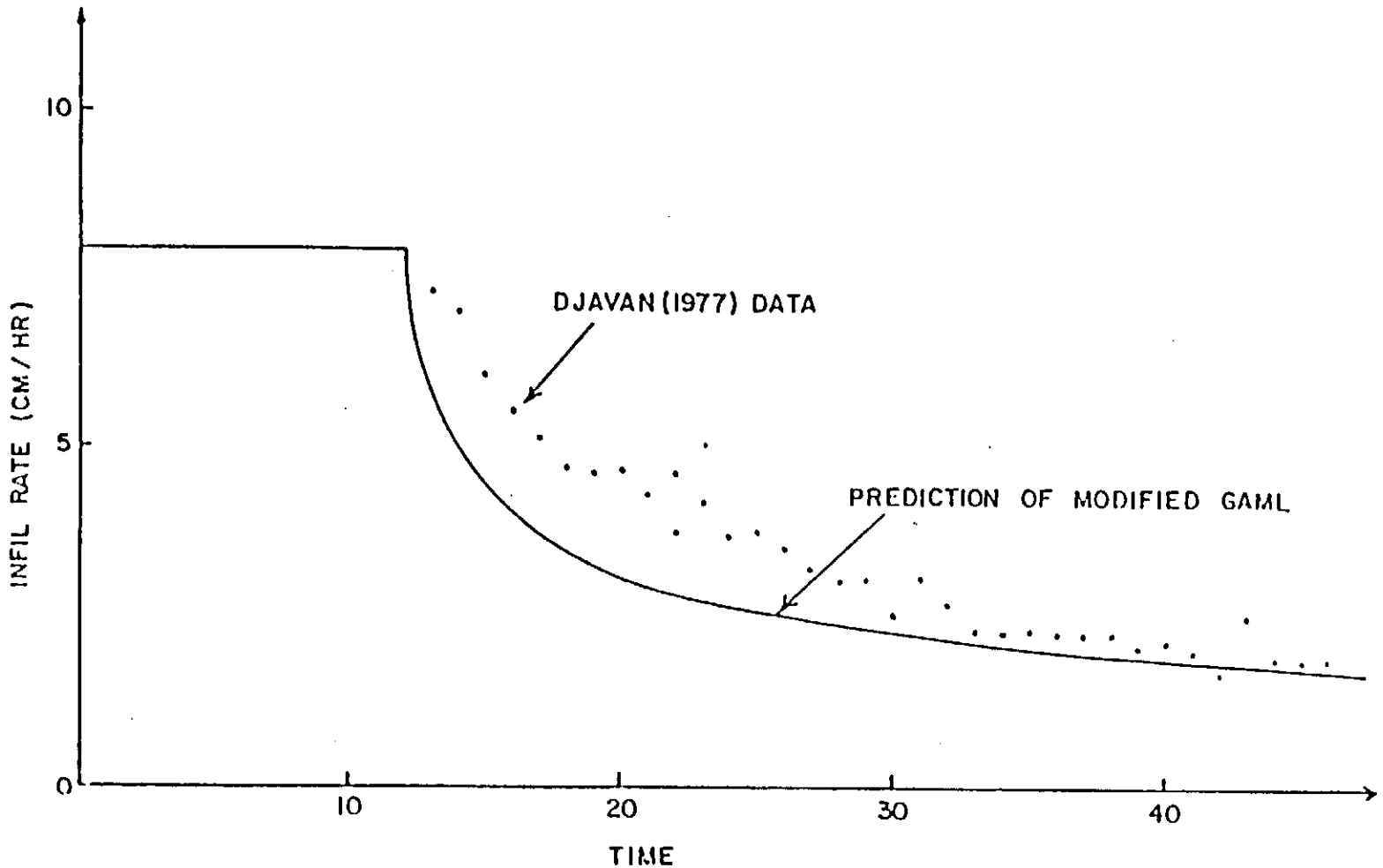

Figure 2.6 **Modified GAML Example Output**

equation is then,

$$RO = (R-f)\left(1 - \frac{(SS - SSF)}{SS} e^{-(P-F)/SS}\right) \qquad (2.7)$$

where SSF is the actual volume of water in surface storage.

The runoff rate on each slope increment during each time step is then available for use in the runoff routing component.

RUNOFF ROUTING COMPONENT

The runoff routing component consists of a sub-main program, RUNROT, and three subroutines, RILLFL, RLFLOW, and RLCSSH. The runoff is routed through the dynamic rill network initially set up in INITIA, whose cross sections are changed with time in the sediment generation component, reflecting detachment of sediment.

In the subroutine RILLFL the flow is calculated in each rill on a slope increment using Manning's equation. In the flow routing routine computations are made in smaller time steps then used in the overall model in order to gain accuracy and stability. In RILLFL flow characteristics are averaged from the previous time step to set the routing time step at or below the critical value for routing method stability. RILLFL then calls the subroutine RLFLOW, in which the routing is calculating.

In the subroutine RLFLOW, a four-point kinematic routing procedure, as outlined by Brakensiek (1966), was used. The kinematic wave model for routing has been extensively used in streams and for overland

flow. Weinmann (1977) studied many routing methods including a numerical solution of the complete non-linear St-Venant equations and concluded,

> "In steep regular channels kinematic wave models produce results that can hardly be distinguished from the results of the complete model, but are obtained at far less expense,..."(pg 136).

In the procedure a finite differencing method was used with Manning's equation as the rate equation along with the continuity equation. The known flow rate and area at previous time and space steps where used to calculate the flow rate and area at the current location and time, as shown in Figure 2.7. The procedure is essentially an initial value problem in two dimensions. Briefly the development is as follows:

Continuity Equation: $$\frac{\partial Q}{\partial x} + \frac{\partial A}{\partial t} = q \qquad (2.8)$$

Rate Equation: $$Q = \frac{1}{n} R_h^{2/3} (\sin\theta)^{1/2} A \qquad (2.9)$$

where Q is flow rate, A is flow area, q is lateral inflow, n is Manning's coefficient, R_h is the flow hydraulic radius, and θ is the slope angle. The continuity equation (2.8) is set up using a different finite difference approximation for each term. Brakensiek found that a central difference equation was best for $\partial A/\partial t$, but a forward difference equation was best for $\partial Q/\partial x$. The representations are

$$\frac{\partial A}{\partial t} = \frac{A_4 - A_3 + A_2 - A_1}{2\Delta t} \qquad (2.10)$$

and

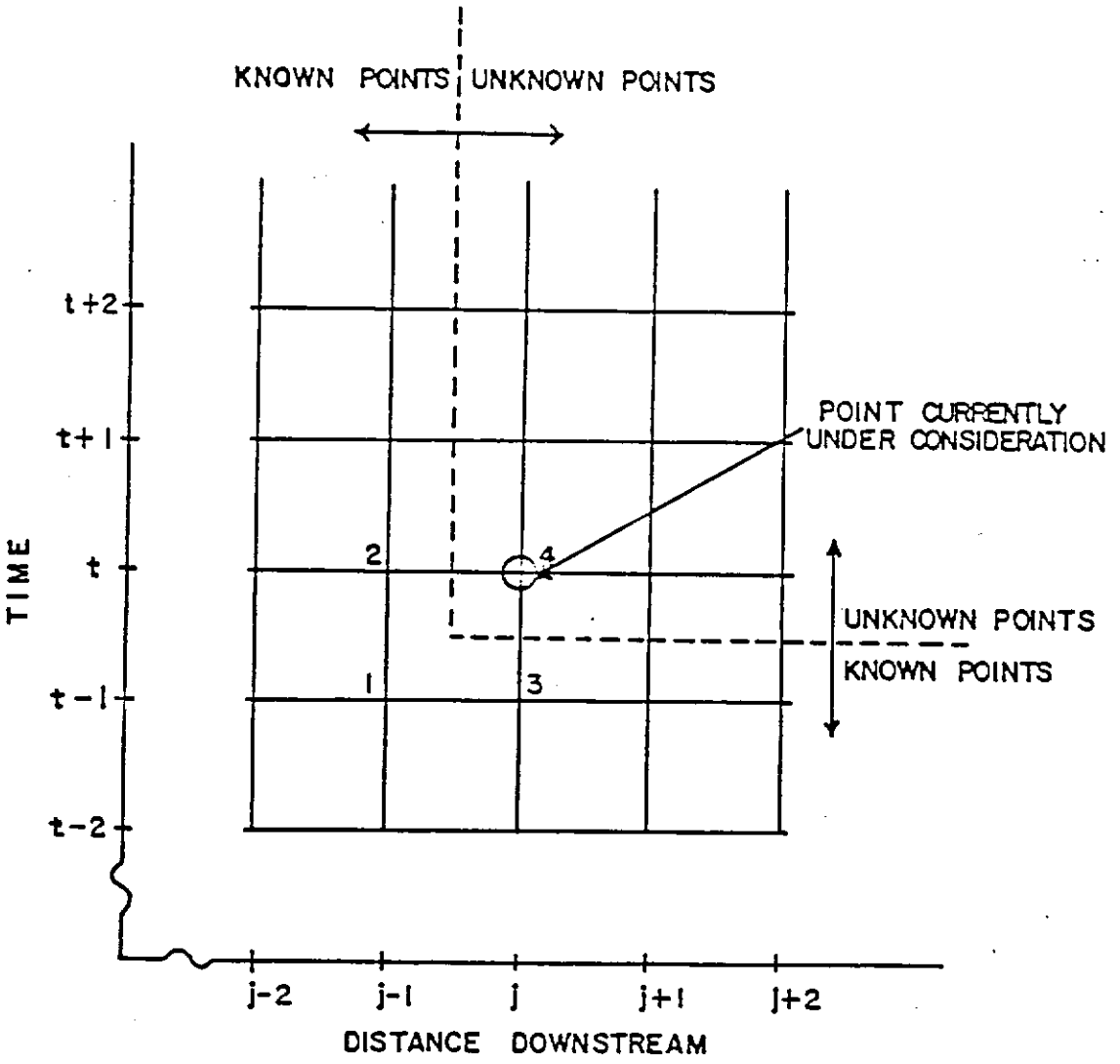

Figure 2.7 Four-Point Kinematic Routing Grid

$$\frac{\partial Q}{\partial x} = \frac{Q_4 - Q_2}{\Delta x} \tag{2.11}$$

where A_1, A_2, A_3, A_4 are flow areas for the grid points in Figure 2.7, Q_1, Q_2, Q_3 and Q_4 are flow rates for the grid points in Figure 2.7, Δt is the time step and Δx is the space step. The continuity equation then becomes,

$$\frac{Q_4 - Q_2}{\Delta x} + \frac{A_4 - A_3 + A_2 - A_1}{2\Delta t} = q \tag{2.12}$$

or

$$\lambda Q_4 + \frac{A_4}{2} = \alpha + \beta \tag{2.13}$$

where,

$$\lambda = \frac{\Delta t}{\Delta x} \tag{2.14}$$

$$\alpha = (A_1 + A_3)/2 \tag{2.15}$$

and

$$\beta = \lambda Q_2 + \Delta t q - \frac{A_2}{2} \tag{2.16}$$

The known quantities α and β are then passed to the RLCSSH subroutine for the calculation of the depth of flow, wetted perimeter and hydraulic radius of the multi-segmented channel cross section using the procedures outlined below. The new flow rate Q_4, and area A_4 are

then calculated, and the routing is continued.

The RLCSSH subroutine is utilized to obtain the new flow depth in response to changing flow conditions and channel geometry. An iterative solution to equations 2.13 and 2.9 is obtained to provide the new flow rate, Q_4 and the new flow area A_4. The corresponding wetted perimeter and hydraulic radius are also calculated and retained. The algorithm is complex due to the segmented channel representation. Briefly, an estimate is made for the maximum flow depth and the corresponding area, wetted perimeter and hydraulic radius are calculated. Equation 2.9 is then solved for Q and both the area A and Q substituted into the left-hand-side of equation 2.13. The result is then compared to the known right-hand-side quantity of equation 2.13, with Q_4 and A_4 accepted if agreement is adequate (within 0.01 percent) or a new depth estimate made by a Newton-Raphson technique if the solution has not been reached. The routing method used can become unstable for backwater conditions. For that reason, abrupt changes in slope must be avoided.

SEDIMENT GENERATION COMPONENT

After the proper flow conditions have been found, the sediment generation phenomena can be considered. The sediment generation component consists of its submain program, SEDGEN, and five subroutines: RADET, RLDET, SHDIST, RLSHAP, and SLUFF. In this component, the process of raindrop detachment, rill flow detachment, rill wall sloughing, and the change of the rill channel cross section

due to detachment are predicted.

In the RADET subroutine sediment detachment due to rainfall impact is calculted by using a soil detachment rate using the final equation of Bubenzer and Jones (1971) with a slope term added as per Quansah (1981), or,

$$SSR = CR^{e_1} E^{e_2} P_{cl}^{e_3} S^{e_4} \qquad (2.17)$$

where SSR is the soil splash in g/cm^2 during Δt, C is an empirical coefficient, e_1, e_2, e_3, and e_4 are exponents, R is rainfall rate in cm/hr, E is the applied rainfall energy during Δt in $joules/cm^2$, P_{cl} is the percent clay of the surface layer, and S is the slope of the soil surface. The splash rate was then obtained by multiplying by the plot increment area and dividing by Δt. This equation was used in KYERMO because it represents the only available relationship utilizing both the rainfall kinetic energy and a soil characteristic to estimate raindrop detachment of soil. These were deemed important due to the use of a rainfall simulator causing energy to not be a function of rainfall intensity and due to the disturbed nature of the plots to be studied. Coefficient and exponent values are input by the user, with Bubenzer and Jones' values being reasonable estimates if actual values are not known.

The energy for each raindrop size class is reduced or enhanced due to the depth of ponding. The modified energy for each class is then summed to get the E-value. Palmer (1965) examined the effect of surface water on soil detachment due to various sizes of raindrops. He

found that detachment rose to a maximum at a depth of about one drop diameter and was almost zero at a depth of three drop diameters. Other researchers, such as Mutchler and Larson (1971) found that the maximum splash occurred at a depth of about 1/6 drop diameter, but agreed with the 3 diameter level for zero splash. The 1/6 value is used in KYERMO. In RADET the user is allowed to specify a maximum coefficient (such as 1.5) and the coefficient at three drop diameters (such as 0.1) and then by fitting a function to the shape of Mutchler's data through those points. Splash is set equal to zero above 3 diameters to guard against numeric instabilities. The 28 raindrop size classes specified in RAINFA are considered separately, with their individual energies weighted by their volume fraction of the rainfall. The weighted individual coefficients are then summed and the resultant "average" energy is used to calculate soil splash for the water depth in question. The energy value, and hence, the soil splash, are determined separately for ponded areas and those covered only by overland flow. A final raindrop detachment rate is obtained by weighting the ponded and overland flow area detachments by their fraction of the surface area. The particles on the soil surface are assumed to be detached according to the fraction specified in INITIA.

The RLDET subroutine and the other called subroutines from RLDET are used to calculate shear distributions, matrix and deposited material detachment and rill wall sloughing. The basis of the rill shear detachment calculation in KYERMO is the excess shear equation of Foster (1982),

$$D_{rc} = a(\tau - \tau_c)^b \qquad (2.18)$$

where D_{rc} is the rill flow detachment capacity in $g/s\text{-}m^2$, τ is the bed shear stress in N/m^2, τ_c is the critical bed shear for particle detachment in N/m^2, and a and b are empirical constants. The constant b is dimensionless and the constant a has the dimension $(g/s\text{-}m^2/(m^2/N)^b$, or $(g\text{-}m^{2(b-1)})/s\text{-}N^b$.

The detachment rate is not always equal to the detachment capacity due to the presence of sediment in the flow. Foster and Meyer (1972a) proposed a balance equation,

$$\frac{D_r}{D_{rc}} + \frac{G_f}{T_c} = 1 \qquad (2.19)$$

where D_r is the actual detachment rate, G_f is the flow sediment load and T_c is the flow sediment transport capacity. All have the same units as D_{rc}. Combining equation 2.18 and 2.19 and solving for D_r, one obtains

$$D_r = (1 - \frac{G_f}{T_c}) \, a \, (\tau - \tau_c)^b \qquad (2.20)$$

with units as given above. Matrix and deposited material have different τ_c values (τ_{cm} and τ_{cd}, respectively), creating a need to treat them separately. If the deposited material covers a fraction of the bed equal to f_{cd}, the detachment rate equations become

$$D_{rm} = (1 - \frac{G_f}{T_c}) \, a(\tau - \tau_{cm})^b (1 - f_{cd}) \qquad (2.21)$$

and

$$D_{rd} = (1 - \frac{G_f}{T_c})\, a(\tau - \tau_{cd})^b f_{cd} \qquad (2.22)$$

where the subscripts m and d indicate matrix and deposited material, respectively.

The rill channel representation utilized in KYERMO consists of a segmented channel with a user-specified number of subsegments on each segment. The detachment on each subsegment is calculated to obtain an accurate average detachment on each segment, and hence for the entire rill channel at the point under consideration. If the rill in question has i segments each with a slope length of l_i (cm) and n_i subsegments, and that rill is representative of a rill reach of length l_s (m), then the detachment rate (g/sec) from each subsegment is given by

$$D_{rm_{ij}} = (1 - \frac{G_f}{T_c}) a(\tau_{ij} - \tau_{cm})^b (1 - f_{cdij}) l_s l_i / n_i / 100 \qquad (2.23)$$

and

$$D_{rd_{ij}} = (1 - \frac{G_f}{T_c}) a(\tau_{ij} - \tau_{cdij})^b f_{cdij} l_s l_i / n_i / 100 \qquad (2.24)$$

where the subscripts i and j denote segment and subsegment, respectively. These detachment rates can then be multiplied by the time step and sediment type fractions to obtain the mass of each

sediment type detached and available for transport during the time step in the rill reach in question.

Each of the parameters in equations 2.23 and 2.24 must be known. The parameters a, b, l_s, and n_i are input by the user. The values of l_i, G_f, and T_c are calculated in other parts of the model. The sediment load, G_f, is the sum of the sheet flow sediment delivery and the sediment load from upslope. The value of T_c is calculated during the previous time step for the flow situation of the rill in question. The value of l_i is calculated during the flow routing procedure. This leaves the values of τ_{ij}, τ_{cm}, τ_{cdij} and f_{cdij} to be calculated.

The shear stress, τ_{ij} is calculated using the area method of Lundgren and Johnson (1964). The volume of water applying a shear to each subsegment is calculated, and the tangential component of the weight of that water is assumed to be the bed shear on that segment. The appropriate volumes are calculated as shown in Figure 2.8. The first step is to calculate the bisector of each angle formed by the rill channel segments. Lines perpendicular to the segments of each subsegment edge are then calculated. The area enclosed by each pair of lines, the bed and the water surface is assumed to be the volume of water, per unit length, supported by the subsegment area, per unit length, in question. The applied shear is then given by

$$\tau_{ij} = \frac{\gamma \, \Delta A_{ij} \, n_i \, \sin\theta}{100 \, l_i} \qquad (2.25)$$

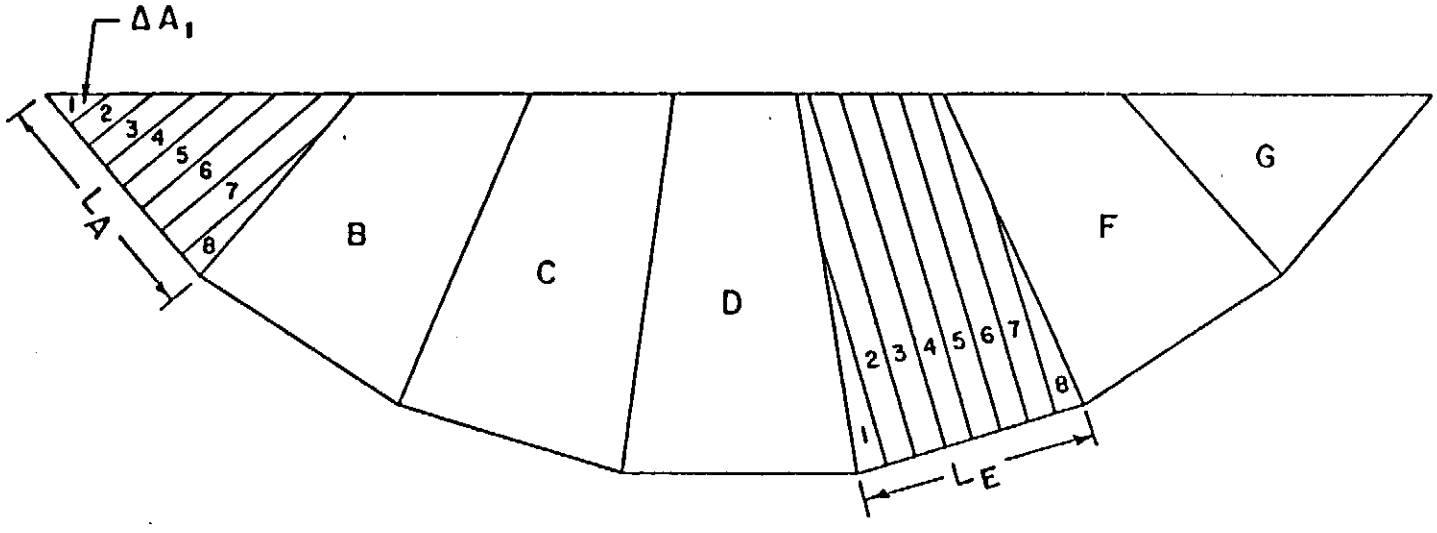

$$\bar{\tau}_{A1} = \frac{\gamma \sin\theta}{L_A} 8\,\Delta A_{A1} \qquad \bar{\tau}_{E3} = \frac{\gamma \sin\theta}{L_E} 8\,\Delta A_{E3}$$

$$\bar{\tau}_A = \frac{1}{8} \sum_{i=1}^{8} \bar{\tau}_{A1}$$

Figure 2.8 Calculation of Effective Areas for Bed Shear Stress

where γ is the unit weight of water in N/m^3, ΔA_{ij} is the area of water applying a shear to subsegment j of segment i in cm^2, n_i is the number of subsegments on segment i, l_i is the slope length of segment i, and τ_{ij} is the applied shear stress on subsegment j of segment i in N/m^2

The next parameters to be determined are τ_{cm} and τ_{cdij}. These parameters represent the τ_{ij} level at which detachment begins for matrix and deposited material, respectively. Currently, the matrix material value, τ_{cm}, is fixed by the user. The value for deposited material is set from the Shield's diagram based upon weighted average characteristics of the deposited material in the rill. The distribution of the deposited material is determined from the difference between the sum of the incoming sediment load and the total rill detachment of each sediment type and the transport capacity for that sediment type.

The remaining parameter to be discussed is f_{cdij}. This parameter is the fraction of each subsegment covered by deposited material. To obtain these fractions, it is assumed that all of the deposited material settles to the lowest part of the rill and that the material had a level surface and a density given by

$$\rho_d = S_{50d}(0.755 + 0.01273d_{50d}^{0.21}) \qquad (2.26)$$

where ρ_d is the deposited material density in g/cc, S_{50d} is the weighted average specific gravity of the deposited material and d_{50d} is the weighted average diameter of the deposited material in mm.

Equation 2.26 is a modification of an equation presented by Vanoni (1975), and is intended to give the "right direction" for the relationship between particle size and density distribution and the deposited material density. The original equation was

$$W = 125 - 7\, d_{50}^{0.21} \qquad (2.27)$$

where W is specific weight in lb/cu ft. and d_{50} is in ft. The particle specific gravity was assumed to be 2.65. Equation 2.26 was derived through unit conversion and through multiplication by the ratio of the average particle specific gravity and 2.65. The relationship is untested.

The example in Figure 2.9 illustrates the general method used to calculate f_{cdij}. The only f_{cd} values not equal to zero or one are those for segment 2, subsegment 3 and segment 4, subsegment 3. Both of these are covered to one-half of their length giving a f_{cdij} value of 0.5. As stated above, this would occur for the general case. However, if the particle diameters and mass of material is such that the bed is covered by less than one particle diameter, the areas covered by the individual particles (assumed spherical) are calculated, and their total area on each subsegment is divided by the subsegment area to determine f_{cd}.

The necessary critical tractive force values are determined through use of the Shields diagram for deposited material and a relationship proposed by Smerdon and Beasley (1961) for matrix material. Their proposed relationship (after unit conversion) is,

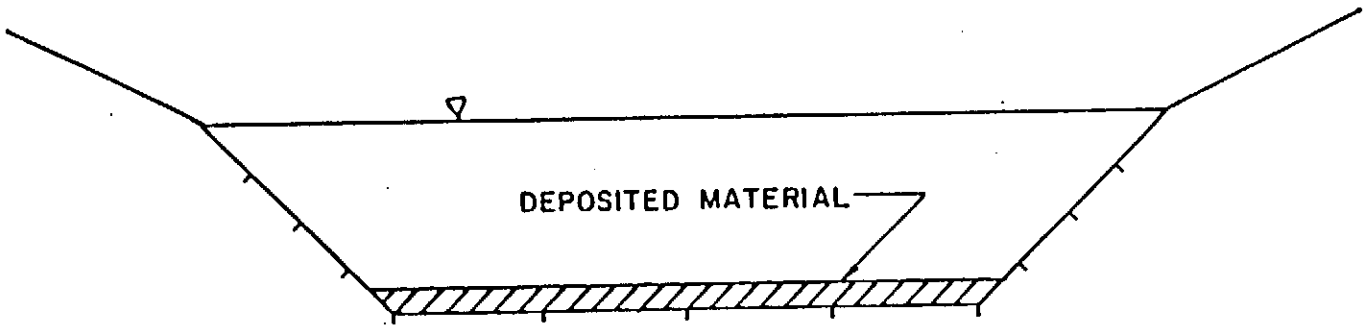

Figure 2.9 Calculation of Fraction-Covered-by-Deposition for Each Segment

$$\tau_{cr} = (0.493)\ 10^{(0.0183\ P_{cl})} \qquad (2.28)$$

where τ_{cr} is the critical tractive force in N/m^2 and P_{cl} is the soil percent clay. This relationship had the lowest standard error of those examined by Smerdon and Beasley and utilized a readily determined soil parameter. A critical shear stress of 0.5 N/m^2 (τ_{cr} for zero percent clay) was used initially for deposited material. After computations begin and the size distribution of deposited material is known, the critical shear stress is calculated from the Shields equation in the subroutine CRITSH.

Once the detachment on each subsegment of the rill cross-section is determined, the shape change due to that detachment is calculated. It is assumed that the water's edge nodal points remain as they are and each point under water is determined based upon the detachment on the segments on either side of the point in question. A removal vector is calculated as the weighted average removal depth on each adjacent segment. The weighting factor is the segment slope length. The removal vector is equal to the displacement of the nodal point. The direction of displacement is determined as the weighted average of the angles of the lines perpendicular to each adjacent segment. The weighting factor is the area of removal on each segment (equal to the average removal depth on each segment multiplied by the segment slope length). This procedure is illustrated in Figure 2.10.

The final step in the calculation of detachment is to determine the

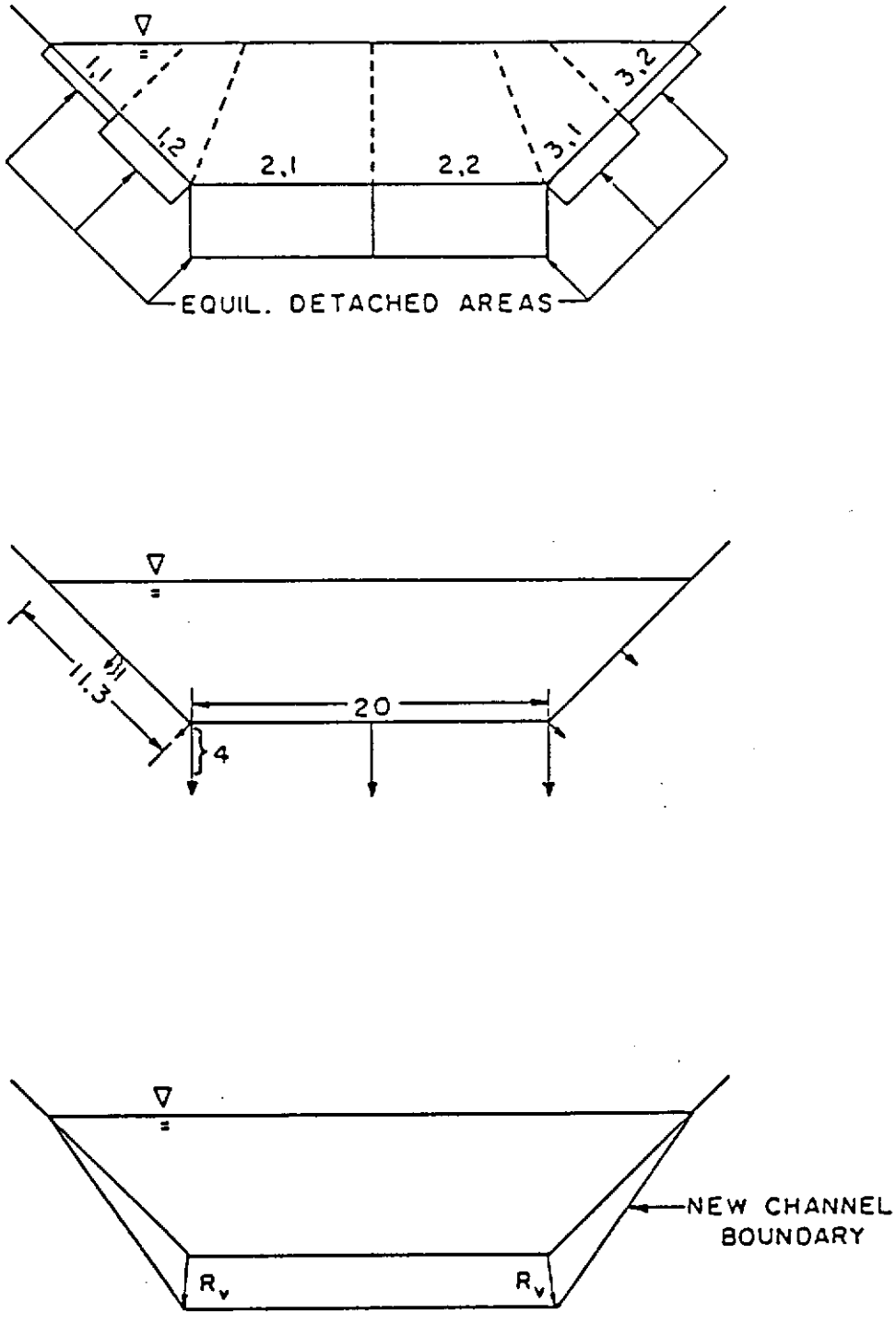

Figure 2.10 New Channel Boundary Calculation Algorithm

detached mass due to rill wall sloughing. Two slopes are input by the user, a critical slope, above which the rill walls are not stable, and an equilibrium slope, which is the slope that occurs immediately after sloughing. This is the same method proposed by Mossaad and Wu (1984). An example of this concept is shown in Figure 2.11. The area of sloughing is calculated using the lines shown in Figure 2.11, and the soil bulk density in them utilized to obtain the total sloughed mass. The total detached mass is now known and is available for transport downslope. The nodal points are then recalculated to reflect the removal of soil due to sloughing.

In summary, the SEDGEN sub-main program and its called subroutines RADET, RLDET, SHDIST, RLSHAP and SLUFF, are used to calculate the sediment detached and available for transport downslope. This value is then used in the sediment routing component described below in which sediment transportation and deposition are calculated.

SEDIMENT ROUTING COMPONENT

The sediment routing component consists of its sub-main program, SEDROT and five subroutines: SHEET, RILLTR, DEPDIS, SEDTRA, and YANGSE. In this component, the transport and deposition of sediment is calculated for both in the sheet and rill flow mechanisms. Two sediment transport equations are provided as options for each.

In the SHEET subroutine sheet flow transport of material detached by rainfall is calculated. Sheet flow rate, wetted perimeter, and depth of flow are calculated based on the runoff rate and a sediment

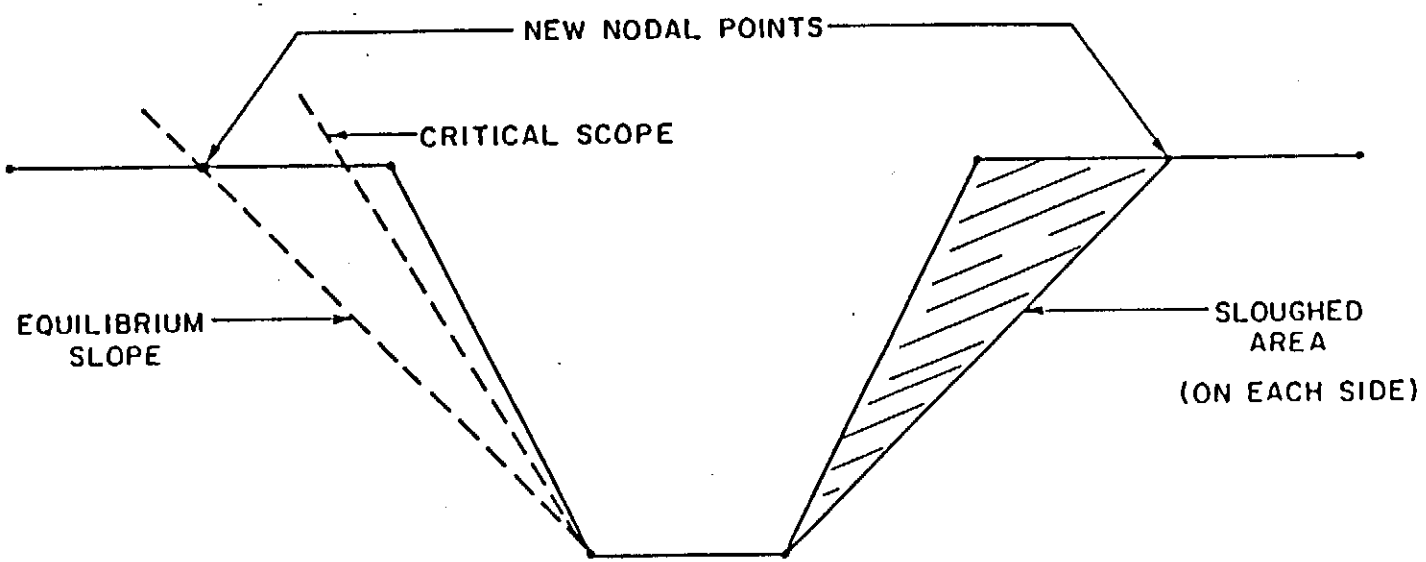

Figure 2.11 Rill Wall Sloughing Conceptualization

transport routine (to be discussed subsequently) is called to calculate the transport. All sediment not transported is considered to be deposited and must be re-detached. The slope for the sheet flow is calculated based upon the plot slope, the rill-watershed-width, and the sideslope of the rill watershed, all of which are user inputs. For this purpose, the rill watershed is assumed to be triangular in cross-section and the flow direction is assumed to be perpendicular to the rill watershed contour lines. This results in a steeper slope for the sheet flow then the plot slope and a wider flow than if the sheet flow were parallel to the rill. It is further assumed that the rill is in the center of its watershed so that the runoff is input equally to each side of the rill.

In the RILLTR subroutine, the same calculations are made for rill flow as are made in SHEET does for sheet flow, except that there are more sources for the sediment load. The sediment load quantities summed to obtain the total load in RILLTR were boundary shear detachment, sediment delivery from upslope, sediment delivery by sheet flow, and detachment due to sloughing of rill walls. Sediment transport capacity is then calculated by one of the transport equations and deposition is calculated as the sediment load of each particle type minus the trasnport capacity for that type.

In the DEPDIS subroutine the size and area distribution of deposited material is calculated for on each of the submerged segments. An iterative routine similar to that of RLCSSH is utilized to calculate the depth of deposited material by assuming that the material moves to the lowest point and has a level surface. The area

of coverage is calculated by assuming that the mass of material is spread over the segment in question. If the layer of particles is less than one particle diameter, the area of coverage is limited to the actual area covered by individual particles to guard against a large particle being "spread out" to cover a segment at a depth less than its diameter. Spherical particles are assumed. The size distribution is calculated as the weight fraction of each particle type deposited to the total deposited mass.

The sheet flow and rill flow sediment transport capacity is calculated using one of two sediment transport relationships. Each of these will be described in the subsequent sections.

The SEDTRA subroutine is the first sediment transport option to be described in which the sediment transport capacity of either sheet or rill flow is calculated using a modified Yalin (1963) equation which is essentially a shear excess relationship. The modification is that of Foster and Meyer (1972b) and involves distributing the transport capability among various particle sizes.

The unmodified Yalin equation was presented by Yalin (1972) as:

$$\frac{q_s \rho^{1/2}}{(\gamma_s D)^{3/2}} = 0.635 \frac{s}{\omega} \left[1 - \frac{1}{as} \ln(1+as)\right] \qquad (2.29)$$

where q_s was the sediment load in lb/ft-s. ρ was the fluid density in slugs/ft^3, γ_s was the sediment specific weight in water in lb/ft^3, D was a typical grain size in ft, ω was a reciprocal mobility number given by:

$$\omega = \frac{\gamma_s D}{\rho V_*^2} \tag{2.30}$$

where V_* was the shear velocity in fps. The other two parameters, a and s, were given by

$$a = 2.45 \frac{Y_{cr}}{W^{0.4}} \tag{2.31}$$

and

$$s = \frac{1}{\omega Y_{cr}} - 1 \tag{2.32}$$

where Y_{cr} is from the Shields curve and is a function of the shear Reynolds' number and W is the solid/fluid density ratio (ρ_s/ρ). The Foster and Meyer (1972b) modification was necessary to consider varying sediment sizes and densities. Foster et al. (1980,1981) used this approach in the CREAMS model. The sediment transport was calculated using the following steps:

1) The excess tractive force of each size of particle was calculated assuming only that size was present (denoted δ_i).
2) The non-dimensional transport for each sediment size was calculated assuming only that size was present (denoted P_i).
3) The total excess tractive force for the mixture was calculated by summing the individual excesses, e.g.

$$T = \sum_{i=1}^{n_s} \delta_i \qquad (2.33)$$

where n_s was the number of different sediments.

4) The individual non-dimensional transport of each size in the mixture was calculated by multiplying P_i by δ_i/T (denoted $(P_e)_i$).

5) The individual transport capacity for each size in the mixture was calculated from

$$W_{si} = (P_e)_i (S_g)_i P_w g d_i V_* \qquad (2.34)$$

where W_{si} was the transport capacity, P_e was the individual non-dimensional transport, S_g is the specific gravity of the particle, and P_w is the fluid density.

6) The transport capacity was distributed according to the sediment load, q_{si}, for each size, and the required non-dimensional transport, $P_{i_{reg}}$, was calculated by,

$$T = \frac{q_{si}}{(S_g)_i g \rho_w d_i V_*} \qquad (2.35)$$

7) The fraction of transport capacity used by those particles with $W_{si} > q_{si}$ was calculated by,

$$SPT = \sum_{i=1}^{n_s} (P_{i_{reg}} / P_i)K_i \qquad (2.36)$$

where $K_i = 1$ for $W_{si} \geq q_{si}$, and $K_i = 0$ for $W_{si} < q_{si}$.

8) The excess transport to be distributed was then

$$E_{xc} = 1 - SPT \qquad (2.37)$$

9) The total excess tractive force for those particles for which $W_{si} < q_{si}$ was determined by

$$SDLT = \sum_{i=1}^{n_s} \delta_i L_i \qquad (2.38)$$

where $L_i=0$ for $W_{si} \geq q_{si}$ and $L_i=1$ for $W_{si} < q_{si}$.

10) The excess tractive force was distributed according to δ_i fractions and q_{si} according to

$$T_{ci} = \left(\frac{\delta_i}{SDLT}\right)(E_{xc})(P_i)(S_g)_i q \rho_w d_i V_* L_i \qquad (2.39)$$

and

$$T_{ci} = q_{si} K_i \qquad (2.40)$$

where L_i and K_i were defined previously.

11) Steps 6-10 were repeated until either all $T_{ci} \leq q_{si}$ or all $T_{ci} \leq q_{si}$. If all $T_{ci} \leq q_{si}$ then proper T_{si}s had been found. If all $T_{ci} \geq q_{si}$ then all of the excess was given to one particle size, and redistribution was calculated by

$$SMUS = \sum_{i=1}^{n_s} \left(\frac{P_{i\,reg}}{P_i}\right) \tag{2.41}$$

and

$$T_{ci} = q_{si}/SMUS \tag{2.42}$$

The Yalin equation in its original form and in its modified form utilized the Shields' diagram to relate the critical shear Reynolds' number to the critical dimensionless lift force. Because Shields' curve was developed for coarse, cohesionless granular solids, modifications were necessary. Mantz (1977) extended the Shield's diagram to include fine grains and flakes. The grains tested ranged in diameter from 15 to 66 μ. Mantz plotted his own data together with data from the literature as a Shields-type diagram. The regression line of the low Reynolds' number data is greatly different in slope from the Shields' curve, crossing at a Reynolds' number of about 1.2. The extended Shields' diagram presented by Mantz has a confidence limit that would allow a multitude of curve shapes including two straight lines intersecting at a boundary Reynolds' number of about 8. The modified Shields curve used in KYERMO and its four segment

representation are shown in Figure 2.12.

The YANGSE subroutine is the second sediment transport options in which the sediment transport is calculated using a modification of the Yang (1973) equation. The modification used in KYERMO involves distributing the sediment transport among particle types by first calculating a transport for an "average" particle type and then distributing that transport among the types according to their relative transport capacities.

The Yang (1973) sediment transport equation was developed to calculate the transportable concentrations of a representative particle type in flowing water. It has been shown (by Alonso, 1980 and others) to be an adequate solution method for the sediment transport capacity of concentrated flow. However, for upland erosion modeling, the transport capacity for each sediment type in a mixture must be known to obtain an accurate size distribution of the delivered material. For that reason, a modification of the Yang (1973) equation was undertaken similar to the Yalin (1963) equation modification of Foster and Meyer (1972b). Ten sediment types were used.

The original Yang (1973) equation was

$$\log_{10} C_t = 5.435 - 0.286\log_{10}\left(\frac{\omega d}{\nu}\right) - 0.457\log_{10}\left(\frac{V_*}{\omega}\right)$$

$$+ \left(1.799 - 0.409\log_{10}\left(\frac{\omega d}{\nu}\right) - 0.314\log_{10}\left(\frac{V_*}{\omega}\right)\right)\log_{10}\left(\frac{VS - V_{cr}S}{\omega}\right) \qquad (2.43)$$

where C_t is the sediment concentration in ppm, ω is the particle fall velocity, d is the particle diameter, ν is the kinematic viscosity, V_* is the shear velocity, V is the flow velocity, S is the channel

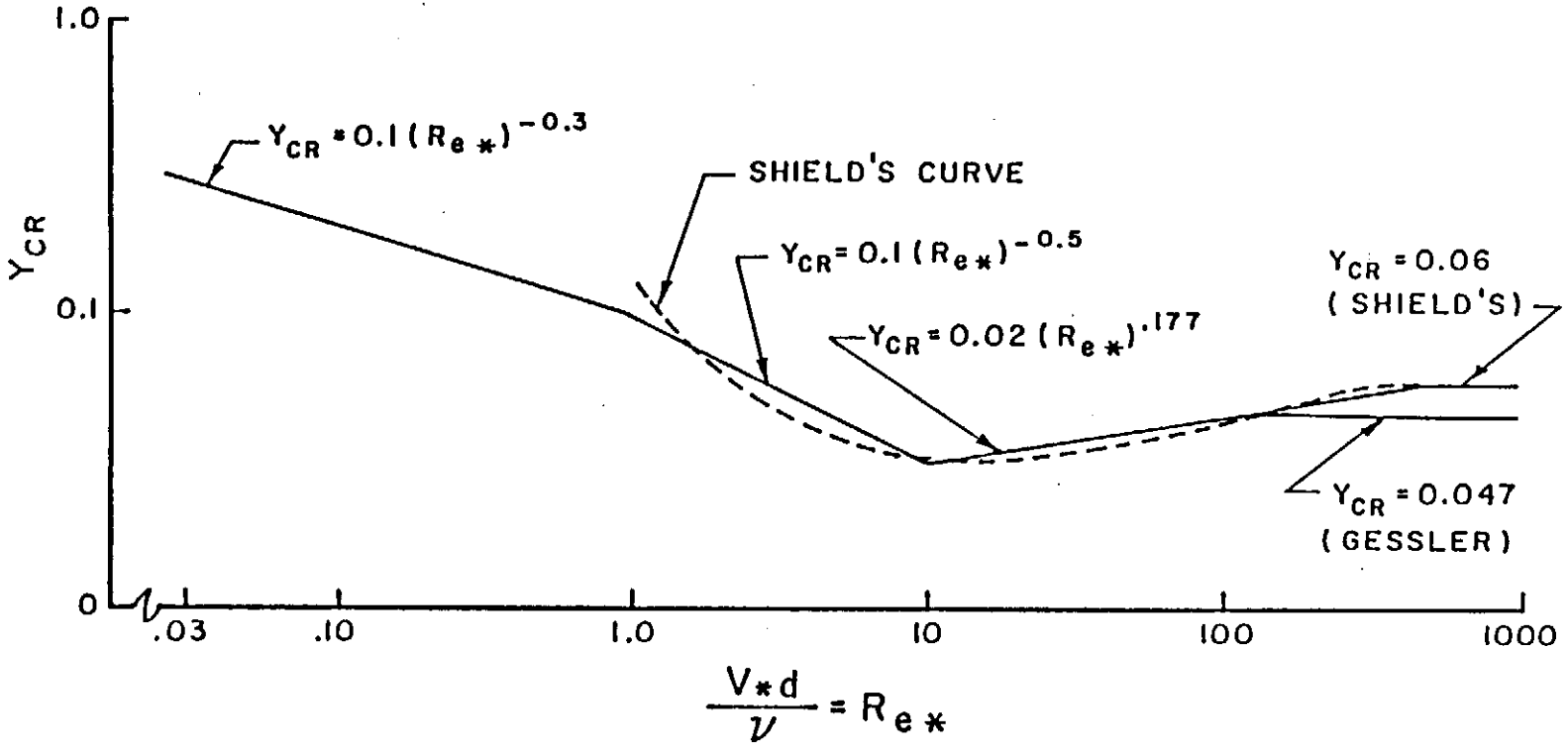

Figure 2.12 Shields Curve Representation used in KYERMO

slope, and V_{cr} is a critical velocity for incipient motion. Units need to be chosen to retain the dimensionlessness of the ratios within the equation. For the remainder of this discussion, equation 2.43 will be

represented by

$$\log_{10} C_t = LHS \tag{2.44}$$

to eliminate unnecessary detail. For this modification scheme, it is assumed that Equation 2.43 provides the proper total concentration for an average particle type,

$$\log_{10} C_{t50} = LHS_{50} \tag{2.45}$$

or

$$C_{t50} = 10^{LHS_{50}} \tag{2.46}$$

The average particle type in determined from the weighted average diameter and weighted average specific gravity of the detached and/or delivered sediment load. The weighting factor for each weighted average is the sediment load of each sediment type. To eliminate bias due to non-transportable particles, an additional "bias factor" equal to zero or one is utilized. The zero values occur whenever the C_t for an individual particle type alone in the flow is equal to zero. The average particle type properties are then given by,

$$d_{50} = \frac{1}{Q_{stot}} \sum_{i=1}^{10} d_i \, Q_{si} \, C_i \qquad (2.47)$$

$$S_{50} = \frac{1}{Q_{stot}} \sum_{i=1}^{10} S_i \, Q_{si} \, C_i \qquad (2.48)$$

where

$$Q_{stot} = \sum_{i=1}^{10} Q_{si} \, C_i \qquad (2.49)$$

d_i, S_i, Q_{si}, and C_i are the particle type diameter, specific gravity, load, and bias factor, respectively. The overall transportable concentration, C_{t50}, can then be calculated using equation 2.46.

The potential concentrations of individual particle types are then estimated by assuming that the fraction of the transportable concentration filled by an individual particle type is the same as its fraction of the sum of the transport capacities of each type if alone in the flow. To clarify, assume that the particle type j is alone in the flow, then

$$C_{tj} = 10^{LHS_j} \qquad (2.50)$$

for each type. Its fraction, f_{tj}, would then be given by

$$f_{tj} = \frac{C_{tj}}{\frac{10}{\sum_{i=1} C_{ti}}} \qquad (2.51)$$

which means that the actual concentration of particle type j would be

$$C(j) = f_{tj}\, C_{t50} \qquad (2.52)$$

The sediment transport capacity for each particle is then compared to the available load. Excess transport capacity is then distributed to each particle type having excess sediment load according to its fraction of the total excess load. A new average particle type is then calculated and the process repeated until the transported concentration changes by less than one percent between calculations. The transported load of each sediment type is then accepted as correct.

Each of the basic sediment transport equations in this model have been shown to be usable for shallow flow applications. The Yang modification has not been tested, but is similar to the Yalin modification of Foster and Meyer (1972b). The user should evaluate the situation and choose which equation is more appropriate. Alonso (1980), Alonso et al. (1981), and Neibling and Foster (1980) presented data supporting the use of either of these equations in small-scale sediment transport situations. The Yalin equation was preferred by them for light materials, such as aggregates.

SUMMARY

An erosion model considering the physical processes occuring during erosion has been developed and described. A summary of the relationships used in KYERMO appears in Figure 2.13. The next step is to evaluate that model using observed data. The field experiments conducted to collect that data will be described next.

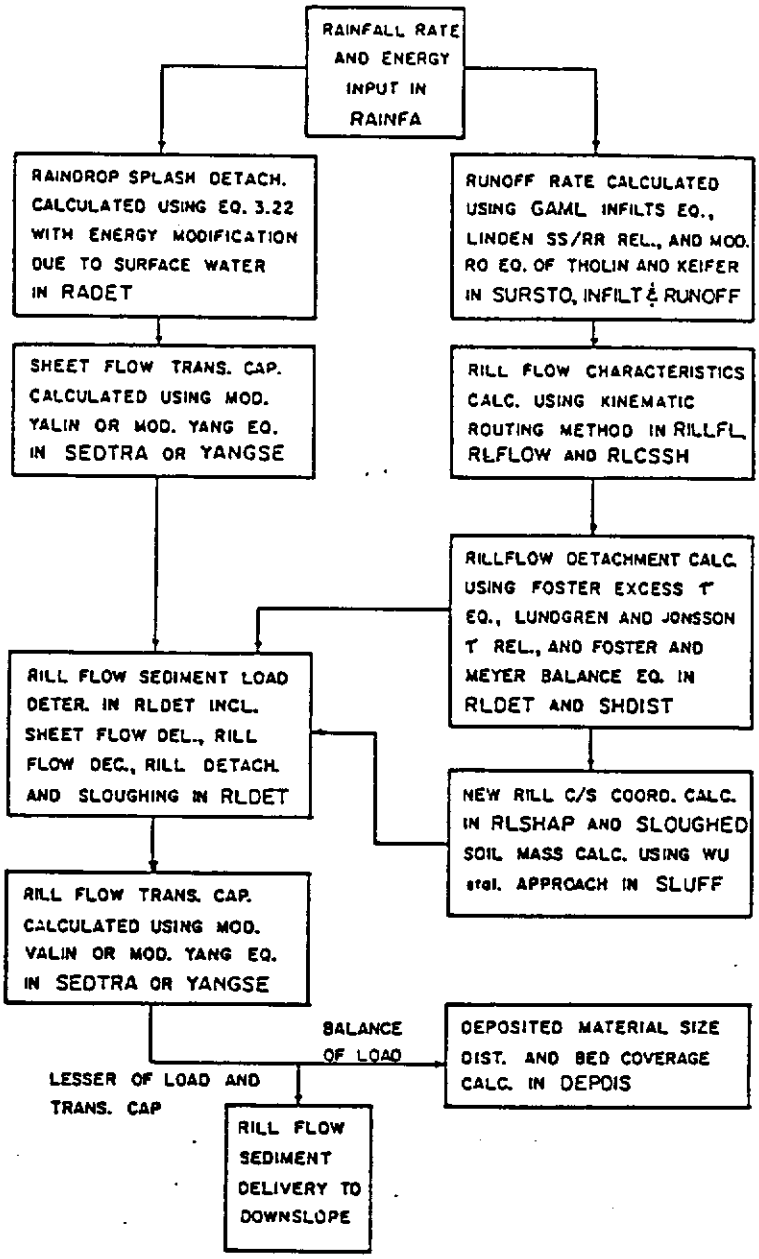

Figure 2.13 KYERMO Calculation Flow Summary

CHAPTER 3 SENSITIVITY ANALYSIS

A brief sensitivity analysis of the erosion model developed in this study was undertaken to determine the important considerations in parameter selection and to evaluate trends predicted by the model. In this analysis, simulation parameters were evaluated for their singular effects upon the simulated sediment yield. The parameters or representations considered were: 1) the number of slope increments, 2) the number of rills (utilizing a fixed rill shape), 3) the initial rill shape, 4) the segmented representation of a known rill shape, 5) the rill detachment equation parameters, 6) Manning's 'n', and 7) the time step. The combined effect of slope and the number of rills was also examined.

SENSITIVITY TRIALS

Numerous sensitivity trials were performed to determine the effects or various parameters upon sediment yield. In the basic simulations a 2 minute time step was utilized, with a total simulation length of 72 minutes, with the plot and rainfall characteristics equivalent to those used in field rainfall simulation run 121. This run was chosen because the initial surface was well defined and the two-rill treatment used for run 121 allowed long computer simulations with relatively little expense. Six slope increments were used. A summary of these base conditions is presented in Table 3.1. The detachment parameters will be discussed first, with rill cross-section representations and plot

Table 3.1 Summary of Base Conditions for KYERMO Sensitivity Analysis

Parameter	Base Value	Units
# of rills (NR)	2	-
# of slope increments (NJ)	6	-
Detachment coefficient (ARDET)	2.5	$\frac{kg - m^{0.1}}{s - N^{1.05}}$
Detachment exponent (BRDET)	1.05	-
Critical shear stress (CSH)	1.98	N / m^2
Manning's 'n' (n)	0.030	-
Time step (Δt)	2	min
Plot Slope (slope)	0.030	m/m

characteristics to follow.

The sensitivity analysis to be presented was conducted almost exclusively for a steep slope condition. The exception to this was the analysis to examine the interaction between the number of rills on a plot, its slope, and the corresponding sediment yield. The steep slope condition dictated, at least for the soil used in this study, that the flow detachment capacity, rather than the flow sediment transport capacity, was the limiting quantity for sediment delivery. The slope-rill number interaction analysis possibly indicates, as will be presented later, that the transport capacity becomes limiting for at least some of the particle types as the slope decreases below about ten percent. After consideration of the objectives of this study, additional sensitivity analyses with limited transport capacity were not performed. However, such analyses are recommended before the model is utilized extensively for situations in which the sediment transport capacity is the limiting factor for sediment delivery.

DETACHMENT PARAMETERS

Five levels of each detachment equation parameter were examined, holding the other parameters constant, for their effect upon the simulated sediment yield. The parameter values as initially used during the model simulations to be described in Chapter 4 were utilized as the "third" or median level. The levels of each are shown in Table 3.2.

The effect of changes in the detachment equation coefficient are

Table 3.2 Detachment Parameter Levels Used for Sensitivity Analysis

Parameter	Units	Level 1	2	3	4	5
ARDET	$\frac{g - m^{0.1}}{s - N^{1.05}}$	.625	1.25	2.5	5.0	10.0
BRDET	-	0.90	1.00	1.05	1.10	1.20
CSH	$\frac{N}{m^2}$	0.50	1	2	4	8

shown in Figure 3.1. It is quite evident that the estimation of this parameter is crucial to accurate erosion simulation. The relationship is very linear, with a unit change in ARDET causing a 4.4 T/ac change in sediment yield for the conditions of run 121. The coefficient of determination (r^2) for the straight line representation of the five data points is equal to 1.000. The sediment yield intercept is 0.5 T/ac, possibly indicating the small contribution of raindrop splash detachment and/or roundoff errors involved in the simulations. The effect of the coefficient levels on the run sediment graph are shown in Figure 3.2.

The effect of the detachment equation exponent is small compared to the coefficient, mainly because the range of reported values is narrow. The effect is shown in Figure 3.3. A change from 1.05 to 1.0 for the exponent value would cause a 1.08 T/ac change in sediment yield for the situation of run 121. This change may be acceptable to obtain the computational benefits of a linear relationship for the detachment equation.

The third detachment parameter is critical tractive force. The effect of this parameter is very important, especially if coarse material is to be considered as will be proposed in Chapter 4. The relationship between critical tractive force and sediment yield is shown in Figure 3.4, and appears to be quite linear for low critical tractive force values. The sediment graph effects due to the levels on τ_c utilized are shown in Figure 3.5. One could conclude from this analysis that the critical tractive force is just as important to the sediment yield as the detachment coefficient.

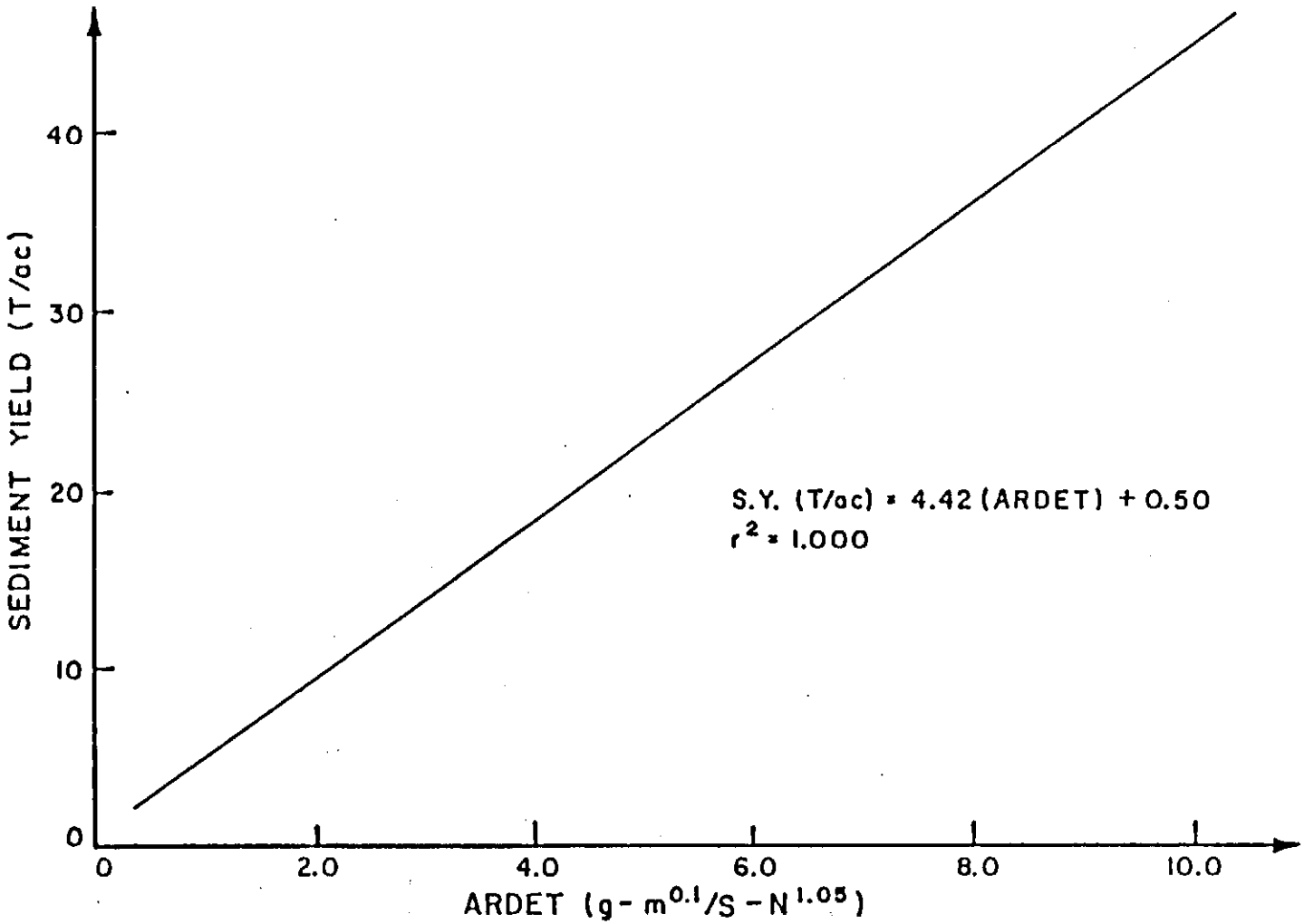

Figure 3.1 Effect of Detachment Equation Coefficient on KYERMO Predicted Sediment Yield (Run 121 data)

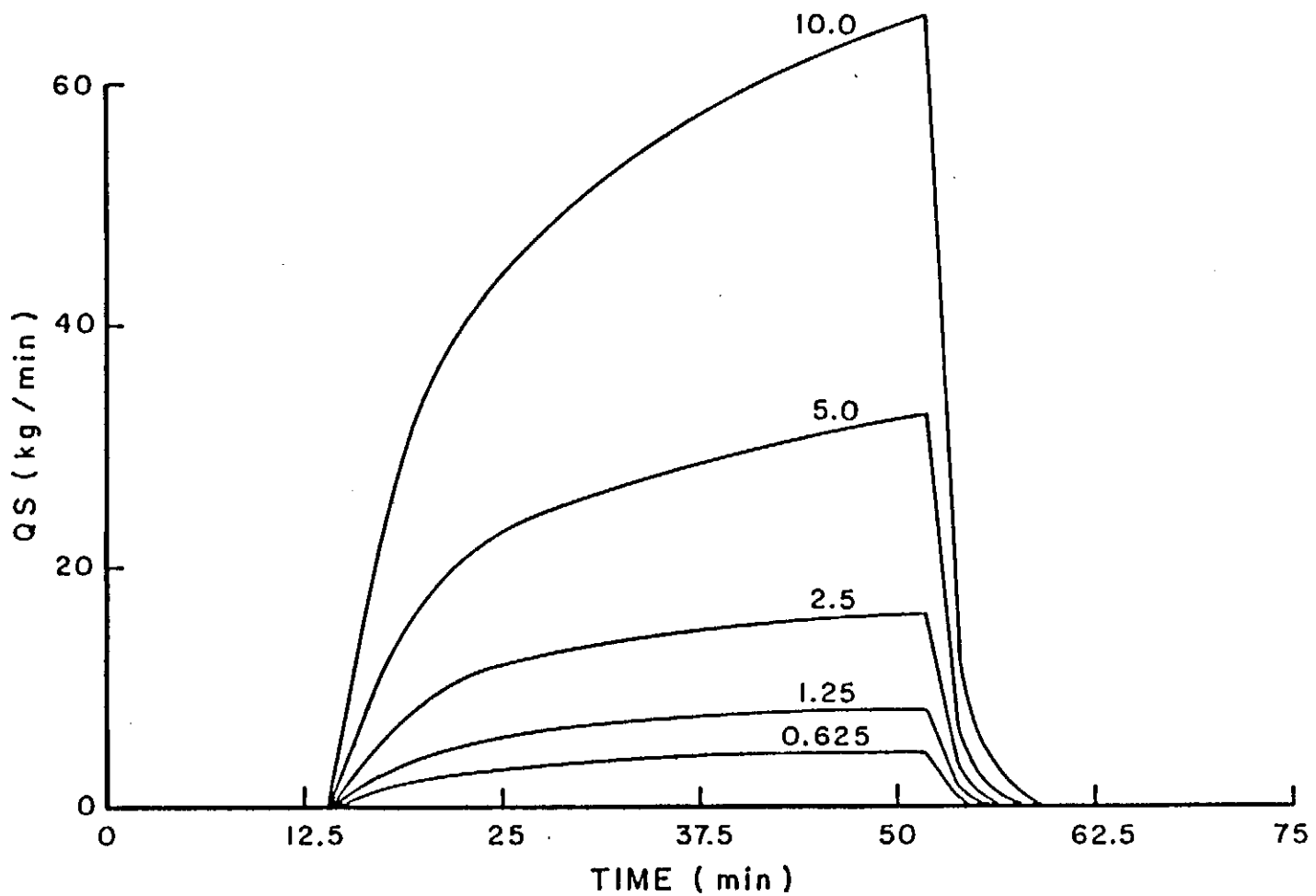

Figure 3.2 Effect of Detachment Equation Coefficient on KYERMO Predicted Sedimentgraph (Run 121 data)

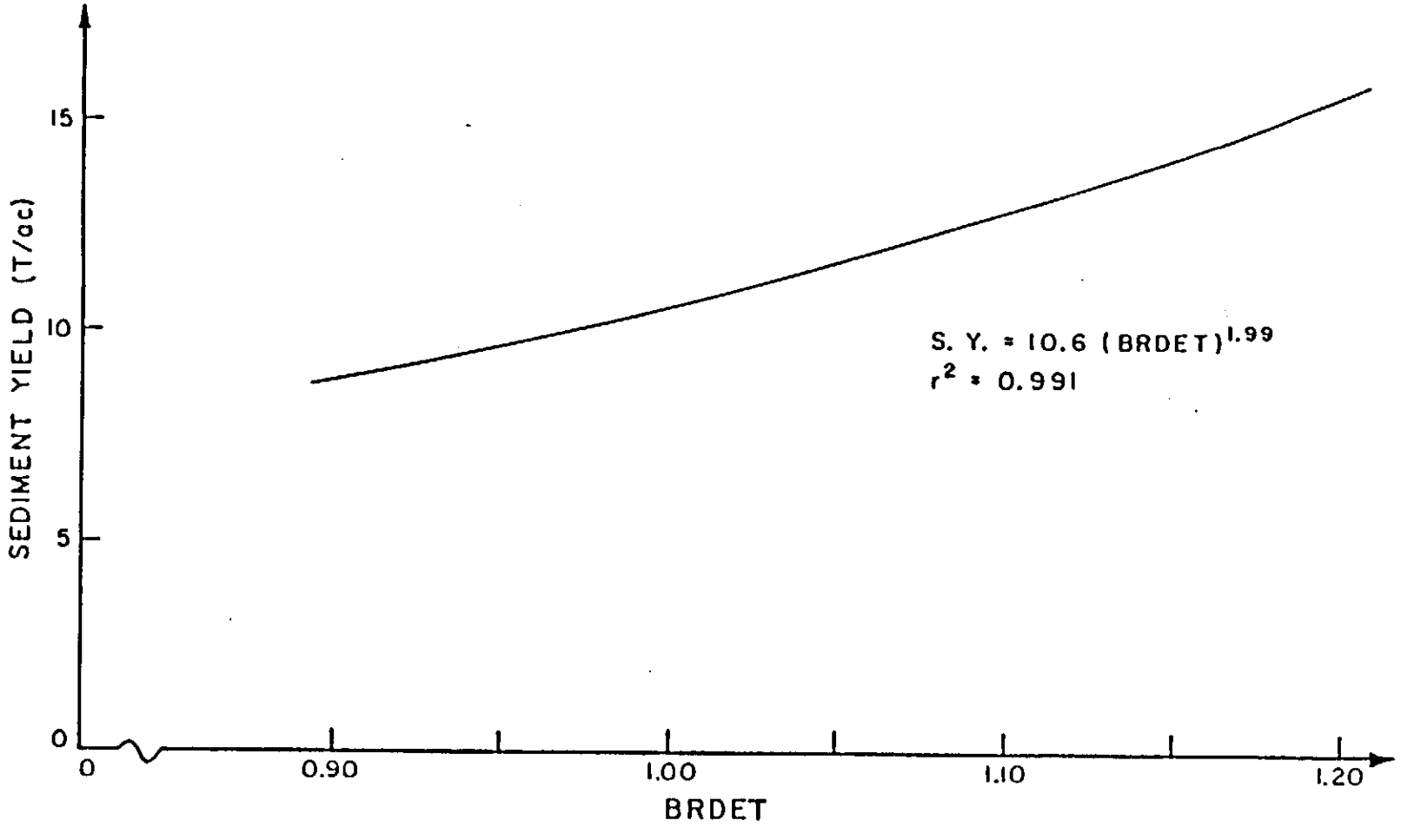

Figure 3.3 Effect of Detachment Equation Exponent on KYERMO Predicted Sediment Yield (Run 121 data)

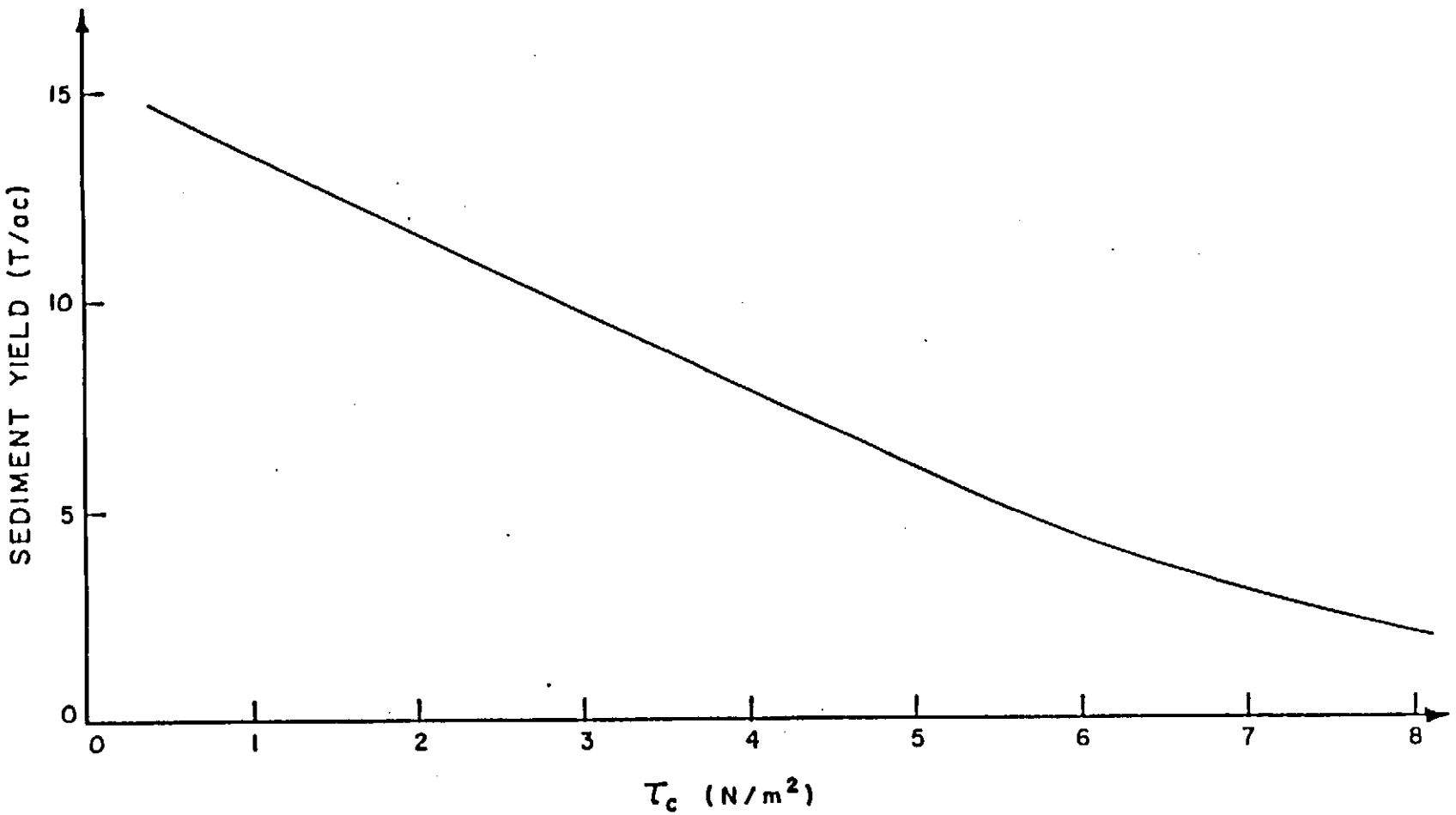

Figure 3.4 Effect of Critical Tractive Force on KYERMO Predicted Sediment Yield (Run 121 data)

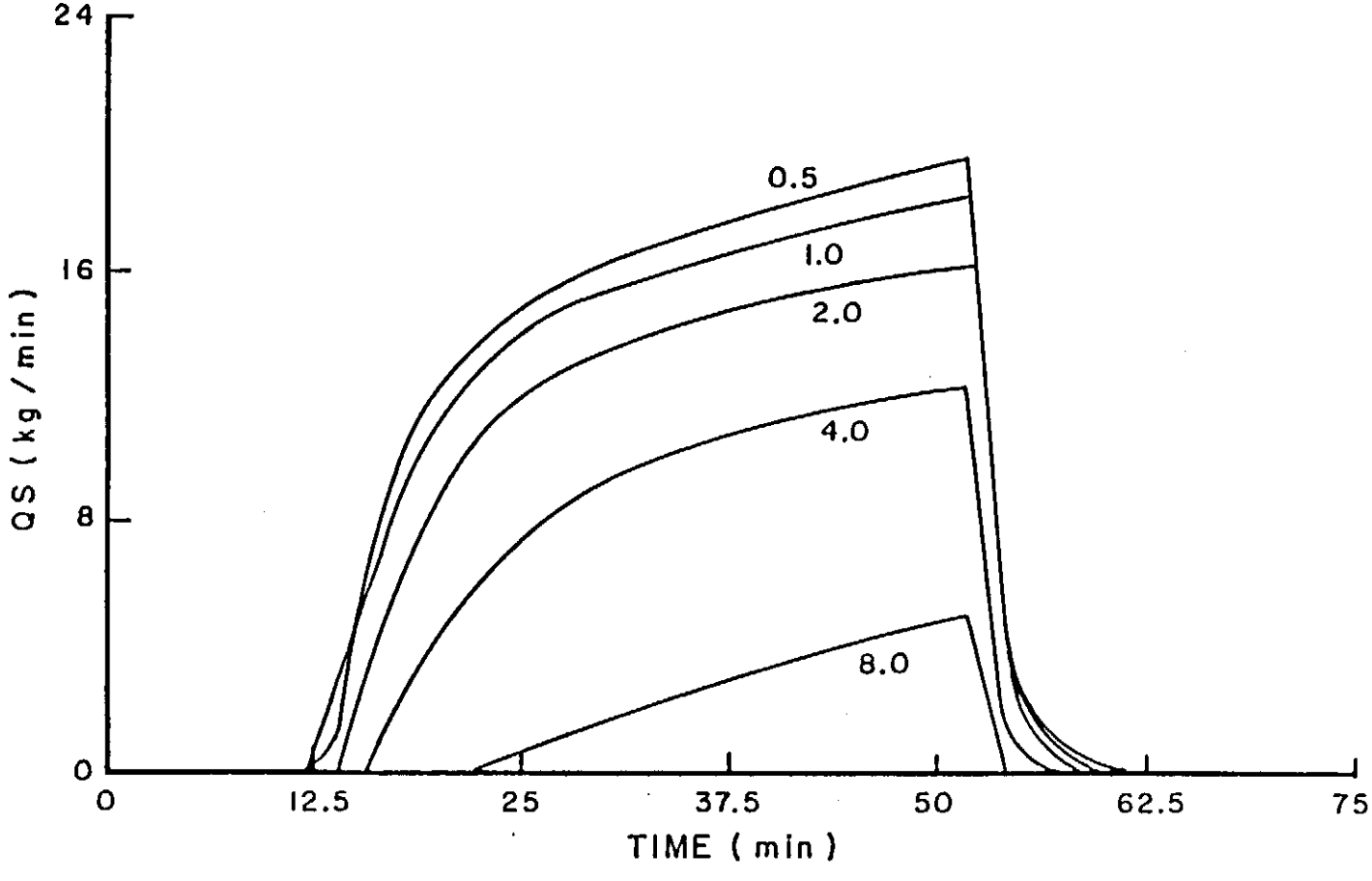

Figure 3.5 **Effect of Critical Tractive Force on KYERMO Predicted Sedimentgraph (Run 121 data)**

RILL CROSS-SECTIONAL SHAPE

The effects of initial rill cross-sectional shape and the representation of a fixed shape upon sediment yield were examined by utilizing three different shapes and three different representations for the situation of run 121. From Figures 3.6 and 3.7 and in light of the effect of other parameters, one can conclude that the effects of rill shape are slight.

NUMBER OF RILLS

The number of rills across a fixed width has an interesting effect upon the sediment yield. In the brief analysis to be presented in Chapter 4, the effect of two rills versus six rills was evaluated with the results indicating that the higher number of rills would cause more detachment. The sensitivity analysis results shown in Figure 3.8 indicate a similar response for the two and six rills, but a decrease for more than six rills.. A postulated cause for the decreasing sediment yield is that the flow is getting shallow enough as the number of rills increases that the tractive force is getting very close to or below its critical value, eliminating detachment under portions of the flow and hence, decreasing overall detachment. The form of the curve, with the maximum detachment occuring at about 6 rills per plot, will be discussed next.

The form of the curve in Figure 3.8 requires explanation. If this shape is appropriate, conservation practices must shape the field or

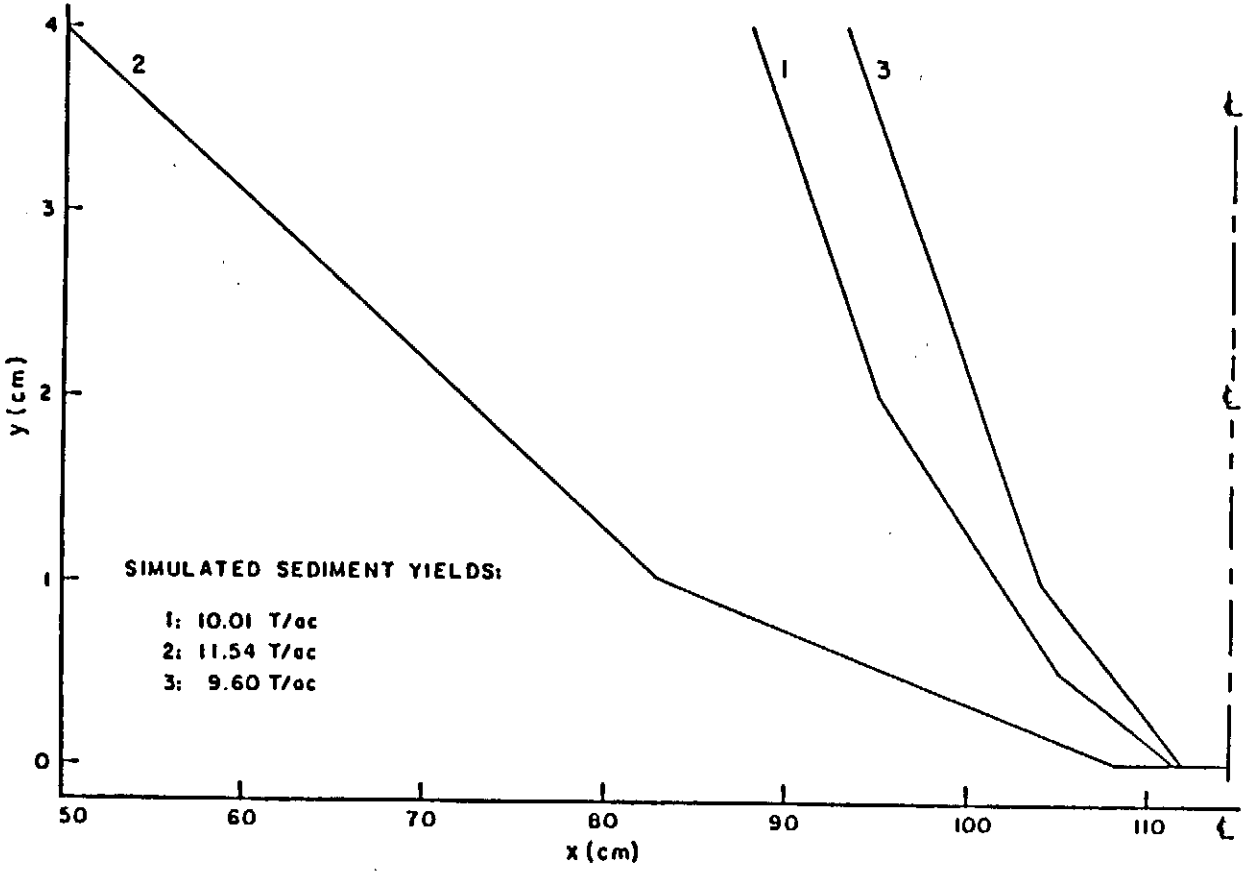

Figure 3.6 Initial Rill Shape and Corresponding Effect on KYERMO Predicted Sediment Yield (Run 121 data)

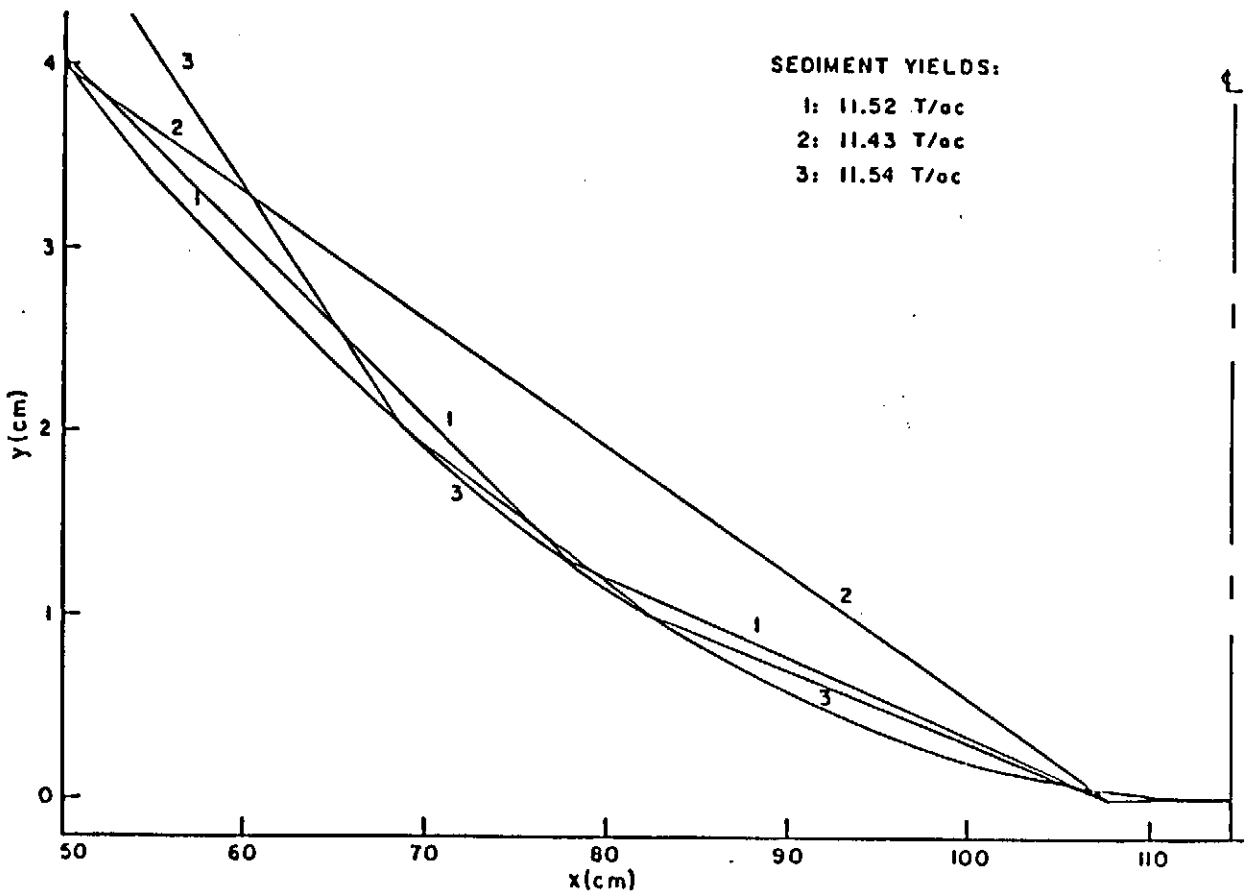

Figure 3.7 Initial Rill Shape Representation and Corresponding Effect on KYERMO Predicted Sediment Yield (Run 121 data)

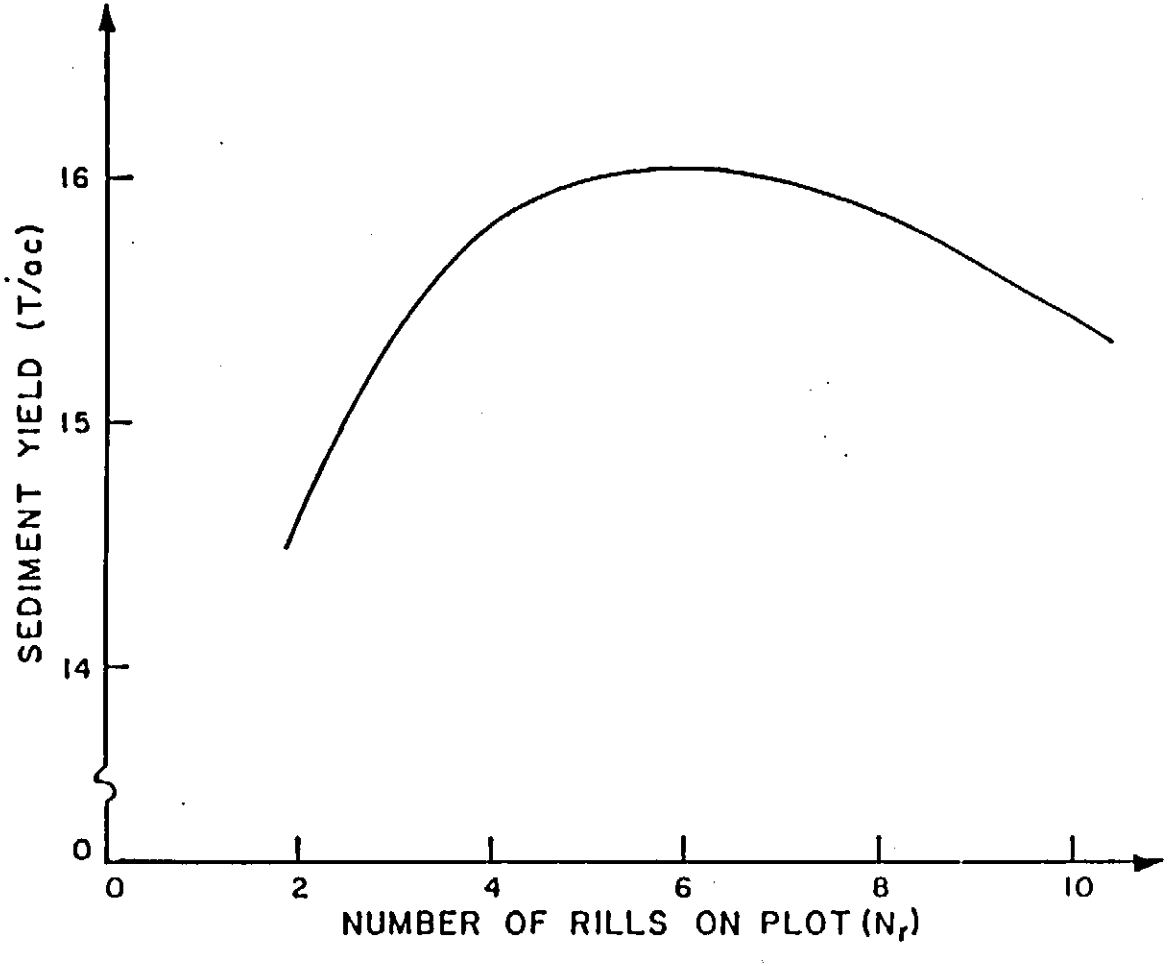

Figure 3.8 Effect of Number of Equal Size Rills on a Fixed Width Plot on KYERMO Predicted Sediment Yield

plot such that the resultant number of flow channels is not near the point of maximum erosion. The brief analysis that follows shows that a shape such as that in Figure 3.8 is a direct result of the form of the detachment equation (equation 2.23) and the form of the tractive force equation .

Consider the detachment equation 2.23,

$$D_{rc} = \alpha(\bar{\tau} - \tau_c)^{\beta} \tag{3.1}$$

where D_{rc} is the soil detachment rate in $g/s\text{-}m^2$, α and β are empirical constants, τ is the average bed tractive force in N/m^2 and τ_c is the critical tractive force in N/m^2. For the purposes of this analysis, β shall be set to 1.0 to allow an analytical solution to be obtained. For various channel geometries, if can be shown that,

$$\bar{\tau} = cQ^d \quad , \quad 0<d<1 \tag{3.2}$$

where c and d are constants and Q is the flow rate in l/min. Therefore,

$$D_{rc} = \alpha(cQ^d - \tau_c) \tag{3.3}$$

for a single rill. For n identical rills and a total flow rate of Q_{tot},

$$D_{rc_{tot}} = n_r\alpha(c(\frac{Q_{tot}}{n_r})^d - \tau_c) \tag{3.4}$$

or

$$D_{rc_{tot}} = n_r^{1-d}\, \alpha c Q_{tot}^{d} - n_r\, \alpha\, \tau_c \tag{3.5}$$

Taking the derivative of both sides with respect to n_r,

$$D_{rc_{tot}}' = (1-d)\alpha\, c\, Q_{tot}^{d}\, n_r^{-d} - \alpha\tau_c \tag{3.6}$$

or

$$D_{rc_{tot}}' = \frac{(1-d)\ \alpha\ c\ Q_{tot}^{d}}{n_r^{d}} - \alpha\ \tau_c \tag{3.7}$$

Which indicates a local minimum or maximum for the situation in which,

$$\tau_c = \frac{(1-d)\ c\ Q_{tot}^{d}}{n_r^{d}} \tag{3.8}$$

The second derivative was obtained to indicate whether the point where Equation 3.8 holds is a maximum or a minimum. The second derivative is given by

$$D_{rc_{tot}}'' = \frac{(1-d)(-d)\ \alpha\ c\ Q_{tot}^{d}}{n_r^{d+1}} \tag{3.9}$$

and since $0<d<1$,

$$D_{rc_{tot}}'' < 0 \qquad (3.10)$$

which indicates a local maximum as indicated in Figure 3.8. This analysis assumes a constant flow rate, so the exact situation depicted in Figure 3.8 cannot be numerically predicted by Equation 3.8.

NUMBER OF SLOPE INCREMENTS

The effect of the number of slope increments was examined using the conditions of run 121. Five simulations were performed with 2, 4, 6, 8, and 10 slope increments with the results shown in Figure 3.9. It is apparent that 10 or more increments are needed for convergence of the solution to a steady value. However, due to time and storage considerations, one must look to a lower number of increments with acceptable error in some situations. The data indicated that the limit for sediment yield as the number of increments gets very large is about 10.2 T/ac. The use of six increments would then give an error of about 13% compared to a very large number of slope increments. This is adequate for the sensitivity analysis. The model in its current form can only utilize 10 increments. An expansion of the model for further research is warranted.

Further examination of the effect of the number of slope increments were performed in order to determine if the effect was consistent for treatments 1 and 2. It was found that the relationship

$$SY_{NJ} = SY_{\infty} e^{0.72/NJ} \qquad (3.11)$$

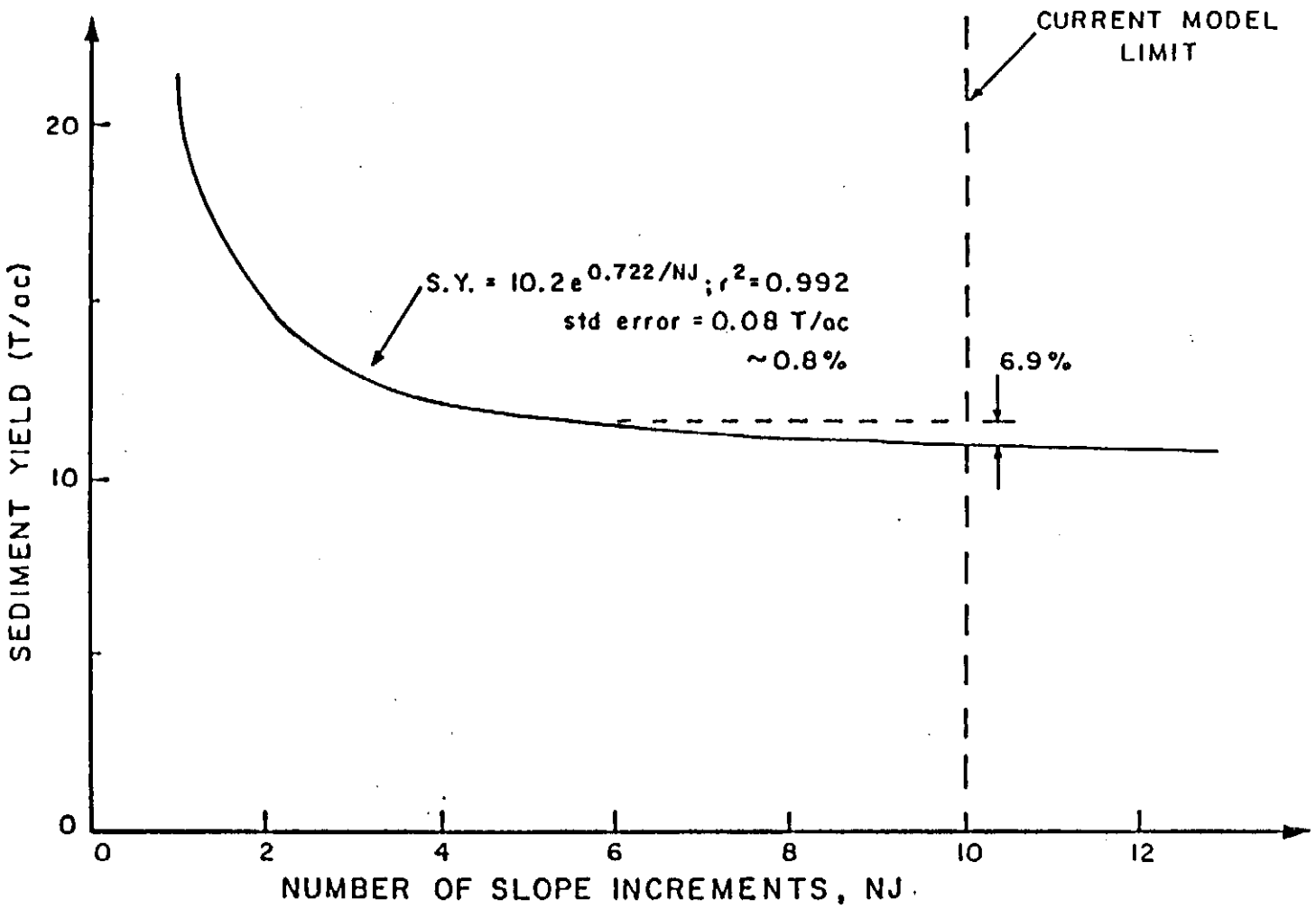

Figure 3.9 Effect of Number of Slope Increments on KYERMO Predicted Sediment Yield

where SY_{NJ} is the predicted sediment yield using NJ slope increments and SY_{∞} is the predicted sediment yield for a very large number of increments, fits the simulated sediment yields very well. The standard error of prediction for equation 3.11 was 0.21% for 8 data points from the two treatments. The sediment yield for simulations using a smaller number of the slope increments than desired for accuracy can then be converted by use of equation 3.11 to the sediment yield that would have been predicted if a large number of slope increments had been used. This also indicates that the use of six slope increments for the sensitivity analysis simulations does not affect the relative effect of those simulations.

EFFECT OF MANNING'S 'n'

The value utilized for Manning's 'n' had a large effect upon sediment yield. Values reported in the literature ranged from 0.010 for overland flow to 0.110 for very rough channels. The values from 0.010 to 0.130 were utilized to examine the effect for run 121. The results, shown in Figure 3.10, indicated that Manning's 'n' is a crucial parameter, and could be used for sediment yield fitting. The effect of 'n' on the sediment yield also points out a problem with the detachment algorithm as used and as accepted by numerous researchers. As the roughness increases for the same flow the detachment increases due to the increased depth, with no regard to the decrease in velocity. If a smoother surface occurs, the detachment would decrease for the same flow, due to a smaller flow depth. The increased velocity

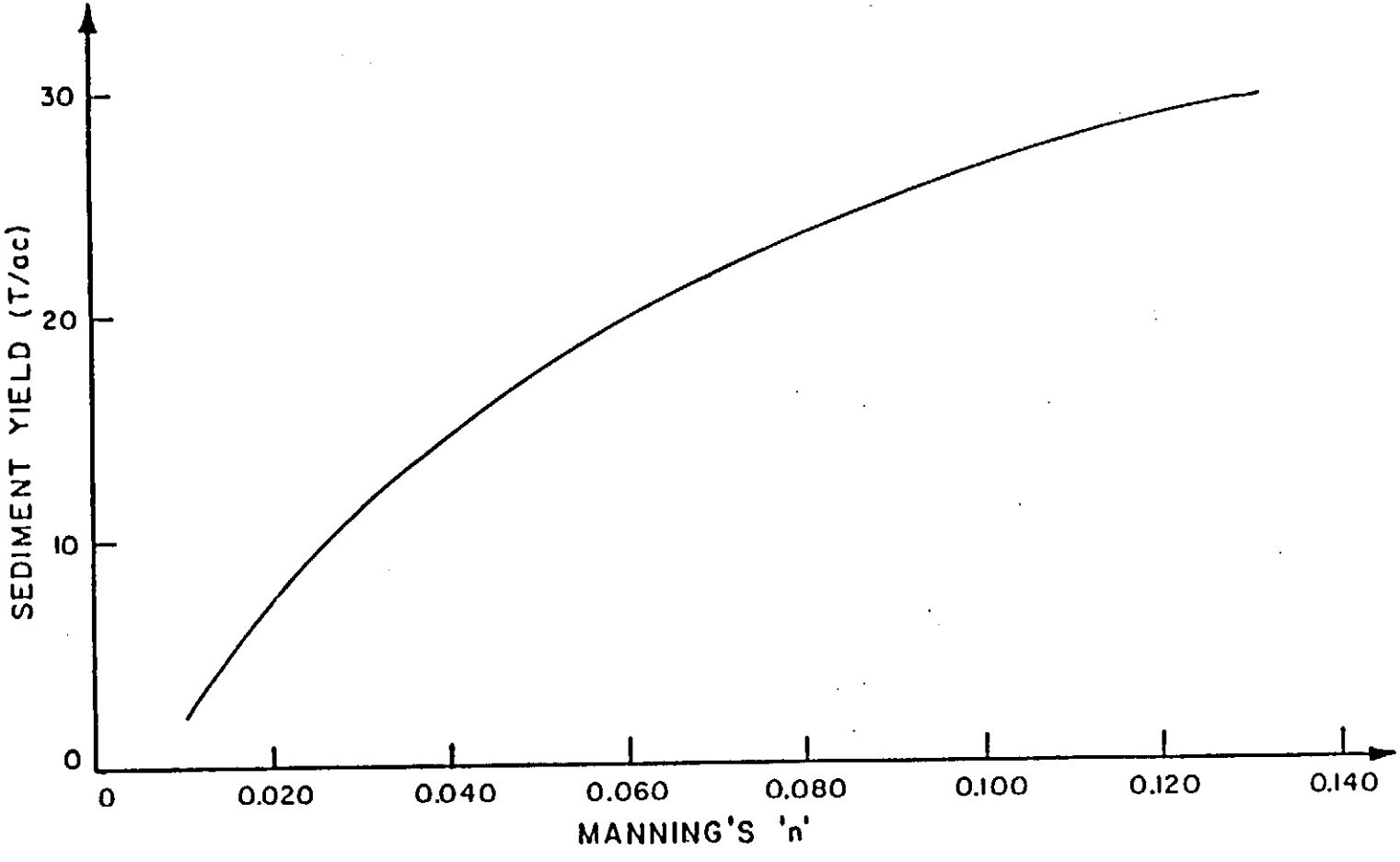

Figure 3.10 Effect of Manning's 'n' upon KYERMO Predicted Sediment Yield (Run 121 data)

would have no predicted effect on the detachment. These trends indicate that the excess tractive force equation may not be appropriate for all situations.

LENGTH OF TIME STEP

Various simulation time steps were utilized to ascertain the effect of time step on sediment yield. The time step also affects the runoff volume so comparisons were made on a grams per liter basis. Figure 3.11 shows the effect, which is slightly curvilinear. Much of the problem lies in the runoff hydrograph, which is shown in Figure 3.12. It is evident that the smallest time step possible should be used.

SLOPE-RILL NUMBER INTERACTIONS

The effect of slope and the number of rills upon the sediment yield was examined and compared with the USLE LS factor. This analysis parallels that of Rohlf (1981) and is evidence that the rilling process is not accounted for by the LS factor in the USLE. Rohlf (1981) found that the LS factor and the normalized sediment yields for his model simulations compared favorably for 7.5 to 12.5 percent slopes on a simulated 61 meter by 6.1 meter plot utilizing ten rills and a single rill. His results are shown in Figure 3.13. The sediment yields were normalized by dividing the model output sediment yields by the sediment yield predicted for a single rill in the center of a 0.61 meter wide plot at a slope of 9 percent, which is essentially the sediment yield

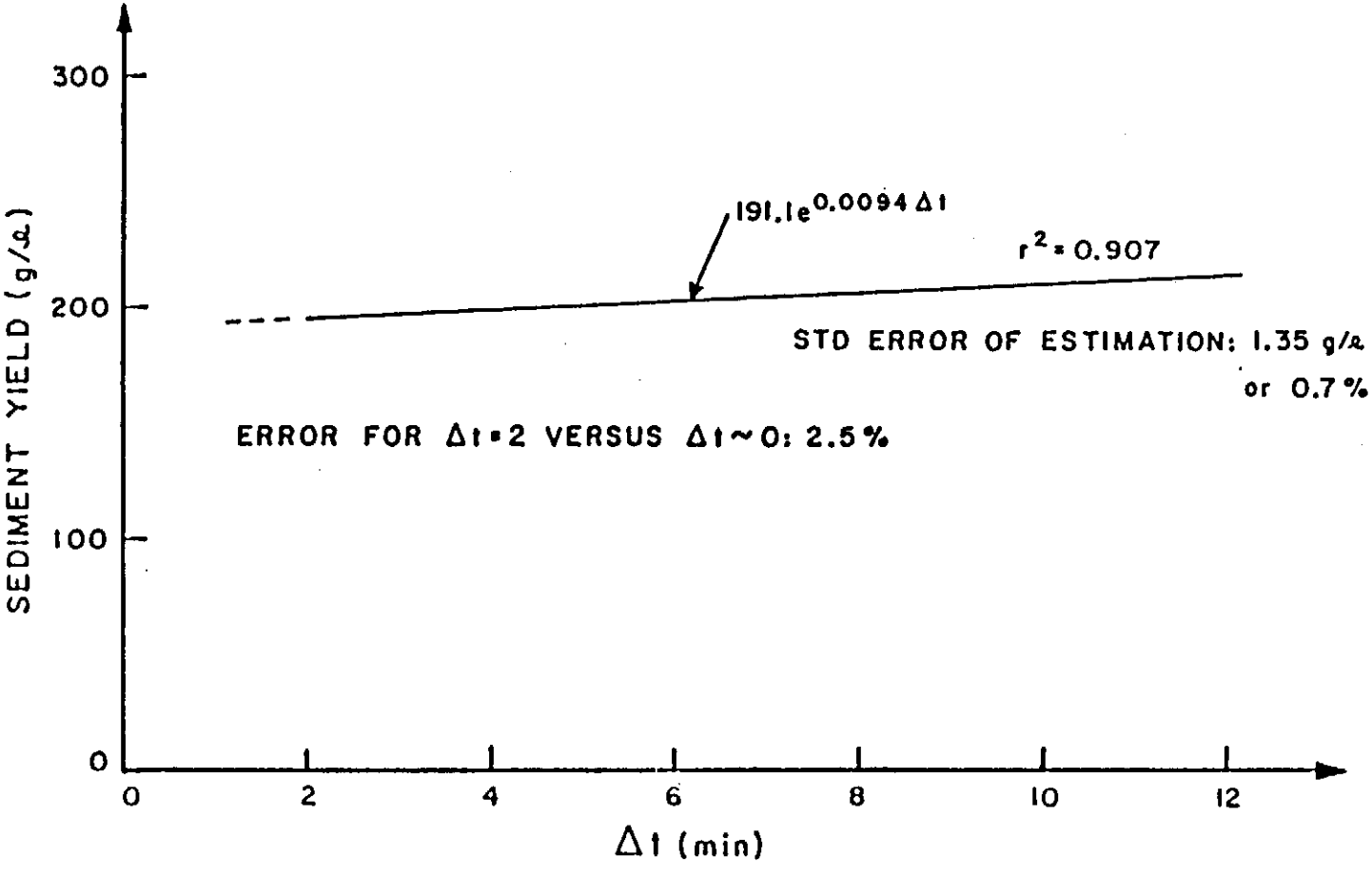

Figure 3.11 Effect of Simulation Time Step on KYERMO Predicted Average Sediment Concentration

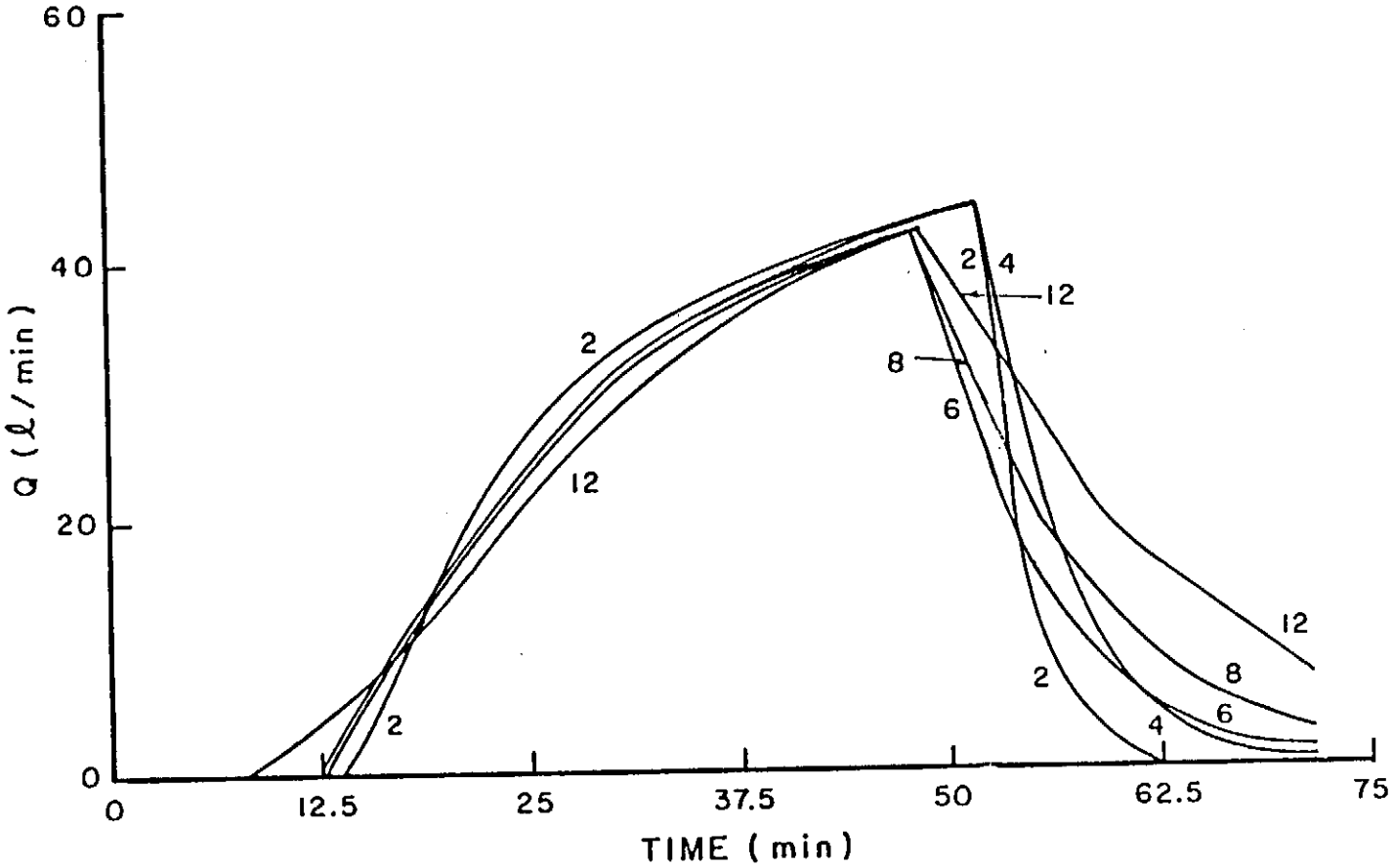

Figure 3.12 Effect of Simulation Time Step on KYERMO Predicted Runoff Hydrograph

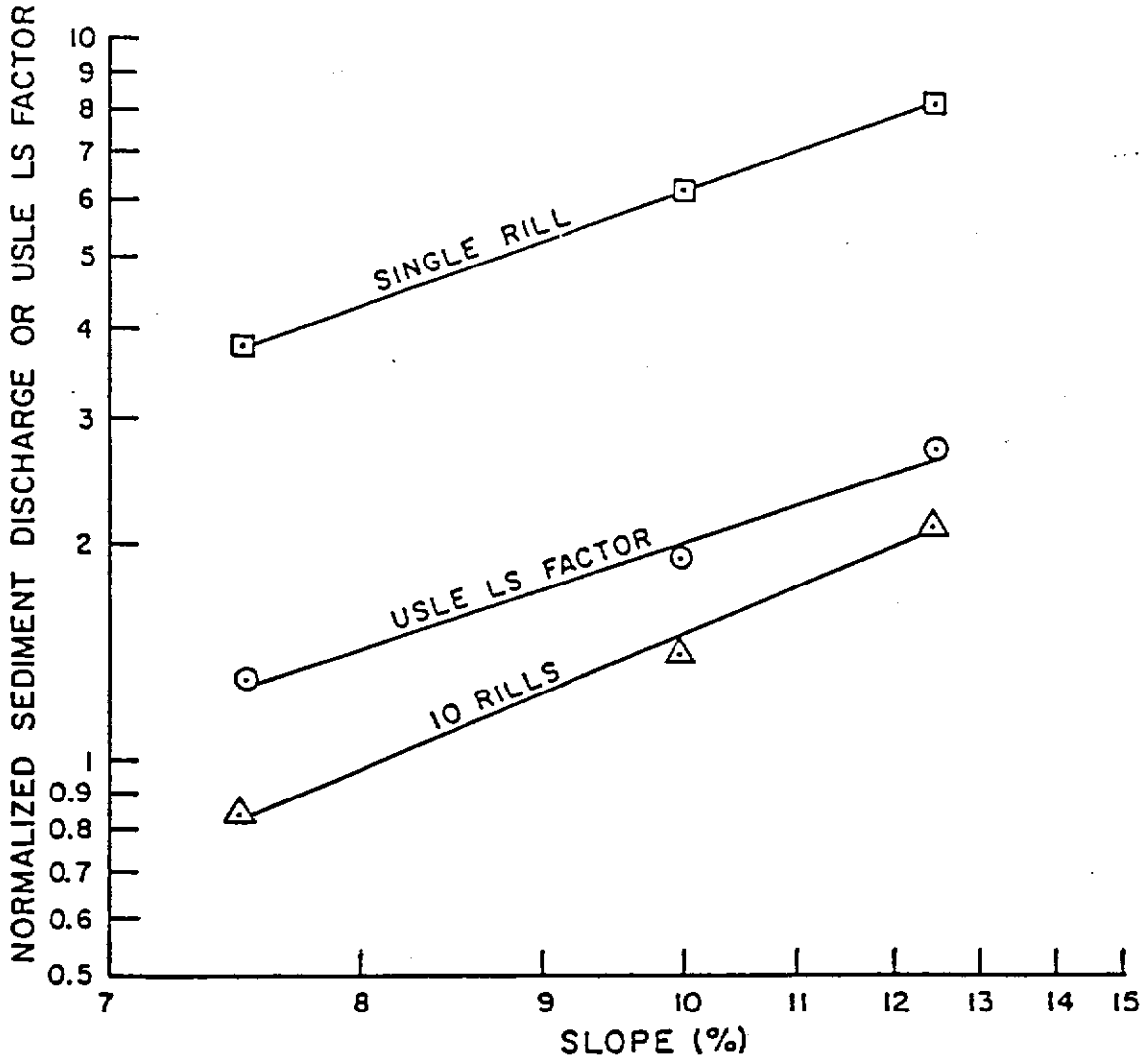

Figure 3.13 Normalized Sediment Yield and USLE LS Factor Versus Slope (from Rohlf, 1981)

from one of the rills on his ten rill wide plots, at a slope of 9 percent.

The results of KYERMO simulations were not as straightforward. Table 3.3 contains the simulation sediment yields, their normalized values using a single rill of the ten rill plot at 9 percent, and the corresponding USLE LS factor. The contents of Table 3.3 are plotted in Figure 3.14. The same general trend of the Rohlf (1981) data is exhibited only in the 10 to 12 percent slope range. Elsewhere, the LS factor is not between the 2 and 10 rill curves as would be expected from the Rohlf data. The curves are also not straight lines as represented by Rohlf, with the 10 rill curve deviating substantially from a straight line, possibly indicating a change from transport-limited to detachment-limited sediment yield, at least for some sediment types, at a slope of about 10 percent. This curvature does not necessarily disagree with Rohlf's results because a close examination of the data points around the 10 rill curve in Figure 3.13 indicated that an upward curve would pass through all three of the data points. Rohlf also reported deposition during his simulations, indicating that his runs were transport limited, at least for certain sediment types.

Figures 3.13 and 3.14 indicate that the LS factor does not account for a varying number of rills per unit width. Figure 3.14 further indicates that the LS factor overpredicts sediment yield by factors of 1.5 and more for slopes over 20 percent, when compared to the KYERMO simulated normalized sediment yield. By virtue of the earlier analyses that indicated that the KYERMO predictions fit expected trends, one can

Table 3.3 KYERMO Simulation LS Comparison

Normalized Sediment Yield

SLOPE	10 Rills	2 Rills	LS
5	0.83	1.07	0.45
7.5	0.89	1.28	0.75
12.5	1.29	1.70	1.60
20	2.09	2.28	3.39
30	3.15	2.98	6.62

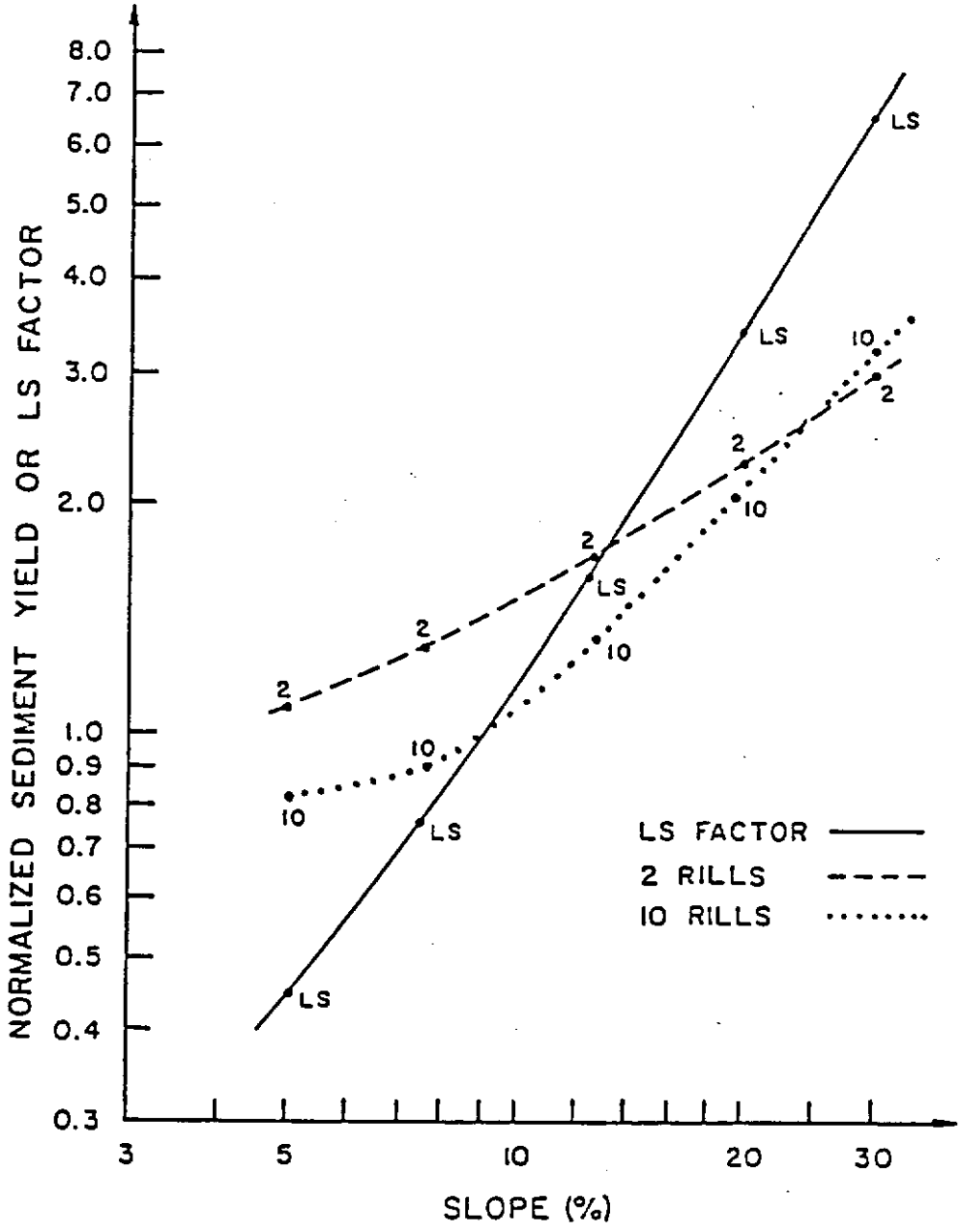

Figure 3.14 Normalized Sediment Yield and USLE LS Factor Versus Slope for KYERMO Simulations

conclude that the use of the LS factor, in its present form, for steep slopes is not warranted. The implications of the shallow slope portion of Figure 3.14 can not be ascertained until extensive tests of KYERMO are made for the limited transport capacity condition.

SUMMARY COMMENTS

The sensitivity analysis discussed in this chapter provided insights for the operation and further development of the erosion model developed for this study. The following conclusions can be drawn from these analyses:

1) The predicted sediment yield is highly sensitive to the detachment equation coefficient, the critical tractive force, and the value chosen for Manning's 'n',

2) The model should be run utilizing 10 slope increments if possible, and modified to handle more than 10 in the near future,

3) The smallest feasible time step should be used for simulations,

4) The maximum sediment yield for a given condition when detachment is limiting may occur for an intermediate number of rills per unit width, and that number of rills is dictated by the flow and plot conditions, and

5) The USLE LS-factor is not appropriate for use on steep slopes.

These conclusions indicate a need for additional development of the Kentucky Erosion Model.

CHAPTER 4 FIELD DATA COLLECTION

The objective of the field experiments was to collect data on steep slopes to justify the algorithms utilized in the erosion model described in Chapter 2 under controlled surface conditions, as a first step to modeling erosion from a more general surface. The first step to meet this objective was to select and develop a field site on which to perform the data collection experiments.

SITE DEVELOPMENT

The site selection criteria for this study were determined by the characteristics of the project under which it was performed. The site selected had to be within a daily commute from Lexington to reduce travel expenditures, with equipment and operators available to construct the plots, and have access to a water source suitable in quality and quantity for rainfall simulation. The choices were few. Fortunately, all these characteristics were available within the Tyrone Power Plant site owned by Kentucky Utilities Company. A research site proposal for this work and other hydrology/sedimentology research was developed in cooperation with Kentucky Utilities Company. The site development survey work for this study began in the spring and summer of 1983. The plots were constructed in the fall of 1983.

PLOT CONSTRUCTION AND WATER SUPPLY

Soil erosion plots were constructed on existing slopes averaging 28 and 30.5 percent. A preliminary soil survey description of the McAfee silt loam soil present on the plots was as follows:

> Moderately deep, acid, droughty soil. Not suited for cultivation because of hazard of erosion. Moderate potential for forage crops.

The plots were constructed by first removing the sod and topsoil using a scraper-pan provided and operated by Kentucky Utilities personnel. The subsoil was then removed to a depth of 24 inches and stockpiled. Similar subsoil from a short distance away was then brought to the plot and placed at a uniform slope using stakes as a guide to form a base for the placement of the removed subsoil. The original subsoil was then placed on top of the base subsoil. A bulldozer then shaped the surface so that a uniform sloping area approximately 40 feet wide and 125 feet long was formed. This area was then covered with plastic sheeting to prevent erosion.

The water supply for this study was Kentucky River water pumped by Kentucky Utilities Company through a 3 inch discharge hose to a water supply tank above the soil erosion plots. The filled tank contained approximately 13,000 gallons of water. This water was then used for rainfall simulation and lab procedures.

EXPERIMENTS CONDUCTED

Experiments to meet the objectives of this study were conducted in August and September, 1984. These experiments were selected to provide data to test the erosion model described in Chapter 2 under controlled surface conditions. The major experiments were rainfall simulations on the plots after one of two surface forming treatments were applied. The first treatment was to form six 76.2 cm (30 inch) interrow areas as subplots over the width of the 4.6 m (15 foot) wide erosion plot. Each subplot had a parabolic surface shape with a 7.6 cm (3 inch) difference between the ridge and center, as shown in Figure 4.1. The second treatment was to form two subplots with a 12.7 cm (5 inch) parabolic shape. Both treatments were applied in the same manner. The plot was first carefully roto-tilled and any surface stones removed. It was then shaped using plywood forms cut to the desired shape.

RAINFALL SIMULATION RUNS

Three sets of runs were performed on each plot for each treatment. These were:

1) Initial run on dry, tilled, shaped surface
2) Run on full-length eroded surface
3) Run on half-length eroded surface

The runs were performed in the listed sequence. Appropriate measurements and samples were taken during each, as described in the following sections. Detailed descriptions of the measurement and

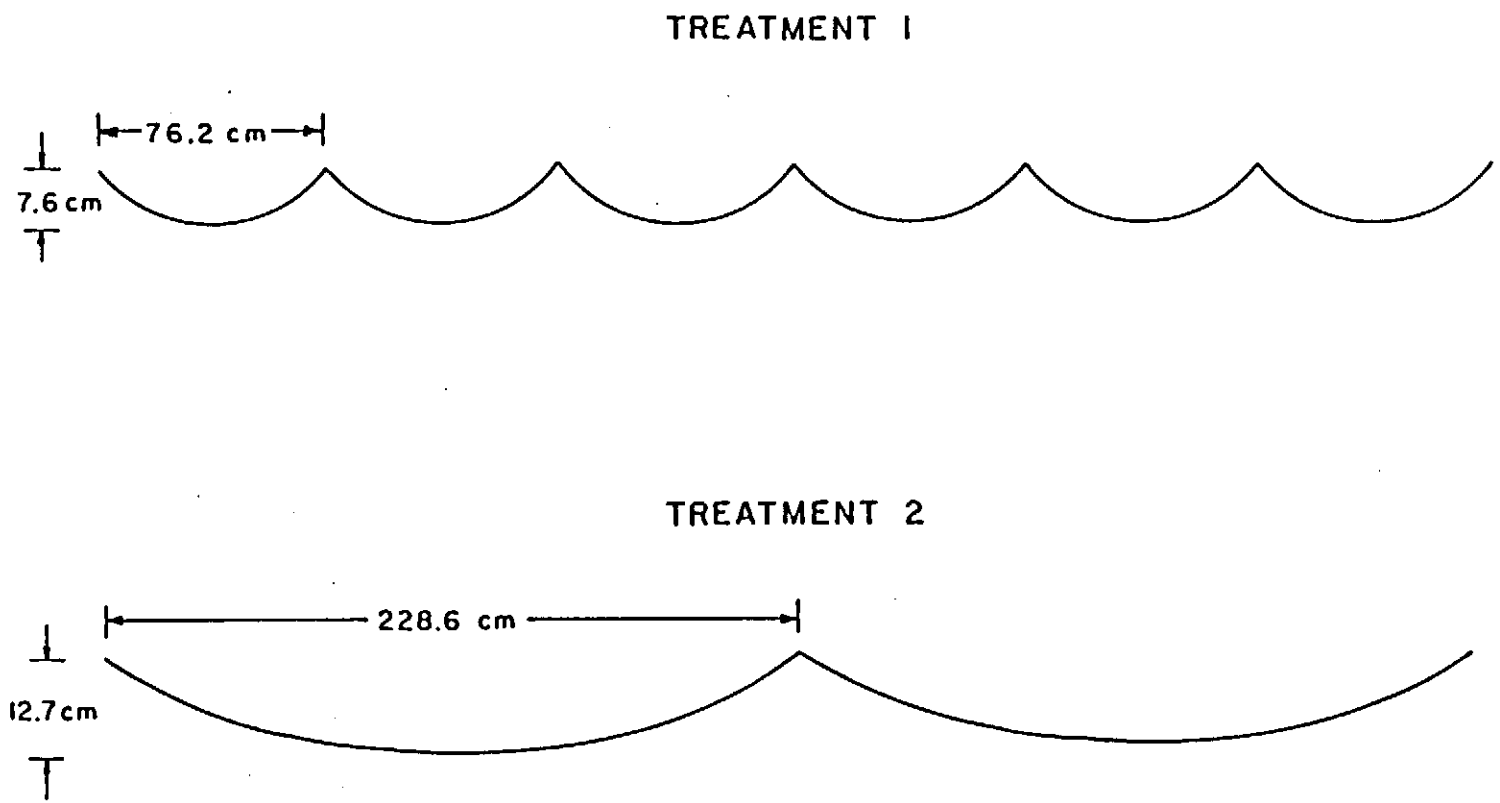

Figure 4.1 Plot Treatment Surface Shapes

sampling techniques are given later in this chapter.

CALIBRATION AND INITIAL RUNS

Rainfall calibration runs were made before the final tillage and shaping for the initial runs took place. Plastic sheeting was laid over the plot and rainfall applied for 20 minutes to determine the rainfall application rate. The plastic was then removed, the plot tilled and shaped, and the plot border replaced. Moisture content and undistributed core samples were taken prior to rainfall application as were soil height profile readings.

The first rainfall simulation was then begun on the dry, tilled, and shaped plot. Rainfall was applied for 60 minutes, the flow rate measured and the runoff sampled for sediment concentration and aggregate size distribution. Runoff measurement and sampling continued after the end of rainfall until runoff ceased. Photographs of the plot were taken from upslope and downslope of the plot every two minutes. The plot was allowed to drain for at least 30 minutes and then soil height measurements and rill cross-sections shape measurements were taken.

The plots were allowed to drain after the initial runs. Rainfall was then applied for an additional 30 minutes, on the eroded surface. This provided erosion event data for an established surface configuration. Runoff measurement and sampling were taken as before, as were plot photographs. The rill cross-sections were measured again after this run.

HALF-PLOT RUNS

Rainfall was applied again for 30 minutes after the surface height data collection for the field capacity runs were concluded and the plot shortened to 11.05 m (36.3 ft) in length. This run supplied data to check model prediction on short plots with an established surface. The same data was taken as with the other two runs.

MEASUREMENT AND SAMPLING METHODS

A brief description of the measurement and sampling methods used during the field experiments is in order. Detailed descriptions of both the field and laboratory data collection procedures were given by Hirschi (1985).

INITIAL AND FINAL PLOT SURFACE SHAPE

The initial and final surface shape of the erosion plots were measured during this study. These data provided a check on the initial shape of the plot and on the overall changes due to the first simulated rainfall. The soil-profile- meter and related instrumentation for these measurements were described by Hirschi et al. (1984) and Hirschi (1985). These data were taken immediately prior to the first simulated rainfall event and prior to any disturbance of the plot after the event. Data collection after the rainfall simulation was delayed until the plot had drained thoroughly (about 30 minutes) so that the

measurement pins would not penetrate the soil surface.

RILL CROSS-SECTIONAL SHAPES

The procedure for cross-section data collection was almost identical to that of the profile meter. Rill cross-sections were only taken after the run and were not on a fixed grid. Major and/or unusual rill cross-sections were measured in addition to measurements every 152.4 cm (60 inches). The rail location and the distance from the right plot border to the right-most pin were recorded. Prior to dropping the pins to the surface, the meter support frame was leveled with a bubble level. This assured that the pins were dropping vertically and from the same height at each point.

RILL DEVELOPMENT DURING SIMULATED RAINFALL

The profile and rill meters provided detailed measurements before and after simulated rainfall, but the surface changes during rainfall were still unknown. For that reason, the plot surface was photographed every two minutes during the simulation. Cameras were set at the bottom and top of the plot on ten foot high stands, assuring total coverage. The rill-meter rails were color coded (red stripes every 5 feet, blue stripes at 1 foot intervals) so that important events during the run could be related to the meter data taken before and after the run.

RUNOFF RATE

The plot runoff was intercepted and metered through the use of the tipping bucket equipment described by Hirschi and Barfield (1984) and Hirschi (1985). The run-control software recorded each bucket tip and the time it occurred. The sediment-laden volumetric flow rate curve was first obtained using a moving average flow rate for each of the buckets, interpolating to a 15 second interval and then summing the flow rates for all four buckets. Stopper removal and insertion times for the buckets delineated their time-interval of contribution.

The clear water runoff hydrograph was obtained after concentration data was available. The sediment volume was subtracted from each time step assuming an average particle density of 2.00 g/cc.

SEDIMENT CONCENTRATION SAMPLE COLLECTION

Runoff samples for determination of sediment concentration were collected continuously during each runoff event. The bottles were filled such that a one-liter bottle was filled every two minutes during runoff. The sample bottle number, the start time and the fill time were recorded. The bottles were then taken to Lexington for analysis.

AGGREGATE SIZE DISTRIBUTION

At the same time as sediment concentration samples were being taken, samples were also taken for aggregate size distribution

analysis. The bottles and their corresponding collection times were recorded just as were the concentration samples. However, the analysis of these samples began at the field site due to possible aggregate breakdown during transport and was concluded after the samples were taken to Lexington. Details of the wet-sieve fractionization procedures as well as the pipette procedures used in the laboratory after wet-sieving were described by Barfield et al. (1983) and Hirschi (1985).

CHAPTER 5 RESULTS AND CONCLUSIONS

The field and lab portions of this study each provided data to use for model simulations and to justify the model algorithms. In this chapter, model simulations and comparisons with field data will be presented and discussed. Details of the parameter measurements and estimates were given by Hirschi (1985).

EVALUATION OF THE ACCURACY OF KYERMO SEDIMENT SIMULATIONS

The KYERMO erosion model described in Chapter 2 was utilized to simulate the field erosion test conducted at the Tyrone site. The aspects of these simulations and comparisons to the observed data that will be presented in subsequent sections are the fitted hydrologic response, the sediment delivery, both fitted and unfitted, the delivered sediment size distribution, and the rill cross section changes.

HYDROLOGIC SIMULATIONS

The hydraulic properties of the plot soils were fitted to match the total runoff volume, the time to runoff, and the peak runoff rate using laboratory parameters as a guide. This assured proper testing of the sediment components of the model. The input parameters for each of the Tyrone runs are presented in Table 5.1. The first digit of the run number is plot number (plot 1 had a slope of 30.5%, plot 2 had a slope

Table 5.1 Hydrologic Simulation Parameters

Run #	K_s (cm/hr)	θ_s (cc/cc)	Campbell B	Campbell X	% SAT	measured IMC (cc/cc)
111	0.45	0.434	6.0	-0.20	0.90	0.197
112	0.45	0.434	6.0	-0.20	0.87	0.267
113	0.45	0.434	6.0	-0.20	0.845	0.300
121	0.45	0.434	6.0	-0.20	0.90	0.190
122	0.45	0.434	6.0	-0.20	0.87	0.277
211	0.45	0.434	6.0	-0.20	0.93	0.178
212	0.45	0.434	6.0	-0.20	0.82	0.307
213	0.45	0.434	6.0	-0.20	0.85	0.324

Run # Code: 1st digit: plot #

2nd digit: treatment # (1: 6 rills, 2: 2 rills)

3rd digit: run #

of 28%), the second digit is treatment (six rills was treatment 1, two rills was treatment 2), and the third digit represents the run number (1: initial 60 minute run, 2: 30 minute run with developed rills, 3: half-plot 30 minute run with developed rills). It was found that the only parameter that required changing between runs within a treatment was the final degree of saturation.

As expected, the results of the hydrologic simulations were good due to the fitting process. The run summary in Table 5.2 contains the simulated and observed runoff volumes, peak runoff rates, and the time to runoff. The entire hydrographs were presented by Hirschi (1985). Instabilities in the observed hydrographs are probably due to clogging of the measurement equipment and the inability to precisely control water application rates with the oscillating sprinkler nozzles. It would be possible to extensively discuss the hydrologic simulations and implications of the fitted parameters. However, the objective of the study was to evaluate sedimentology estimates. In view of this objective and the fact that the hydrology parameters were fitted, such a further discussion seems unwarranted.

SEDIMENT DELIVERY

The prediction of sediment delivery is the first crucial test of an erosion model's performance. To test the accuracy of the KYERMO in predicting sediment yield, simulation runs were first made with detachment parameters from the literature and compared to the results from field tests. The initial detachment coefficient and exponent were

Table 5.2 Hydrologic Simulation Results

Run #	Rainfall Rate (cm/hr)	Rainfall Duration (min)	Runoff Volume (l)		Final Flow Rate Rate (l/min)		Initial Runoff Time (sec)	
			Sim	Obs	Sim	Obs	Sim	Obs
111	4.6	58	1566.3	1492.2	46.4	47.0	735	800
112	4.6	30	990.2	979.8	49.5	49.5	255	270
113	4.6	30	713.8	668.2	29.2	29.0	135	135
121	4.6	52	1288.5	1161.9	44.5	46.5	735	885
122	4.6	30	1056.8	997.6	50.4	52.0	255	270
211	4.6	50	673.5	639.6	33.8	28.0	1215	810
212	4.6	30	1673.5	1588.5	63.0	67.0	0	60
213	4.6	30	796.3	753.7	30.6	29.0	15	90

average values of those presented by Foster (1982) which were fitted from field trials of Meyer et al. (1975). The values reported were 2.76 and 2.34 with units of $g\text{-}m^{0.1}/s\text{-}N^{1.05}$. A third value, 11.4, from unpublished data of Foster was also reported but was not used due to a high fitted τ_c value in the evaluation. The initial critical tractive force was estimated using the plot dispersed percent clay as determined in the lab analyses and the relationship proposed by Smerdon and Beasley (1961). The initial Manning's 'n' value for rill flow, 0.030, was taken from the default value used in the CREAMS model for concentrated flow (Knisel, 1980). The input parameters from the literature are summarized in Table 5.3. Utilizing these parameters, the model overpredicted erosion from the Tyrone runs for treatment 1 on both plots. Treatment 2, on the other hand, was under predicted for both runs. The predicted and observed sediment yields and average sediment concentrations are reported in Table 5.4 and plotted in Figure 5.1. The standard error of estimation of these simulations is compared with other studies in Table 5.5. This comparison indicates that the model prediction is in the same range as other models reported in the literature.

Although the model yields reasonable results without fitting compared to other models, it seems appropriate to examine the increase in accuracy gained from parameter adjustments. Optimization was performed on a term-by-term basis rather than for all terms at once to gain insights to the individual parameter effects. This allows more evaluation of the physical "reasonableness" of the fitted parameters. If better accuracy can be gained through parameter adjustments

Table 5.3 Summary of Input Detachment Parameters Selected from the Literature

Parameter	Value	Units	Source	Comments
ARDET	2.5	$\frac{g - m^{0.1}}{s - N^{1.05}}$	Foster (1982)	Average of fitted values from Meyer et al. (1975) study
BRDET	1.05	-	Foster (1982)	Average of fitted values presented
n_{rill}	0.030	-	Knisel (1980)	Default value for CREAMS model
n_{sheet}	0.010	-	Knisel (1980)	Default value for CREAMS model

Table 5.4 Simulation Summary

Run	Slope (%)	# Rills	Run Duration (min)	Horiz. Plot Length (m)	Sed. Del. (T/ac) Obs.	Sed. Del. (T/ac) Sim.	Ave. Conc. (g/l) Obs.	Ave. Conc. (g/l) Sim.
111	30.5	6	58	21.3	8.62	13.6	126.1	190.8
112	30.5	6	30	21.3	6.9	9.1	154.0	200.5
113	30.5	6	30	10.7	3.9	4.1	62.2	63.0
121	30.5	2	52	21.3	17.8	10.8	335.1	184.5
122	30.5	2	30	21.3	14.8	6.9	325.1	143.3
211	28.0	6	50	21.3	5.2	5.5	117.8	179.1
212	28.0	6	30	21.3	7.9	11.9	108.8	156.2
213	28.0	6	30	10.7	1.0	5.1	15.1	140.0

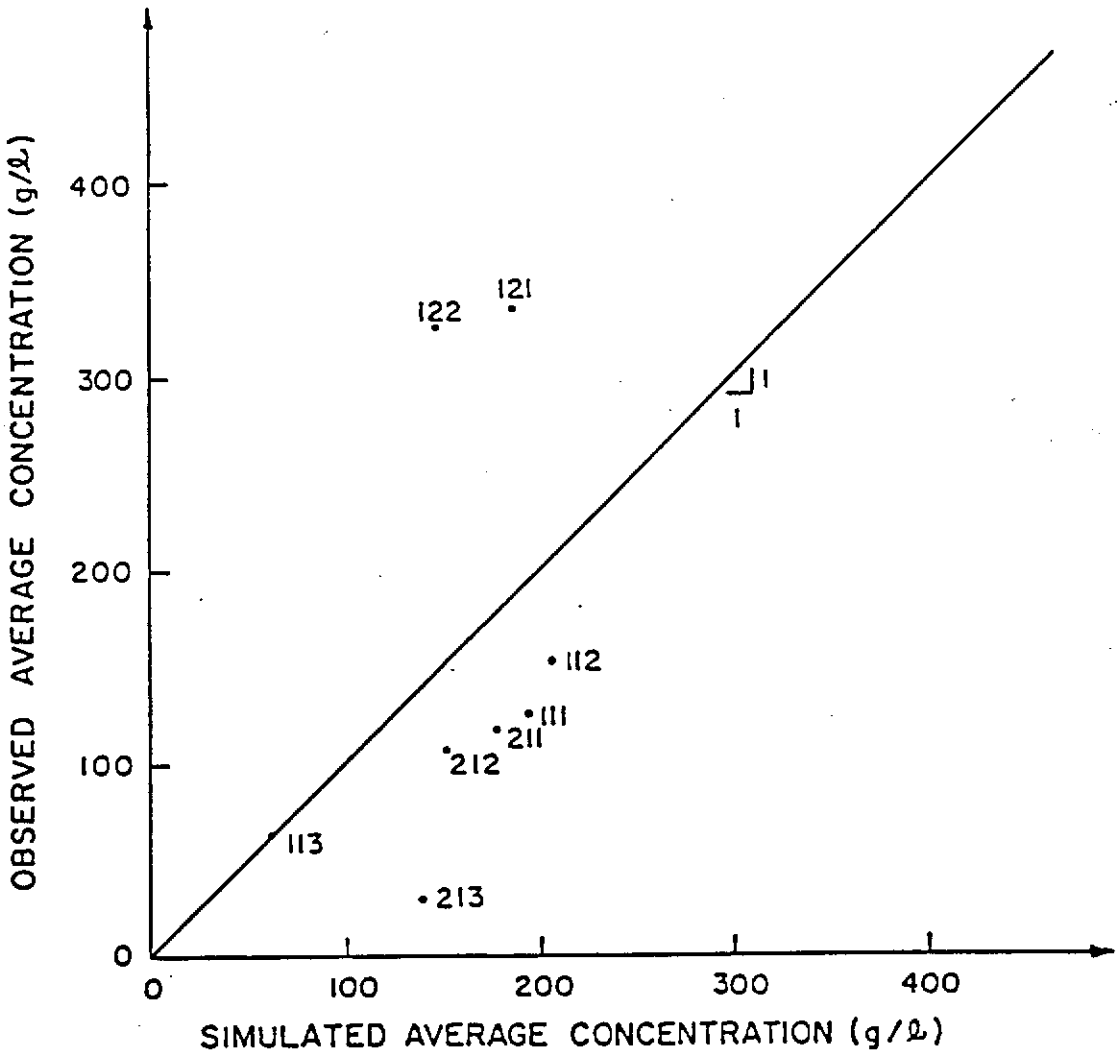

Figure 5.1 Accuracy of Initial KYERMO Simulations

Table 5.5 Simulation Accuracy Comparisons

Model	# Runs	Equations Used	Std. Error (T/ac)	Ref.
KYERMO	8	as in Chapter 3	4.95	this study
Foster and Meyer closed form	3	Foster and Meyer closed form	3.72	Foster and Meyer (1976)
Onstad and Foster	11	Modified USLE	2.50	Onstad and Foster (1975)
CREAMS Erosion Component	4	Mod. USLE for interrill areas excess tractive force for rills using Foster shear distribution	10.72	Foster and Lane (1981b)

consistent with field conditions and lab estimated values, then the algorithms will be further justified and the parameters that require further study will be brought to light. Three parameters can be adjusted that directly affect detachment. They are: 1) the rill detachment coefficient (ARDET), 2) the rill critical tractive force (CSH), and 3) the rill Manning's 'n' value. Foster (1982) stated "... parameter values in a rill erosion equation can vary without apparent reason for similar soils". This indicates that many unknowns exist pertaining to these parameters. Hence, the use of fitted values may be necessary as recommended by Foster (1982). The effects of each of the parameter adjustments upon the Tyrone simulations will be discussed separately.

The adjustment of ARDET would change the detachment proportionally. The fitting is therefore very straightforward. The required values, in most cases, are within the range of values reported in the literature. For example, Foster (1982) presents results of the Meyer et al. (1975) tests with coefficients of 2.76, 2.34, and 11.4 with approximate units $g\text{-}m^{0.1}/S\text{-}N^{1.05}$ (actual units depend upon equation exponent value). These values were fitted, along with the critical tractive force and the detachment equation exponent, and represent the only values reported in the literature based upon actual data. The CREAMS model (Kinsel, 1980) utilized a default of 0.135 with units $ft^{0.1}/lb^{0.05}/s$ which converts to 11.3 for the units of this study ($g\text{-}m^{0.1}/s\text{-}N^{1.05}$). The required coefficients are presented in Table 5.6, leaving CSH and 'n' as input. It can be concluded, from this analysis, that individual simulations can be matched to the

Table 5.6 Estimated Parameters for Fitting

	Original Input Parameter Values			Match Parameter Values		
Run #	ARDET	CSH	n	ARDET	CSH	n
111	2.50	1.98	.030	1.47	4.11	0.015
112	2.50	1.98	.030	1.74	2.22	0.009
113	2.50	1.98	.030	2.22	2.17	0.026
121	2.50	1.98	.030	3.87	0.00*	0.052
122	2.50	1.98	.030	4.93	0.00*	0.070
211	2.50	1.98	.030	2.20	2.24	0.026
212	2.50	1.98	.030	1.63	3.48	0.018
213	2.50	1.98	.030	0.47	2.78	0.004

*Actual match value would be negative

observed sediment yields by using appropriate values of ARDET. Each of these values are within the range of reported values.

The adjustment of CSH would not change the detachment as simply as would ARDET changes, but reasonable estimates can be made by calculating the "run average" shear assuming the total sediment delivery is equal to the total detachment. The "run average" shear is obtained by solving equation 2.18 for τ, using the total simulated sediment yield (SSY) as the detachment capacity,

$$\bar{\tau} = \left(\frac{SSY}{2.5}\right)^{1/1.05} + 1.98 \qquad (5.1)$$

The approximate τ_c value necessary for matching the simulated sediment yield to the observed sediment yield (OSY) is then

$$\tau_c' = \bar{\tau} - \left(\frac{OSY}{2.5}\right)^{1/1.05} \qquad (5.2)$$

or

$$\tau_c' = \left(\frac{SSY}{2.5}\right)^{1/1.05} - \left(\frac{OSY}{2.5}\right)^{1/1.05} + 1.98 \qquad (5.3)$$

The resultant values can then be used as a first approximation to the correct fitted value. Simulations utilizing these values exhibited excellent agreement with the observed sediment yield; therefore the values shown in Table 5.6 are the optimized values.

It is appropriate to compare proposed match critical tractive force values in Table 5.6 to those reported in the literature to check the reasonableness of the values in Table 5.6. The fitted critical shear

values from Foster (1982) were 2.87, 4.16 and 4.78 (all in N/m^2). In the CREAMS model, however, (Kinsel, 1980) used 0.40 lb/ft^2 was used for a default value which converts to 19.2 N/m^2. This value seems extremely high. The full range of CSH based upon the percent clay equation of Smerdon and Beasley (1961) indicated a minimum of 0.493 N/m^2 for zero percent clay and a maximum of 33.3 for 100 percent clay. The 19.2 N/m^2 would indicate 87 percent clay, whereas the average Foster (1982) value of 3.94 N/m^2 would indicate 49 percent clay. If these values are correct, the cohesiveness of the matrix material was not the sole factor contributing to the critical shear. The approximate CSH values presented in Table 5.6 are within the range of the Foster (1982) values and the Smerdon and Beasley values (although the clay content would have to be much higher than measured in most cases), but fall far below the CREAMS default value. The fitted CSH values seem appropriate, but the fact that they are high compared to the Smerdon and Beasley values may indicate that coarse material is present or that the ARDET value is too high. This problem is discussed in a subsequent section. One could conclude from the above discussion that the critical tractive force can be adjusted to match the observed and simulated sediment yield, but that the cohesiveness of the material, as represented by the Smerdon and Beasley (1961) percent clay relationship alone cannot be used to explain the physical reason for the high critical tractive force necessary for fitting. The presence of exposed coarse material on the boundary may explain these high values.

The third fittable parameter is Manning's 'n'. The CREAMS model

used a bare soil 'n' value of 0.030 for all concentrated flow, although it is known that cover and "cultural practices" increase this value. The overland flow Manning's 'n' value in the CREAMS model was lower, with a range of 0.010 to 0.035, which is unusual compared to other recommended 'n' values for shallow flow, such as those of Schwab et al. (1966). The evaluation of 'n' for shallow flow is very subjective. Much information is available for deeper flow, but little is known about the effect of shallow flow on 'n', especially in the presence of roughness elements larger than the depth of flow. The materials that are normally assigned the 'n' values necessary to fit the observed sediment yield data are much 'smoother' than the channels in this study, therefore the values necessary for fitting seem low, in most cases, for this application. However, the lowering of 'n' would also have the effect of moving the recession limb of the simulated runoff hydrographs closer to the observed. It can be concluded that the values used for Manning's 'n' should probably be left as input from the literature. The values necessary for fitting would require that the channel bed be much smoother than the observed rill channels for the case of treatment 1. The sensitivity analysis discussed in Chapter 3 pointed out other problems with Manning's 'n'.

Based upon the initial simulations and the values of the parameters necessary for fitting, it can be concluded that the model represents the erosion process as accurately as other available models. However, it is evident that parameter estimation procedures for the detachment process are badly needed.

Another test of a model, in addition to the actual values

predicted, is the reasonableness of the predictions. For this reason, the apparent discrepancy between the predicted values for sediment yield for treatments 1 (6 rills per plot) and 2 (2 rills per plot) of the simulations must also be addressed. Initially, one might assume that the same volume of water divided into three rills would cause less erosion than if sent down one rill. Simulated sediment yields for runs 111 and 121 do not indicate this trend. The average sediment delivery concentration in simulated run 111 was 190.8 g/l whereas the average simulated sediment delivery concentration in run 121 was 184.5 g/l. This phenomenon can can be at least partially explained by the fact that, although both channels began as parabolic, the rill watersheds in treatment 2 were much flatter than in treatment 1. This allowed two changes to occur: 1) the concentrated flow at the lowest point of the watersheds was wider, and hence, shallower for treatment 2 than for treatment 1 for the same flow rate, thus lowering the shear and the detachment, and 2) the rill that formed in the watersheds of treatment 2 were wider, which allowed them to carry more flow for the same applied shear. Further analyses to verify that the model prediction followed expected trends were presented by Hirschi (1985).

It can be concluded, therefore, from the above simulations and analyses and from those of Hirschi (1985), that

1) The erosion model predictions fit expected trends based upon the form of the detachment relationship utilized,

2) The erosion predictions of this study utilizing available parameters from the literature are as accurate as those presented in the literature for other studies,

3) The erosion prediction can be improved through parameter adjustments, and

4) The parameter adjustments to improve accuracy are in accordance with the physical characteristics of the plot, indicating the need for parameter estimation based upon those characteristics.

SEDIMENT SIZE DISTRIBUTION

The input size distribution for the matrix material during the simulations was obtained from the lab aggregate size distribution results. The size distributions output by the model as the distribution delivered off the plot is the same as the input matrix material distribution. This is due to the fact that the transport capacity of the flow was always in excess of the sediment load, so no depositional sorting occurred in the simulations. Little deposition was observed in the Tyrone field runs. The measured size distributions varied with time. Each distribution was presented by Hirschi (1985). The combination of no deposition and a varying size distribution in the delivered material may indicate the need for a detached size distribution other than the soil matrix fraction, which is used in KYERMO, that is also time and/or flow varying.

From the above, it can be concluded that the model does not predict the delivered size distribution of material on plots where sediment transport is not limiting. A new approach, with selective detachment for varying particle sizes, is needed for the steep slope application.

RILL DEVELOPMENT AND CHANGES

The rill development and rill changes due to runoff were major modeling efforts within the development of KYERMO. The simulations provided time varying rill cross-sections that can be used to study the changes occuring in the field. Only the initial and final shapes can be compared with field data. A difficulty in this comparison arises from the fact that the field rills are quite non-uniform, even over a few feet, due to heterogeneities, such as rocks, which diverted the flow to the side of the rill, or limited rilling altogether. For example, Figures 5.2 and 5.3 show three rill shapes measured in the field at 1 foot increments along the plot over each rill after run 121. The rill meter was located at the same lateral location for each measurement over each rill. The fourth shape is the simulated rill shape for run 121 after parameter adjustment for that portion of the plot. The shape of the simulated rill seems appropriate, but the model did not predict the difference in rill shape and size between the two rills. On the average, the simulated rill size seems reasonable, but if compared with only one of the observed rills, the simulation would be poor. This situation emphasizes the stochastic nature of the rilling process. Further evidence of this stochastic nature is shown in Figures 5.4 and 5.5. In the top portion of each of these figures, the six rill cross sections measured at one slope location after run 111 are shown. The variability is quite evident. The average of these cross sections and the simulated cross section for that plot location are shown in the lower half of the figures. It can be concluded that

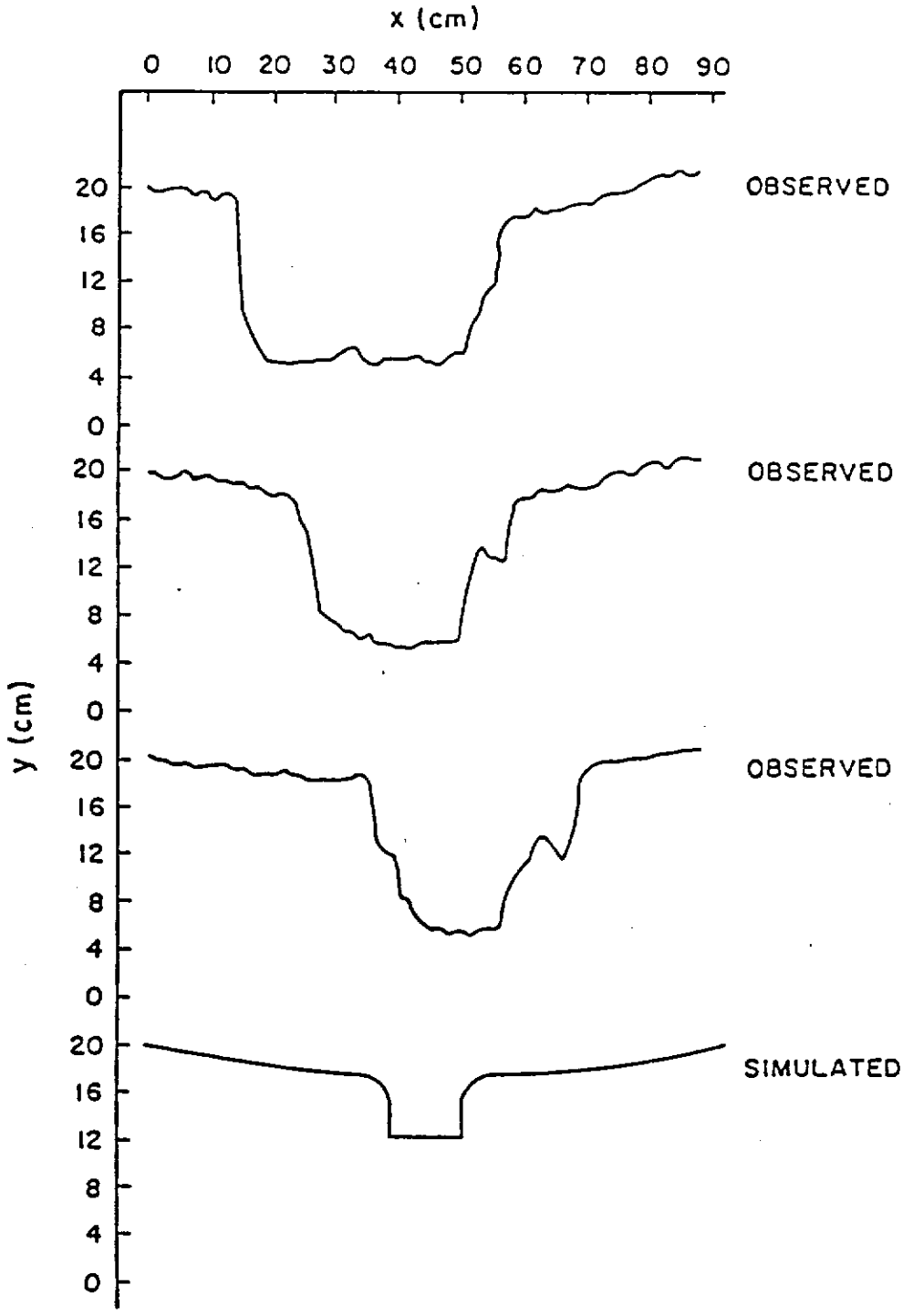

Figure 5.2 Run 121 Left-Side Rill Cross-Sections (1 foot intervals) Compared to KYERMO Simulated Shape

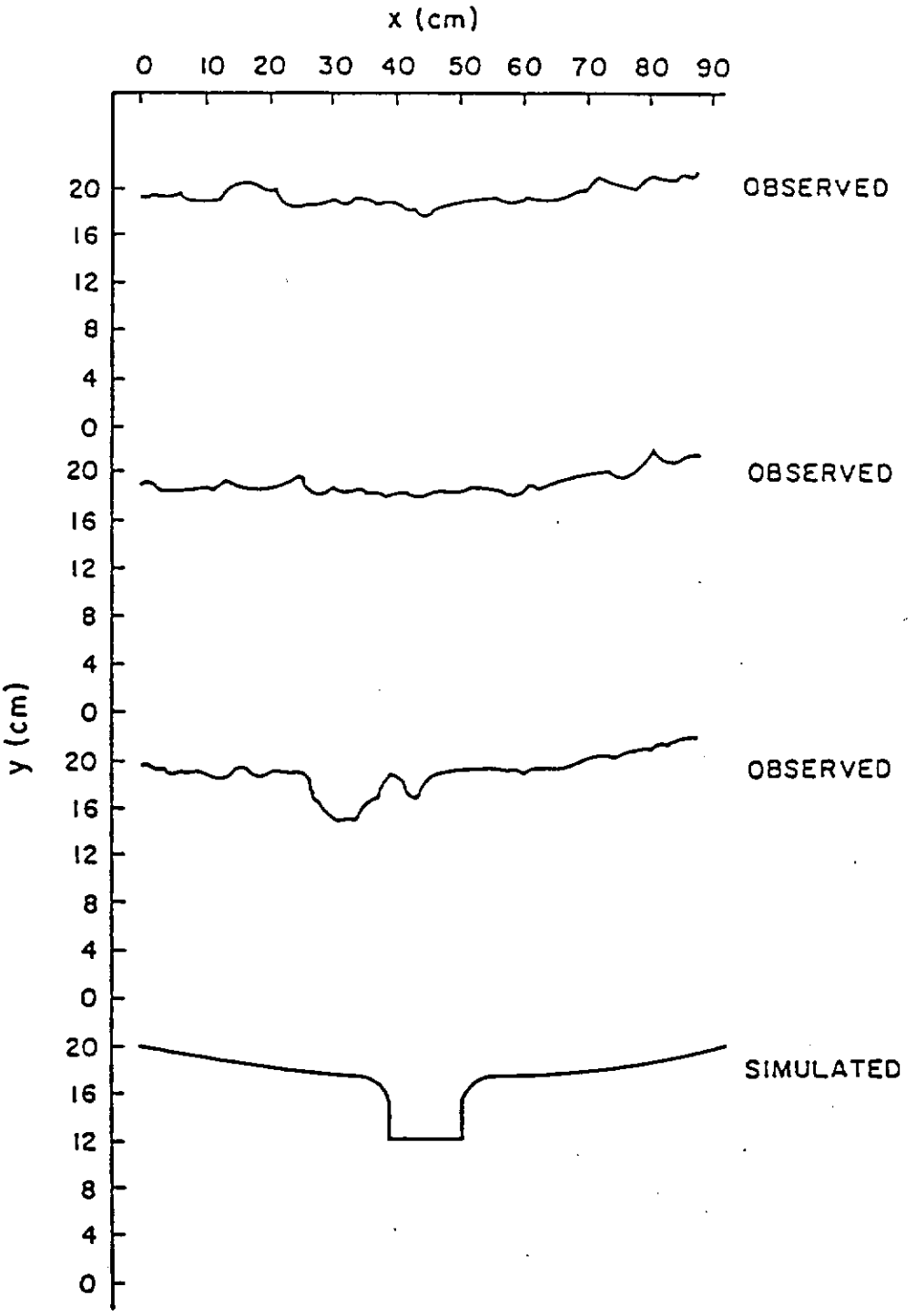

Figure 5.3 Run 121 Right-Side Rill Cross-Sections (1 foot intervals) Compared to KYERMO Simulated Shape

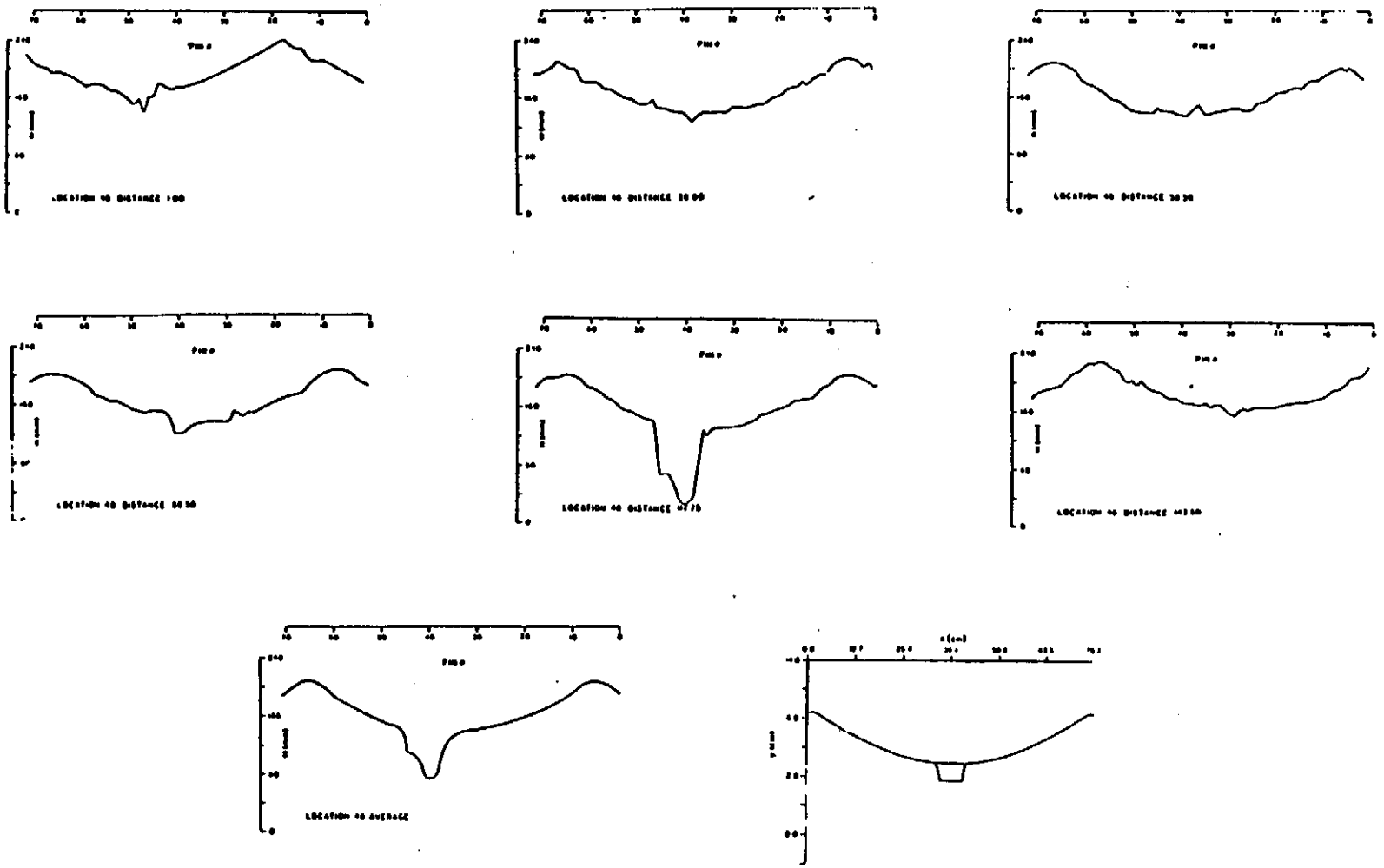

Figure 5.4 Run 111 Mid-plot Rill Cross-Sections and Average Cross Section Compared to KYERMO Simulation

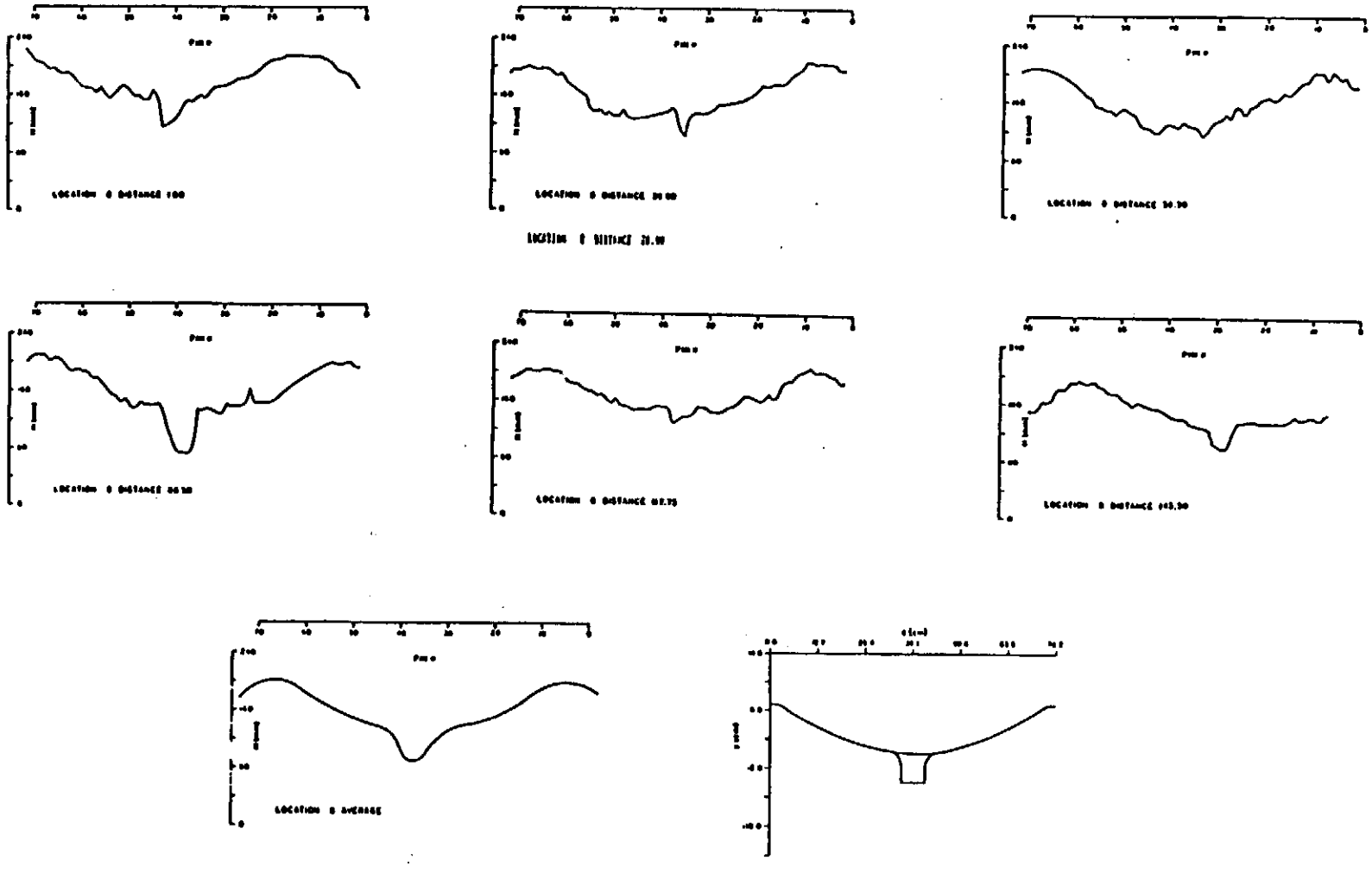

Figure 5.5 Run 111 Lower Plot Rill Cross-Sections and Average Cross-Section Compared to KYERMO Simulation

the model simulated rill cross sections only predict the average measured cross section.

It can be concluded from the above that the rilling process is highly variable, with a modeling approach such as in KYERMO giving a correct representation only on the average. This points out the need for a stochastic approach to the rill erosion process.

SUMMARY COMMENTS

The justification simulations described in this chapter pointed to areas of the model that require further research. The most obvious area is that of the rill detachment and its parameters. Reasonable prediction is attainable if these parameters can be estimated. At the present time, fitting is the only alternative, although the initial estimates based upon parameters available in the literature gave results comparable to other studies. The size distribution prediction and the rill shape prediction are also directly affected by the detachment process. A sensitivity analysis of that process is in order.

CONCLUSIONS

The objectives of this study were divided into two parts, the model development objectives, and the field experiment objective. The model development objectives were to:

1) Develop an overall frame work for the erosion process to

facilitate further research,

2) Predict overall sediment yield and average rill cross-sections under controlled surface shape conditions on a steep slope as a first step to modeling the erosion process on a random surface, and

3) Model the rilling process due to its importance and a lack of knowledge about its prediction.

The objective of the field experiments was to collect justification data for the algorithms used in the erosion model, under controlled surface conditions on steep slopes. This was viewed as a first step to modeling the erosion of a more general surface. The drawing of conclusions based upon these objectives, the results of simulations, and the sensitivity analysis is now in order.

The conclusions to be drawn deal directly with the simulation model's ability to adequately represent the data collected for justification, and the simulated and observed rill cross-sectional shape changes.

KYERMO JUSTIFICATION

The erosion model developed during this study and described in Chapter 2 simulated the hydrologic response of the field plots very well. The good agreement between the magnitude of the simulated response and that of the observed response was due to parameter fitting. However, the shape of the simulated and observed responses were not optimized and their agreement indicates that the model is

representing the hydrologic processes quite well.

The model also simulated the field erosion data with reasonable accuracy, with a standard error within the range of other studies reported in the literature. The simulation accuracy could be greatly increased by utilizing optimized parameters. The need for parameter value optimization methods was quite evident in the analysis. This is consistent with the results from other researchers. It can be concluded that the erosion model produces the proper trends, and that the relative effects of parameters may be evaluated with reasonable confidence for steep slopes, but the lack of information for estimating detachment parameter values limits the use of the model for determining absolute erosion amounts. The need for research in this area will be addressed in a later section.

The sensitivity analysis indicated that the model predictions followed the expected trends for the steep slope (detachment limiting) case. These analyses further indicate that predictions should be based on the highest practical number of slope increments and the smallest practical time step. The results also indicate that the number of rills on a given plot that causes a maximum erosion rate are different for different soil conditions and storm runoff volumes.

Average rill cross sections were predicted with only fair accuracy (due to total sediment yield errors) and the individual rill cross-section with poor accuracy. This occurred because of the highly stochastic nature of the rilling process. The presence of coarse material in the observed rills and a possible change in soil structure between treatments also contributed to this lack of accurate prediction. The general shape of the predicted rills were reasonable when

compared to the observed rill shape.

RILL DEVELOPMENT

The rill processes merit further conclusions. It was quite evident from the measured rill cross-sections that the cross-sectional shape was highly variable, both between different rills and within the same rill, even over very short distances. These changes were largely due to heterogeneities in the plot soil, pointing out the stochastic nature of the rilling process. From this and the model predictions it can be concluded that the model developed in this study can only predict the dynamic rill shape on the average, and that if individual rills are to be modeled, a new modeling approach must be developed which accounts for this stochastic behavior.

RILL CROSS-SECTIONAL CHANGES

The changes that occur in the rill cross-section during an erosion event were examined only in the slides taken of the plots during the field simulations and in the results of the model simulations. Few conclusions can be drawn from the field data, however the model indicated that the rill shape is dictated largely by the initial shape and the location of the rill on the plot. Field observations indicated that major changes in rill shape were due to heterogeneities, such as large rocks. These random processes are not predicted by the erosion model.

SUMMARY OF CONCLUSIONS

1) The erosion model developed during this study represents the hydrologic processes well, and can be used to predict the hydrologic response with parameter inputs,

2) The erosion model prediction accuracy compares favorably with that of other erosion models as reported in the literature,

3) The erosion model predictions follow expected trends for the detachment limiting case,

4) The erosion model can only be used to predict rill cross-sections on the average, and

5) The rill erosion process is stochastic in nature, with large variations over short distances.

REFERENCES

Allmaras, R. R., R. E. Burwell, W. E. Larson, R. F. Holt and W. W. Nelson. 1966. Total porosity and random roughness of the interrow zone as influenced by tillage. USDA Conservation Report. No. 7.

Alonso, C. V. 1980. Selecting a formula to estimate sediment transport capacity in nonvegetated channels. In CREAMS - A field scale model for Chemicals, Runoff, and Erosion from Agricultural Management Systems, Volume III, Supporting Documentation, Chapter 5, USDA-SEA, Conservation Report #28, pp. 426-439.

Alonso, C. V., W. H. Neibling and G. R. Foster. 1981. Estimating sediment transport capacity in watershed modeling. Transactions of the ASAE, 24(5):1211-1220, 1226.

Barfield, B. J., R. I. Barnhisel, J. L. Powell, M. C. Hirschi, and I. D. Moore. 1983. Erodibilities and eroded size distribution of Western Kentucky mine spoil and reconstructed topsoil. Institute for Mining and Minerals Research Final Report, University of Kentucky, Lexington, KY.

Brakensiek, D. L. 1966. Storage flood routing without coefficients. USDA-ARS, 41-122.

Bubenzer, G. D. and B. A. Jones, Jr. 1971. Drop size and impact velocity effects on the detachment of soils under simulated rainfall. Transactions of the ASAE, 14(4):625-628.

Campbell, G. S. 1974. A simple method for determining unsaturated conductivity from moisture retention data. Soil Science, 117(6):311-314.

Foster, G. R. 1982. Modeling the erosion process. In Hydrologic Modeling of Small Watersheds, C. T. Haan et al., editor, ASAE Monograph No. 5, pp. 297-380.

Foster, G. R., L. J. Lane, J. D. Nowlin, L. M. Laflen and R. A. Young. 1980. A model to estimate sediment yield from field-sized areas: development of model. In CREAMS - A field scale model for Chemicals, Runoff, and Erosion from Agricultural Managements Systems. Volume I: Model Documentation, Chapter 3. USDA-SEA, Conservation Report #26, pp. 36-64.

Foster, G. R., L. J. Lane, J. D. Nowlin, J. M. Laflen, R. A. Young. 1981. Estimating erosion and sediment yield on field-sized areas. Transactions of the ASAE, 24(5):1253-1262.

Foster, G. R. and L. D. Meyer. 1972a. A closed-form soil erosion equation for upland areas. In Sedimentaion: Symposium to Honor Professor H. A. Einstein. H. W. Shen, Editor, Fort Collins, CO, Chapter 12, 19pp.

Foster, G. R. and L. D. Meyer. 1972b. Transport of soil particles by shallow flow. Transactions of the ASAE, 15(1):99-102.

Hirschi, M. C. 1980. Hydraulic conductivity and degree of saturation during infiltration: A preliminary investigation. Unpub. M.S. paper, Department of Agricultural Engineering, University of Minnesota, St. Paul, MN.

Hirschi, M. C. 1985. Modeling soil erosion with emphasis on steep slopes and the rilling process. PhD Dissertation, University of Kentucky, Lexington, KY.

Hirschi, M. C. and B. J. Barfield. 1984. Tipping bucket flow measurements on large erosion plots. ASAE paper #84-2008, presented at the ASAE Summer Meeting, June 24-27, Knoxville, TN.

Hirschi, M. C., B. J. Barfield, and I. D. Moore. 1983. Modeling erosion on long steep slopes with emphasis on the rilling process. Research Report No. 148, Water Resources Research Institute, University of Kentucky.

Hirschi, M. C., B. J. Barfield, and I. D. Moore. 1984. Rillmeters for detailed measurement of soil surface heights. ASAE paper #84-2534, presented at the ASAE Winter Meeting, December 11-14, New Orleans, LA.

Hirschi, M. C., C. L. Larson and D. C. Slack. 1980. Hydraulic conductivity and degree of saturation during infiltration. ASAE paper #80-2007, presented at the ASAE Summer Meeting, June 15-18, San Antonio, TX.

Knisel, W. G., editor. 1980. CREAMS: A Field Scale Model for Chemicals, Runoff, and Erosion from Agricultural Managment Systems. U.S. Department of Agriculture, Conservation Research Report No. 26, 640 pp.

Linden, D. R. 1979. A model to predict soil water storage as affected by tillage practices. Ph.D. Disseration, Department of Soil Science, University of Minnesota, St. Paul, MN.

Lundgren, H. and I. G. Jonsson. 1964. Shear and velocity distribution in shallow channels. Jour. of Hydr. Division, ASCE, 90(HY1):1-21.

Mantz, P. A. 1977. Incipient transport in fine grains and flakes by fluids-extended Shields diagram. Jour. of Hydr. Division, ASCE, 103(HY6):601-615.

Mein, R. G. and C. L. Larson. 1971. Modeling the infiltration components of the rainfall-runoff process. WRRC, University of Minnesota Grad. School Bull. 43.

Meyer, L. D., G. R. Foster, and S. Nikolov. 1975. Effect of flow rate and canopy on rill erosion. Transactions of the ASAE, 18(5):905-911.

Meyer, L. D. and D. L. McCune. 1958. Rainfall simulator for runoff plots. Agricultural Engineering, 39(10):644-648.

Moore, I. D. 1979. Infiltration into tillage affected soils. Unpub. Ph.D. thesis, University of Minnesota, St. Paul, MN.

Moore, I. D. 1981a. Infiltration equations modified for surface effects. Jour. of the Irr. and Drain. Div., ASCE, 107(IR1):71-86.

Moore, I. D. 1981b. Effect of surface sealing on infiltration. Transactions of the ASAE, 24(6):1546-1552, 1561.

Moore, I. D. and J. D. Eigel. 1981. Infiltration into two-layered soil profiles. Transactions of the ASAE, 24(6):1496-1503.

Moore, I. D., M. C. Hirschi, and B. J. Barfield. 1983. Kentucky rainfall simulator. Transactions of the ASAE, 26(4):1085-1089.

Mossaad, M. E. and T. H. Wu. 1984. A stochastic model of soil erosion. Int'l Jour. for Num. and Analy. Meth. in Geomech., 8:201-224.

Mutchler, C. K. and C. L. Larson. 1971. Splash amount from waterdrop impact on a smooth surface. Water Resources Research, 7:1:195-200.

Neibling, W. H. and G. R. Foster. 1980. Sediment transport capacity of overland flow. In CREAMS- A Field Scale Model for Chemicals, Runoff, and Erosion from Agricultural Management Systems, Volume III, Supporting Documentation, Chapter 10, USDA-SEA, Conservation Report #26, pp. 463-473.

Palmer, R. S. 1965. Waterdrop impact forces. Transactions of the ASAE, 8(1):69-70.

Quansah, C. 1981. The effect of soil type, slope, rain intensity, and their interactions on splash detachment and transport. Journal of Soil Science, 32:215-224.

Richards, L. A. 1931. Capillary conduction through porous mediums. Physics, 1:313-318.

Rohlf, R. A. 1981. Developemnt of a deterministic mathematical model for interrill and rill runoff and erosion. Unpub. M.S. Thesis, Department of Civil Engineering, University of Kentucky, Lexington, KY, 84 pp.

Schwab, G. O., R. K. Freuert, T. W. Edminster, and K. K. Barnes. Soil and Water Conservation Engineering, 2nd Edition. New York: John Wiley and Sons, 683pp.

Slack, D. C. 1978. Predicting ponding under moving irrigation systems. Jour. of Irr. and Drain. Div., ASCE, 104(IR4):446-451.

Smerdon, E. T. and R. P. Beasley. 1961. Critical tractive forces in cohesive soils. Agricultural Engineering, 42(1):26-29.

Tholin, A. L. and C. J. Keifer. 1960. Hydrology of Urban Runoff. Transactions ASCE, 125:1308-1355.

Vanoni, V. A., editor. 1975. Sedimentation Engineering. New York: American Society of Civil Engineers, 745pp.

Weinmann, P. E. 1977. Comparison of flood routing methods for natural rivers. Civil Engineering Research Report No. 2/1977, Monash University, Clayton, Victoria, Australia.

Wilson, B. N., D. C. Slack, and R. A. Young. 1982. A comparison of three infiltration models. Transactions of the ASAE, 25(2):349-356.

Wischmeier, W. H., C. B. Johnson, and B. V. Cross. 1971. A soil erodibility nomograph for farmland and construction sites. Jour. of Soil and Water Cons., 26(5):189-193.

Wischmeier, W. H. and J. V. Mannering. 1969. Relation of soil properties to its erodibility. Soil Sci. Soc. of Amer. Proceedings, 33(1):131-136.

Yalin, M. S. 1963. An expression for bed-load transportation. Jour. of the Hydr. Div., ASCE, 89(HY3):221-250.

Yalin, M. S. 1972. Mechanics of Sediment Transport. 2nd Edition. New York: Pergamon, 298 pp.

Yang, C. T. 1973. Incipient motion and sediment transport. Jour. of Hydr. Div., ASCE, 99(HY10):1679-1704.